

FAA-ADS-82



SOME EFFECTS OF BLADE CHARACTERISTICS ON COMPRESSOR NOISE LEVEL

AD647221

TECHNICAL REPORT

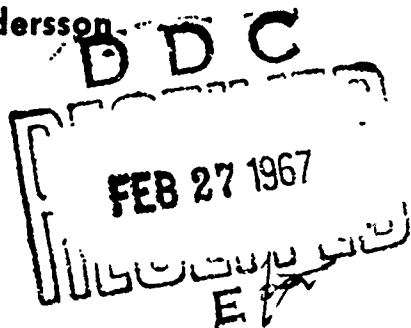


OCTOBER 1966

By

B. Hulse, C. Pearson, M. Abbona, and A. Andersson

THE **BOEING** COMPANY
COMMERCIAL AIRPLANE DIVISION
RENTON, WASHINGTON



Under Contract FA65WA-1263
For
FEDERAL AVIATION AGENCY
Aircraft Development Services

ARCHIVE COPY

**SOME EFFECTS OF BLADE CHARACTERISTICS
ON COMPRESSOR NOISE LEVEL**

**TECHNICAL REPORT
FAA-ADS-82
CONTRACT NUMBER FA65WA-1263**

by

**B. Hulse, C. Pearson,
M. Abbona, and A. Andersson**

October 1966

Prepared for

**THE FEDERAL AVIATION AGENCY
Under Contract No. FA65WA-1263**

by

**THE BOEING COMPANY
Commercial Airplane Division
Renton, Washington**

Mr. John B. Large, Chief of the Acoustics Staff/SSTD served as Program Manager. This report has been approved for general availability. The contents of this report reflect the views of The Boeing Company, which is responsible for the facts and the accuracy of the data presented herein, and do not necessarily reflect the official views or policy of the FAA. This report does not constitute a standard, specification, or regulation.

ABSTRACT

Sound power level and airflow measurements were obtained for flat, cambered, and airfoil blades, with and without twist. A single-stage axial flow compressor or fan of low pressure ratio was used, the simplified design being dictated by the variety of blade shapes tested. Data are given for the dependence of sound power level on flow coefficient, air weight flow, relative tip velocity, and rotational speed. The sound power per unit weight flow appears to be independent of blade shape. The discrete-frequency noise from a freely running rotor is predicted to an order of magnitude in agreement with experimental results by an equation that is intuitively derived from an extension of propeller theory.

CONTENTS

<u>Section</u>	<u>Page</u>
1 INTRODUCTION	1
2 CHARACTERISTICS OF FAN AND COMPRESSOR NOISE	3
3 PHYSICS OF PROPELLER AND FAN NOISE	5
4 ANALYTICAL CONSIDERATIONS, ROTOR ALONE	11
5 EXPERIMENTAL PROGRAM	15
6 CONCLUSIONS	29
7 RECOMMENDATIONS	31
REFERENCES	33
GLOSSARY OF SYMBOLS	35
ACKNOWLEDGMENTS	37
APPENDIX A SOUND LEVEL DATA	A-1
APPENDIX B FAR-FIELD NOISE FROM JET-ENGINE COMPRESSORS	B-1
APPENDIX C MEASUREMENT APPARATUS	C-1

ILLUSTRATIONS

<u>Figure</u>		<u>Page</u>
1	Principal Shape of a Narrow-Band Spectrum of a Rotor-Stator Combination	3
2	Flat and Cambered Blades	17
3	Twisted, Cambered, and Airfoil Blades	18
4	Rotor With Twisted Blades	19
5	Rotor With Twisted Airfoil Blades	19
6	Inlet Guide Vane Assembly With Flat Blades	20
7	Inlet Guide Vane Assembly With Tilted Blades	20
8	Stacked Tube Inlet Guide Vanes	21
9	Honeycomb Inlet Guide Vanes	21
10	Different Blade Shapes, Sound Power Level 6 Inches From Rotor ($m = 1$)	24
11	Sound Power Level (Normalized With Weight Flow) Compared With V_{rel}^5	25
12	Sound Power Level (Normalized With Weight Flow) Compared With Slope of Proposed SAE Prediction Curve	25
13	Flat Blades, Rotor Alone, Rotational Speed and Sound Power Level 6 Feet From Rotor: Comparison Between Calculated and Measured Values	26

SECTION 1

INTRODUCTION

When a subsonic aircraft powered by turbofan engines approaches an airport, a distinctive whine can be heard above a background of broad-band noise. This whine originates in the first few compressor stages and is especially noticeable when the first stage rotor is that of a turbofan. This study emphasizes physical interpretations of fan-noise generating mechanisms and experimental estimates of the influence that variations in blade geometries have on these mechanisms.

Techniques for reducing fan noise by means of inlet or fan duct sound-absorbing treatments are not considered, nor are such remedial procedures as inlet choking, partial choking of the fan periphery, and blowing inlet guide vanes. The nature of fan or compressor noise as it would be heard by an observer in the acoustic far field is described in Sec. 2.

The literature on the physics of propeller sound generation is reviewed in Sec. 3. This material is used as background for an intuitive discussion of inlet noise in a turbofan engine. A general equation governing sound pressure fluctuations produced by a number of different acoustic sources is then used to link aerodynamic and acoustic identifications of noise sources.

A particular mathematical model of a fan rotor in which blades are aerodynamically loaded at an effective radius (R_e) is discussed in Sec. 4. A theoretical prediction of the far-field sound pressure levels is available when blade loads are constant in magnitude and direction with respect to the blades, and the rotor blades do not sense the presence of such obstructions in the flow as inlet guide vanes or stator blades. The prediction equation, often referred to in the literature as the Gutin formula, accurately predicts propeller noise but is unsatisfactory for estimating noise produced by freely running fan or compressor rotors. (A freely running rotor is one that operates without obstructions.) The point of view taken here is that flow irregularities causing fluctuations in blade loads are more effective in producing noise from many-bladed rotors than from propellers. A quasi-analytical argument is presented to stimulate other analytical extensions of the Gutin formula to include the effects of fluctuations in blade loads.

In Sec. 5 the experimental program is described critically with future work in mind; results are discussed in parametric terms and, where possible, are compared with experimental results of other investigators and with available prediction equations.

Section 6 relates the physical and analytical arguments of Sec. 3 and 4 to the experimental results of Sec. 5. The assumption that fan noise generation can be explained in terms of fluctuating aerodynamic forces acting at an effective blade radius is believed by Boeing to be compatible with experimental results now available.

Design objectives for a compressor rig that might be used in a more ambitious extension of this program are presented in Sec. 7. Additional critical experiments that could be performed on the existing ducted fan are also described.

SECTION 2

CHARACTERISTICS OF FAN AND COMPRESSOR NOISE

A listener in the vicinity of an axial-flow fan or compressor may distinguish two distinct sound components known as "discrete-frequency noise" and "broad-band noise." The first component consists of a number of pure, or nearly pure tones, which combine to form a high-frequency noise best described as a whine. The second component is a background hissing noise caused by a superposition of sounds over a continuous band of frequencies from the lower audible range to the higher, and without pronounced peaks at any particular frequencies.

The relative importance of the two noise components depends on the type of fan or compressor. Noise from a many-bladed fan, working at subsonic tip speed in an unobstructed airflow, has broad-band characteristics. Noise from a high-speed propeller has predominately discrete-frequency characteristics. From a compressor in which the rotor interacts with stators, or a fan with bearing support struts or other obstacles near the rotor face, the noise is a mixture of the two components. Generally, the discrete-frequency noise dominates. The principal shape of a narrow-band spectrum of a rotor-stator combination is shown in Fig. 1.

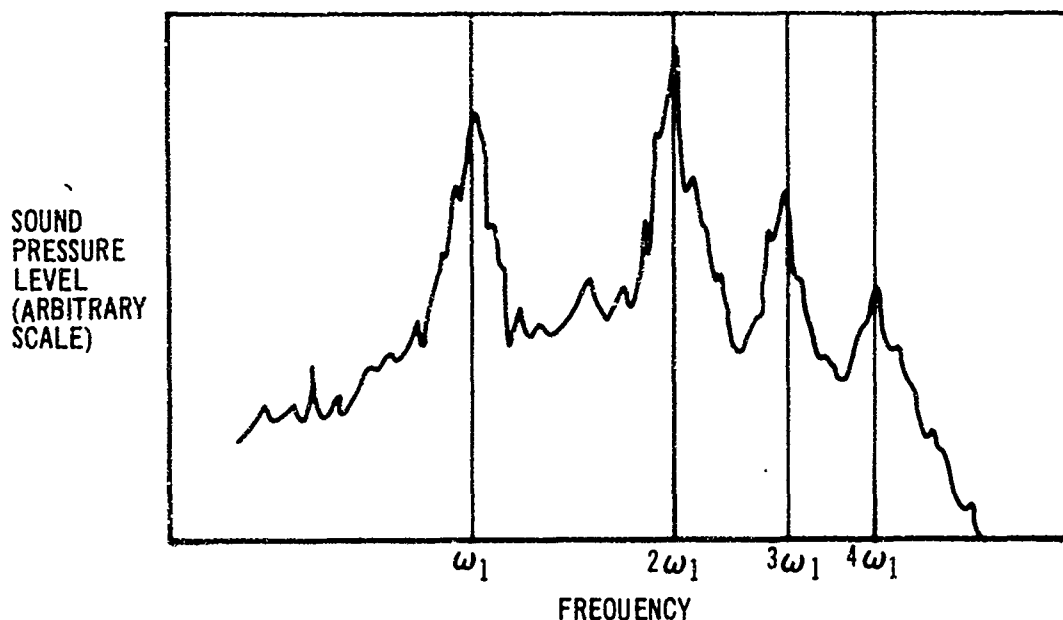


Fig. 1. Principal Shape of a Narrow-Band Spectrum of a Rotor-Stator Combination

The discrete-frequency noise has its fundamental frequency at the "blade passage frequency," $f = N \times B$, where N is the rotational speed of the fan measured in rps, and B is the number of rotor blades. When listening to the fan noise, filtered through a narrow-band filter, centered at blade passage frequency, the observer will experience a tone that is modulated, i. e. the sound level varies with time. In the case of a compressor with predominantly

discrete-frequency noise, this modulation is due to the mixing of the fundamental tone with that part of the broad-band noise which, at considerably lower level, occurs in the same frequency band. In the case of a freely running fan of low tip speed where the fundamental frequency may only be distinguishable through the narrow-band filtering, the tone occurs in bursts, presumably when patches of large-scale turbulence pass through the fan.

If the listener moves in an arc of constant radius from the noise source, he will experience a change in the sound level and character of the noise, since each component of the noise has different directivity characteristics. The broad-band noise radiation is more or less omnidirectional, i. e. the level is almost the same in all directions. The discrete-frequency noise, on the other hand, has a pronounced directivity pattern, with "lobes" of maximal noise level separated by deep minima. The number and position of these lobes is determined by many parameters, e. g. frequency, fan diameter, number of rotor and stator blades, and the presence of an inlet duct. The lobal pattern is therefore different for the fundamental blade passage frequency than for its harmonics. Most lobal patterns have one feature in common: the sound level is at a minimum on the fan axis. An exception occurs when the sound source is a compressor with the number of stator blades being a multiple of the number of rotor blades.

SECTION 3

PHYSICS OF PROPELLER AND FAN NOISE

A typical fan or compressor noise spectrum can be considered as composed of two basic parts. One is a broad-band spectrum and the other consists of discrete-frequency peaks superimposed on the first. The broad-band spectrum covers a wide range of frequencies, whereas the peaks of discrete noise are practically concentrated at the rotor blade passage frequency and its harmonics.

The generation mechanisms of the two forms of compressor or fan noise are related in a broad sense to those of propeller noise, but contain some additional characteristic features. These are the results of the different geometry and aerodynamic behavior of fans or compressors as compared with a propeller. For the first, the boundary layers and wakes resulting from the presence of ducts and fixed blade rows before and after a rotor represents one of the most important sources of noise. On the contrary, for propellers (including pusher-type) the effects of turbulence are of much less importance than other factors of noise generation.

It is then obvious that fan or compressor noise is more complex than that of a propeller. However, in spite of the differences between the two types of noise a brief review of the mechanisms of propeller noise generation, for which more data are available, is useful. Finding the counterparts of these generation mechanisms for the fan noise, together with the sources and mechanisms peculiar to it, will give a better understanding of the physics and basic problems of fan noise.

It is generally assumed that propeller noise is produced by three different mechanisms, and therefore it is considered here as composed of the following parts:

- thickness noise
- lift noise
- vortex noise

This classification is only an approximation to the real phenomenon, where a net separation of these concomitant and interrelated noise mechanisms does not exist. It is adopted here only to simplify the description of propeller noise. However, since workers in the field use these noise designations with different meanings, clarifications will be introduced when confusion might otherwise arise.

Richards and Sharland presented an up-to-date résumé of propeller and fan noise (Ref. 1). Their scheme is used to give a short description of the sources of propeller and fan noise.

"Thickness noise" designates the part of propeller noise that arises from the transverse displacement of the air adjacent to a passing blade element. This displacement, in a fixed frame of reference, is equivalent to a periodic introduction of mass at each element of air near the propeller disk, and the

rate of mass introduction at a point depends on the peripheral speed, blade profile, and pitch and incidence angles. This is the accepted definition of thickness noise, but some investigators (Refs. 2 and 3) designate with this term the noise from a propeller with symmetrical profiles, zero blade angle, and zero forward speed. In this case, a better separation between thickness and other noise mechanisms is obtained and theoretical treatment of thickness noise can be made easily. Thickness noise then becomes related only to the so-called "propeller volume," which is the product of the number of blades, blade thickness and chord, and propeller tip radius. Here, the first designation is adopted as the one reflecting the real conditions of propeller operation.

"Lift noise" arises from the pressure field that surrounds each blade as a consequence of its motion. In a moving blade, the pressure distribution on each section along the blade span produces force fluctuations on the surrounding air; this is the origin of lift noise. The force produced on the air by each blade is equal and opposite to the force produced on each blade by the air, and the latter force can be resolved into two different sets of components. In one, the components are lift and drag, in directions perpendicular and parallel to the flow velocity, respectively. In the other, they are the thrust in the direction of the propeller axis and a component in the plane of the propeller disk, which is associated with the propeller torque. This noise, which is a combination of torque and thrust noises, is usually referred to as "lift noise," taking its name from one of the components of the force on the blade along its aerodynamic axis. The pressure field around each blade rotates with the rotating propeller and then lift noise contributes to the periodic component of the propeller noise spectrum, together with thickness noise.

"Vortex noise" is produced by the vortices shed in the propeller wake by the blades as a consequence of their motion. It represents the broad-band or nonperiodic component of the propeller noise spectrum. The exact physical mechanism of this type of noise is not yet known. Investigators agree that it is caused by the vortices in the blade wake. However, some of them ascribe the noise directly to the vortices, which, being random both in size and point of release from the blade, cause the broad-band noise spectrum. Others suggest that the shedding of vortices in the wake results in a corresponding change of circulation over the blade section. This change, in turn, sets up on the blade a randomly fluctuating lift, which is the final cause of noise. Apart from this difference on the explanation of vortex noise, all agree on the factors determining its existence. These are represented by von Kármán vortices, vortices coming from the separation region on the convex side of the blade, and vortices produced by every cause of turbulence on the flow. Even for ideal conditions, the von Kármán vortices, shed alternately from opposite sides of the blade, are present in the flow because of the finite thickness of the blade trailing edge, but then vorticity is shed in a regular manner.

It is appropriate to emphasize once more that the classification of propeller noise and the contributing mechanisms is only an idealization. For example, lift noise was considered only as a source of discrete-frequency noise. However, a more detailed analysis of lift generation would show that it also contributes to the broad-band noise.

After this brief review of propeller noise, general considerations on fan or compressor noise and an examination of the pertinent spectra suggest that the latter must be produced by the same mechanisms described for propellers. But to this must be added the important noise contributions brought about by the presence of both fixed blade rows before and after each rotor and a duct around all these rows of blades. This ducting of the flow produces an essentially axisymmetrical flow in an annulus as compared with a three-dimensional flow for propellers.

A brief correlation between propeller and fan noise based on the three mechanisms previously considered, and a description of the new mechanisms peculiar to fan or compressor are made in the following paragraphs:

"Thickness noise," produced by a mechanism similar to that found for propellers, must also exist in the case of fans or compressors. However, for typical engines and speed regimes, the contribution of this mechanism to overall fan noise does appear unimportant. This can be explained as a consequence of both the smaller thickness of rotor blades with respect to that of propeller blades and the greater relative importance of lift and vortex noise in a fan than in propeller.

"Lift noise" is also found because a fan rotor has an associated rotating pressure field such as that determining propeller "lift noise." The resulting periodic force fluctuations are then contributing in a similar way to the discrete frequency of fan noise. But this is only a part of the fan "lift noise" and precisely that due to the rotor alone. In a fan or compressor the rotor of the first stage, which contributes more to noise, is generally preceded by bearing support struts and by inlet guide vanes, and is always followed by a stator.

Consequently, a further source of "lift noise" appears because of the motion of the rotor in the wakes of upstream objects. In these wakes, the air velocity is small compared to its value in the remainder of the annulus, and a blade rotor moves in and out of regions of different velocity. These variations of velocity, which are due not only to the effects of the viscous wakes, but also to the potential flow field of the upstream blade row (Ref. 4), produce variations of incidence. On the rotor blade subjected to these variations of incidence, a fluctuating lift is originated and, therefore, periodically varying forces are applied to the air. In this way the mechanism contributes to discrete frequency noise together with the rotor "lift noise," and thus can be called "discrete frequency interaction noise."

"Vortex noise," in contrast to that of propeller noise, is a very important source of fan noise. It is produced by the same causes analyzed in propeller noise. However, the two additional mechanisms represented by the interaction effects of fixed and moving blade rows and the effect of duct boundary layer can add considerably to vortex noise. In the first, the wakes shed by the upstream blades on reaching the leading edge of a rotor blade are distorted and can represent a source of noise. In the second, the turbulence produced by the boundary layers on the fan or compressor casings adds to any turbulence present in the intake flow to produce vortex noise. As pointed out by Sharland (Ref. 5), who made a detailed study on the subject, this source of broad-band

noise can be dominant when the intensity and spatial scale of the turbulence are large enough. Because of their origin and the type of noise produced, these additional sources can be designated as sources of "vortex or broad-band interaction noise."

At this point, to illustrate that also for the interaction noise the discrete-frequency and broad-band contributions cannot be separated completely, an example is given of two concurrent effects due to the oncoming turbulence. This may affect the positions of the separation points on both the fixed and moving blades and thus cause fluctuating lift leading to broad-band noise. The variations of the separation point along the fixed blade, in turn, produce changes in the form of their wake and contribute to the discrete-frequency interaction noise from the rotor.

From the brief description of the mechanisms of interaction noise, both discrete frequency and broad band, it can be inferred that similar noise radiations come from the blades of a stator placed in the induced field of a rotor. Furthermore, the flow from the rotor, when reaching the stator inlet, finds new obstructions represented by the stator blades. Consequently, local pressure variations are again produced, which, since the flow is generally subsonic (even in the case of transonic rotors), are propagated upstream, causing variations of force on the rotor blade—a further cause of noise.

Fincher (Ref. 6), extending the work of Sharland on interaction noise, performed experiments on a model composed of inlet guide vanes and rotor with variable separation between the two adjacent rows of blades. The primary object of his investigation was to find the more effective cause of noise between the following two mechanisms: (a) wake-induced pressure fluctuation on the rotor blades or (b) a disturbance of the upstream pressure field associated with the rotor blade by the presence of the stator. Experiments showed that for axial spacing greater than a certain critical amount, the first mechanism was the most important, whereas the second was the prevalent one when the rows of blades were brought very close.

From the previous consideration of the mechanisms of interaction noise, it can be expected that it will become minimum if care is taken to make the aerodynamic interference between adjacent blades as small as possible. This can be done by reducing the mutual effect of their pressure fields, decreasing the size of the wakes, modifying their form, and diminishing the size of the boundary layer on the inlet duct walls. For the first stage of a fan or compressor, some practical means of obtaining these effects are: omit inlet guide vanes, increase axial spacing between adjacent blade rows, reduce the boundary layer thickness on the duct walls, and remove or reduce the boundary layer on the inlet guide vanes.

It is possible to compare the above aerodynamic descriptions of noise sources to the basic sources of Lighthill's noise theory. There, following Lowson (Ref. 7), the fundamental equation describing noise generation can be written in tensor notation as

$$\frac{\partial^2 \zeta}{\partial t^2} - a_0^2 \nabla^2 \zeta = \frac{\partial Q}{\partial t} - \frac{\partial F_i}{\partial x_i} + \frac{\partial T_{ij}}{\partial x_i \partial x_j}$$

where the left-hand side represents the equation of sound propagation in a uniform acoustic medium at rest, and ζ and a_0 denote, respectively, the fluctuating density and the sound velocity in the medium. The three terms on the right side account for the various sources of sound radiation. The first term, $\partial Q/\partial t$, where Q is the mass per unit volume, represents the sound produced by mass introduction at a point of the medium. It describes the sound radiation due to a single pulsating mass source, which has no definite directionality associated with it, and is known as the "monopole" or "zero order" type of radiation source. "Thickness noise," which arises from a periodic introduction of mass at each element of air near a propeller or rotor, is an example of this type of noise.

The second term, $\partial F_i/\partial x_i$, where F_i is the force per unit volume in the x_i direction, represents the sound produced by the fluctuating forces acting at a point of the medium. The sound radiation due to these forces can be associated with that of a dipole having its axis in the direction of F_i and of strength equal to the magnitude of F_i . This dipole radiation has a definite directionality, with the maximum radiation occurring in the direction of action of the force. "Lift noise," which arises from force fluctuations on the air surrounding a propeller or rotor, is an example of this type of radiation and therefore is described as dipole in origin. For typical subsonic propellers, where lift noise is the most important, the noise contributions come from two arrays of dipoles, one with axis in the direction of the propeller axis and the other with axes in the propeller disk aligned in the torque direction.

The third term, $\partial T_{ij}/\partial x_i \partial x_j$, where $T_{ij} = \zeta V_i V_j + V_{ij} - a_0^2 \zeta \delta_{ij}$ is the "acoustic stress tensor," accounts for the noise produced by turbulence. For most practical purposes, $T_{ij} \approx \zeta V_i V_j$, where $\zeta V_i V_j$ is the momentum flux tensor, or rate at which momentum in the x_i direction crosses the unit surface area normal to the x_j direction. A full discussion of all the effects described by the term $\partial T_{ij}/\partial x_i \partial x_j$ can be found in Lighthill's aerodynamic noise theory (Ref. 8). Here it is sufficient to recall that from the acoustical standpoint the noise due to this term radiates as a quadrupole field whose strength per unit volume is T_{ij} and has a double directionality pattern. Vortex noise of propellers and fans is an example of this type of noise.

SECTION 4

ANALYTICAL CONSIDERATIONS, ROTOR ALONE

Much of the literature on fan and compressor noise has evolved from analyses of aircraft propeller noise such as the one published by Gutin (Ref. 9) in 1936. Garrick and Watkins reviewed the Gutin theory in 1954 (Ref. 10) and obtained good agreement with measurements of propeller noise. In 1964, Sharland (Ref. 5) described experimental results obtained on a single-stage axial-flow fan. He found that when a rotor with 16 blades was rotated in the absence of inlet guide vanes or stators, measured noise spectra exhibited prominent peaks at the blade passage frequency and the second and third harmonics, as might be expected from propeller theory. However, the amplitude levels of these tones were much higher than predicted. He attributed this discrepancy to the presence of wakes behind bearing support arms upstream from the rotor. Noting that the Gutin theory supposes that aerodynamic forces on blades are constant, Sharland argued that fluctuating forces, not accounted for by the theory and due to passage of the blades through the wakes, would result in an increase in level of the discrete components of fan noise.

As reported in Appendix B, an effort was made to find whether the Gutin result was valid for rotors with large numbers of blades and, if so, to determine whether or not it may be extended to include effects of fluctuating blade loads. The conventional result predicts a drastic reduction in sound level of discrete tones for a rotor as the product mB is increased (where m is the order of the harmonic and B the number of blades).

Since earlier derivations of the Gutin formula involved a first term approximation to an asymptotic expression, this result was extended to include a second-order term. However, it was found that the Gutin result, in the usual deterministic form, is indeed valid for large B , in spite of the first-order approximation.

Garrick and Watkins (Ref. 10) used rather arbitrary blade pressure distributions in their review of the Gutin theory, yet the resulting equation pertains to constant thrust (T) and torque (Q) applied at an effective radius (R_e). The discussion presented in Appendix B shows that the Gutin result can be obtained by assuming at the outset that the distributed blade loading can be replaced by concentrated loads at a fixed effective blade radius.

The following is a heuristic discussion of the possible effects of adding fluctuations to the concentrated loads on the rotor blades:

It is important to note that even slight irregularities in these instantaneous forces can have a marked effect on the higher order harmonics generated by a single blade, and also on the intensity of the fundamental blade passage frequency corresponding to B blades. The far-field noise pattern corresponding to a single blade is very roughly sinusoidal, with a period equal to $2\pi/\Omega$. If we now replace the single blade with B blades, and if each blade produces exactly the same far-field pattern except for the appropriate time displacement, all Fourier components of the single-blade pattern will cancel out, except for

the B^{th} harmonic, which will be reinforced. (Similarly, the next higher harmonic to be reinforced is the $2B^{\text{th}}$ harmonic, and so on). Since the magnitude of the B^{th} harmonic of our nearly sinusoidal signal is so small (via the Gutin formula), even this reinforcement will not be effective, and the overall signal level will be extremely small. If there are slight irregularities in the forces exerted by the blades, the magnitude of the higher order harmonics can be very much larger because it is in those harmonics that the irregularities show.

As a result it is reasonable to expect the B^{th} harmonic of the single blade pattern to be much larger than that given by Eq. (15) in Appendix B, particularly for small values of y . To obtain a careful estimate of the expected value of the B^{th} harmonic of a signal possessing some randomness requires an investigation of the correlation features of that randomness. An order of magnitude estimate can however be made if we assume that the random signal has an average angular frequency β , and that its bandwidth is neither very narrow nor very broad. The B^{th} harmonic will then have a magnitude of the order of

$$\frac{\Omega}{\pi} \int_0^{2\pi/\Omega} \sin \beta t \cdot \cos B\Omega t = 0 \left(\frac{1}{B} \right) \quad (1)$$

assuming $\beta \ll B\Omega$. As an estimate of the magnitude of the B^{th} harmonic of the far-field signal, $1/B$ of that of the fundamental thus can be taken.

Secondly, in considering the cumulative effect of B blades, the randomness of phases between the B^{th} components emanating from each blade means that the net resulting magnitude should be taken as \sqrt{B} times the magnitude of the effect resulting from a single blade.

For a single blade the Gutin formula reads [cf. Eq. (1), Appendix B]:

$$|p| = \frac{\Omega}{2\pi a s_0} \left| T \frac{x}{s_0} - Q \frac{a}{\Omega R_e} \right| J \left(\frac{\Omega y R_e}{a s_0} \right) \quad (2)$$

This formula gives the correct order of magnitude for the fundamental single-blade signal, as has been borne out by experiment for propellers. If we now assume that the fluctuating thrust and torque can be approximated by the steady values of thrust and torque, the above formula can be applied; if it is corrected for the influence of the number of blades. First replace Q by GR_e , where G is the equivalent force per blade at radius R_e , in the plane of the propeller. Also replace $\Omega R_e/a$ by M , the rotational Mach number of the blade at radius R_e . We also choose average values for x/s_0 and for y/s_0 (again more realistic for the random situation); via conventional solid angle weighting,

each is replaced by 1/2. For the m^{th} harmonic of the B-bladed case, our previous considerations now lead us to multiply this result by $1/(m\sqrt{B})$, to give as the final result

$$p_{\text{rms}} = \frac{\Omega}{2\sqrt{2}\pi a s_0} \sqrt{\left(\frac{T}{2}\right)^2 + \left(\frac{G}{M}\right)^2} \cdot J_1\left(\frac{\pi}{4}M\right) \frac{1}{m\sqrt{B}} \quad (3)$$

One questionable point remains. Because of the randomness, the $(B-1)^{\text{st}}$ harmonics, say, of the single-blade pattern, should not cancel when the patterns of B blades are superimposed. Consequently, for the case in which a rotor alone is tested, there should be peaks in the spectrum at $\frac{B}{2\pi}\Omega$, $\frac{B\pm 1}{2\pi}\Omega$, $\frac{B\pm 2}{2\pi}\Omega$, etc. Experimental tests on a rotor alone show that such peaks are not necessarily evident. This matter deserves future investigation.

It must be recognized from the foregoing discussion that the existence of subharmonics of the blade passage frequency is not a necessary consequence of the assumption of "random" irregularities in the instantaneous blade forces, but is rather a result of incomplete specification of the properties of this randomness. To illustrate this, consider the following example: Imagine a fan rotor working in a flow with irregularities that are in the form of "patches" with a different speed or direction of flow than the mean flow. Whenever such a patch is cut by the rotor blades, a train of pulses at blade passage frequency occurs. The only reason for production of frequencies other than the blade passage frequency and its harmonics is thus the finite length of the pulse trains that shows up in the spectrum as a modulation, or broadening, of the discrete frequency peaks.

The procedure described in Appendix B for estimating sound pressure at an observation point where a blade with a concentrated aerodynamic force is rotated about an axis could be extended to the case where the force is time and space dependent. In this way the effects of flow irregularities caused by obstacles or turbulence could be taken into account. An analysis along these lines is being conducted and the results will be published when they are available.

SECTION 5

EXPERIMENTAL PROGRAM

Description

In the initial phase of this program, flat blades were selected for experimental convenience and analytical simplicity. Sound level and air flow measurements were made on a model compressor consisting of a single stage with or without inlet guide vanes. Preliminary results were presented in Ref. 11. Although the blades were aerodynamically substandard in comparison with actual compressor blades, they did embody the more significant noise-producing characteristics discussed in Sec. 3 of this report.

The need for performing a variety of tests on blade rows differing from each other both in the number and shape of their blades and in their attachment to the inner and outer casings dictated the design of the test rig. For this reason, the stage was designed with constant hub and tip diameters, a configuration rarely found in the first stage of an actual compressor or fan, but frequently used in simple test rigs. In our tests the choice of a stage with constant hub and tip diameter appears realistic. The level of stage pressure ratios achievable with the use of the rather unconventional shapes and mountings of the blades to be investigated here is low and, consequently, the airflow can pass through the inlet and outlet areas with only moderate adjustments in axial velocity.

The diameters at the rotor inlet were chosen as 12 inches for the tip and 4 inches for the hub, i.e. the hub-tip-diameter ratio was 0.33. No attempt was made to select a design point and to compute the flow characteristics according to it, because widely differing blade configurations were used.

In spite of the feasibility of changing the number of blades of the rotor and stator in this phase of the investigation, tests were conducted mostly with equal numbers of blades (8) for both rotor and stator. The study was initiated to investigate the relative sound source strength associated with different blade shapes. Sound wave propagation modes were not a primary concern for this program.

In the present phase of the program, several different blade geometries were used, including flat, cambered, and airfoil shapes both with and without twist. The following rotor blades configurations were tested:

- Flat blades
- Flat blades with sharp trailing edges (STE)
- Flat blades with 20 degrees of twist
- Cambered blades (6-inch radius of curvature)
- Cambered blades with 20 degrees of twist
- Airfoil blades NACA 65 - 12 (A₁₀) 10
- Airfoil blades NACA 65 - 12 (A₁₀) 10 with 20 degrees of twist

These blades were operated at relative tip speeds under $M = 0.5$ in the experimental model. Higher Mach numbers were not contemplated because of limits imposed on the blade tip rotational speed by the geometry of the available test rig.

The angle between the blade chord and the plane of the rotor face, β_r , was 30 degrees for the flat blades and for the tips of the twisted blades. All of the rotor blades except the airfoil blades were 4 inches long, with a chord of 1.5 inches and a thickness of 0.050 inch. The airfoil blades were 0.150 inch thick.

The blade solidities at the tips and hubs of both the rotors and stators are then 0.32 and 0.95, respectively. These are rather small values when compared with those adopted in actual practice. The same can be said for the blade thickness ratio, which, except for the NACA 65 - 12 (A_{10}) 10 airfoil blade, amounts to 3.3 percent. The size of bolts required for fixing blades to the rotor hub was the determining factor in selecting blades of small chord and thickness. Large bolts on blades of larger chord and thickness might have perturbed the flow excessively. For manufacturing reasons the same blades were then used for both rotor and stator.

For higher speeds, in the transonic region, blades with double circular arc, J-blade, or blades with other suitable profiles should be used. The blading should be designed for specified stage operating conditions.

The effect on noise level of the relative position of fixed and moving blade rows was investigated for some of the blade geometries by varying the spacing between them from 0.135 to 1.35 of the common value of blade chord.

Since the subject of the experimental part of this study was primarily comparative noise-generating properties of compressor blades of different shape, the model for this work was not selected to perform detailed sound propagation and far-field sound level distribution studies. It was selected to make relative power level measurements for different rotor-stator configurations. The influence of the duct on the radiation has been studied by Filleul (Ref. 12) for the same range of frequencies and fan dimensions as in the present experiments. The increase in noise level at blade passage frequency that occurred when the rotor was shrouded by a ring can be attributed to flow separation at the sharp edges of the ring. When the fan was fitted with a bellmouth inlet, the increase was negligible. It can thus be assumed that the inlet used here has no appreciable effect on noise generation or radiation from the fan; that is, the duct may alter spatial distribution of the radiated noise, but not its total power.

No serious attempt was made to study the test rig behavior from the standpoint of its aerodynamic performance. Difficulties would be encountered in producing a stage map for the following reasons:

- No design point was specified for the stage
- The needed parameters were determined only at the three rotational speeds of 4000, 6000, and 8000 rpm
- The pressure ratios turned out small and with values close to each other at the three speeds

The relationship between noise and the stage performance characteristic, described by pressure ratio vs airflow weight, can be obtained only if some device for throttling the test system either upstream or downstream is available. Future test rigs should be designed for both aerodynamic performance and flexibility for changing those parameters that most affect noise generation.

Flat blades with and without a sharp trailing edge are shown in Fig. 2; also shown are cambered blades with and without twist.

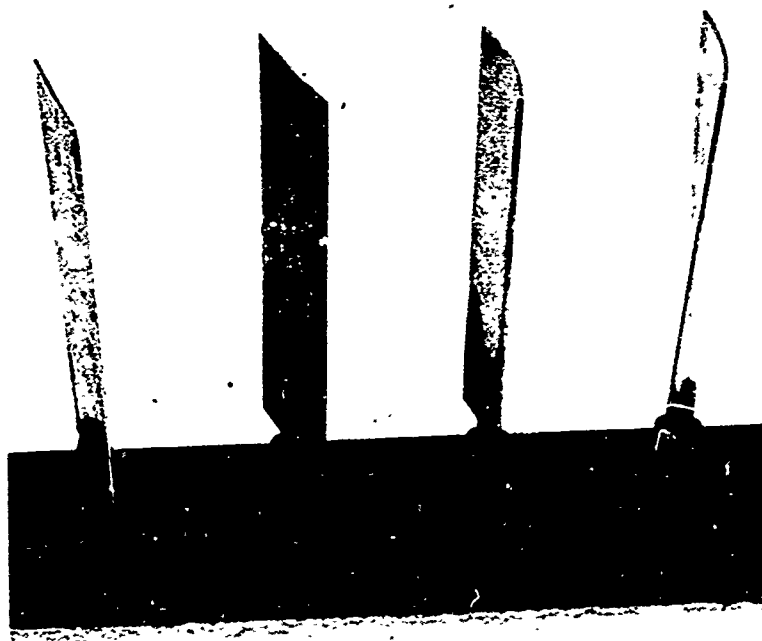


Fig. 2. Flat and Cambered Blades

Twisted, cambered, and airfoil blades are shown in Fig. 3. For comparison, these are shown alongside a rotor blade from the first compressor stage following the turbofan of a Model JT3D-1 engine.

Figure 4 shows a rotor assembly with flat, twisted blades. The amount of twist between the blade chord adjacent to the hub and that at the tip was 20 degrees. Near the hub the blade made an angle of 50 degrees with the rotor face; at the tip, the angle with the face was, therefore, 30 degrees. A rotor assembly with twisted airfoil blades is shown in Fig. 5. These blades have a section profile designated as NACA 65 - (12A₁₀) 10.



Fig. 3. Twisted, Cambered, and Airfoil Blades

An inlet guide vane (stator) assembly is shown in Fig. 6. The blades are adjusted to 90 degrees with respect to the rotor face. The stator blades are identical to the flat blades described for the rotor, having a length of 4 inches, chord of 1.5 inches, and thickness of 0.050 inch.

An inlet vane assembly with tilted blades is shown in Fig. 7. The inlet guide vane assembly with tilted blades was investigated to determine the feasibility of affecting the sound generation due to the wakes of a fixed blade row. As it is known, in the case of radially fixed inlet guide vanes a rotor blade enters and leaves the wake produced by an inlet guide vane at the same instant along its length. With tilted inlet guide vanes, the sections of the rotor blade from hub to tip enter and leave that wake at different times. Therefore it is to be expected that the replacing of instantaneous changes of the circulation, lift, etc., along the rotor blade with gradual ones will reduce sound generation due to wake. An example of nonradial fixed-inlet guide vanes can be found in the Rolls-Royce Spey turbofan, but data about their usefulness for sound reduction are not available. Figure 8 shows stacked tube inlet guide vanes, and honeycomb is shown in the place of the inlet guide vanes in Fig. 9. The honeycomb for this assembly is 1.5 inches thick and the cells are $3/16$ inch wide between parallel faces.

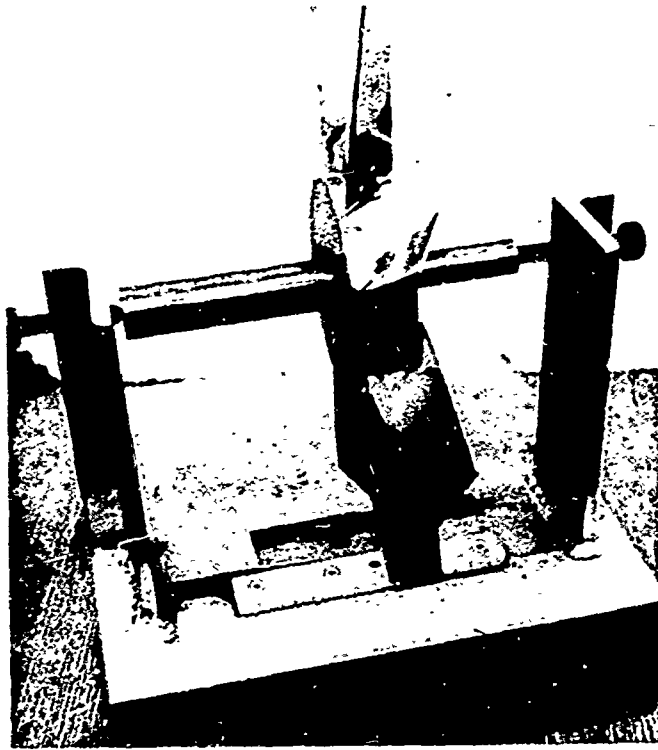


Fig. 4. Rotor With Twisted Blades

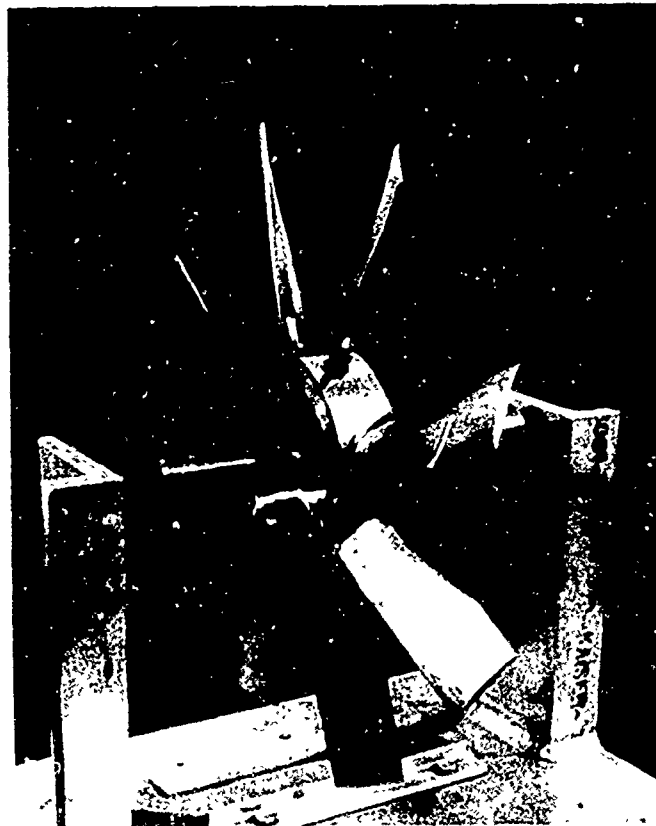


Fig. 5. Rotor With Twisted Airfoil Blades

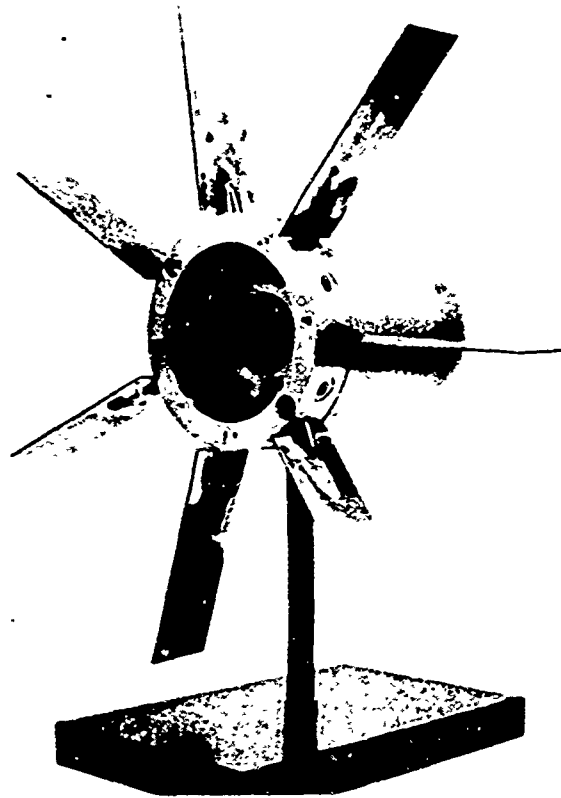


Fig. 6. Inlet Guide Vane Assembly With Flat Blades



Fig. 7. Inlet Guide Vane Assembly With Tilted Blades

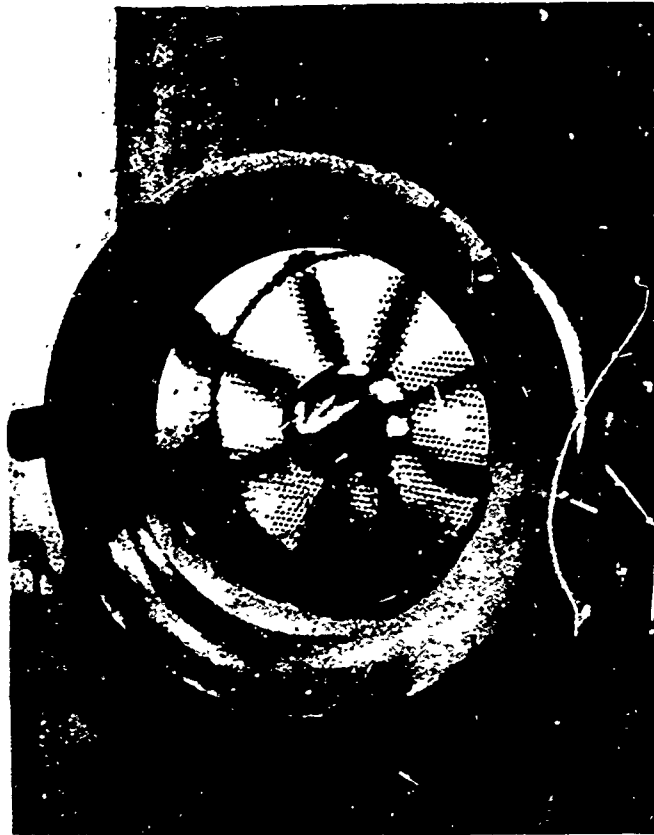


Fig. 8. Stacked Tube Inlet Guide Vanes

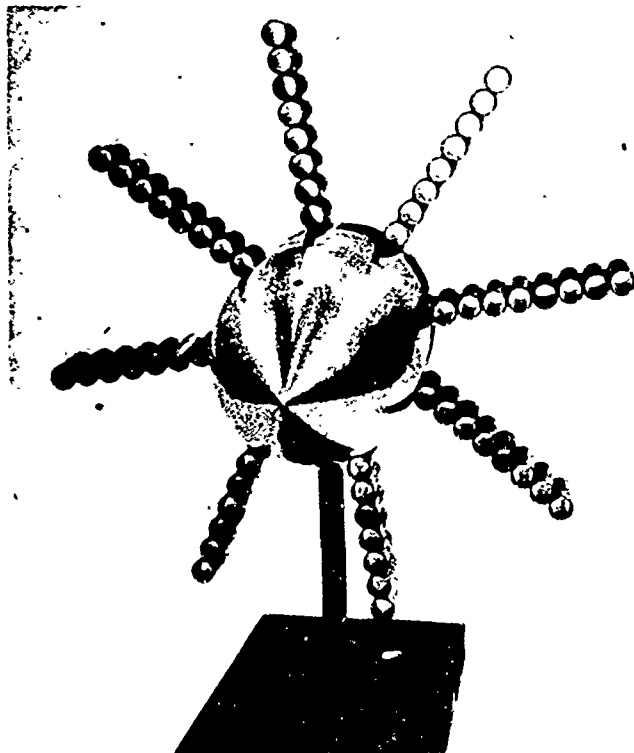


Fig. 9. Honeycomb Inlet Guide Vanes

Both of these devices represent unusual solutions. They were considered here only for the purpose of investigating their effect on sound reduction. Their use is impractical in an actual engine for takeoff and cruise conditions because of the associated inlet efficiency losses, ice formation problems, weight, etc. Consequently, they must be regarded as devices to be used only in the approach and landing phase of airplane flight. They should be retractable and in the extended position should form a screen in front of the radial portion of the rotor inlet surface, which contributes most to the noise generation. Since the radial height of this rotor inlet surface is between 20 and 30 percent of the blade length, according to the value of the radial hub-tip ratio, the use of honeycomb or stacked tubular inlet guide vanes could be feasible if their usefulness for sound level reduction has been established and their installation does not endanger the compressor operation because of the associated inlet flow distortion.

Discussion of Results

Sound level measurements were made at a radius of 6 feet from the rotor center and, in some cases, in the duct at a distance of 6 inches from the rotor face. Sound power levels for these two cases were calculated numerically using the formula

$$PWL = 10 \log_{10} \int_A \log_{10}^{-1} \left(\frac{SPL}{10} \right) dA \quad (4)$$

where A is the area of the forward hemisphere in the 6-foot case, and the duct cross section in the 6-inch case. A is in units of m^2 . The sound power level will then be given relative to the reference power of 10^{-12} watts. For sound measurements under similar conditions, the agreement between the two calculations is good, which indicates that far-field conditions prevailed even at the 6-inch distance. This is in agreement with the measurements of Filleul (Ref. 12) who reports far-field conditions (validity of the inverse square law) down to a distance of 2 or 3 blade chords from the rotor face. It must be noted that the assumption of far-field conditions at a distance as close to the rotor face as reported here may only apply to the following special configurations, i. e. rotor alone and rotor-stator combination with the same number of blades in both rows. For configurations with a different number of rotor and stator blades, it can be argued that in order for cancellation between the sound pressure contributions from different blades to take place (which is the case for these configurations), measurements should be made at large distances compared with the wavelength.

The principal data presented in this report relate sound power level to:

- Flow coefficient (V_a/u)
- Air weight flow (\dot{w})
- $\log_{10} V_{rel}$
- Rotor RPM ($60\Omega/2\pi$)

Other presentations relate RPM to the following:

- $\log_{10} V_{rel}$
- Flow coefficient (V_a/u)
- Air weight flow (\dot{w})

Some important data are shown in Fig. 10, and the rest are in Appendix A.

The dependence of PWL on flow coefficient, air weight flow, and $\log_{10} V_{rel}$ is given in Fig. 10 for the blades of different shapes that were tested. The flow coefficient was somewhat different for each blade design and was approximately constant for different rotor rotational speeds.

The change of PWL with changes of rotor shaft speed for different blade shapes is shown in Figs. A9 and A10 in Appendix A. The relation is approximately the same for blade passage frequency and its harmonics.

Irregular IGV angular spacing does not appreciably change the sound generation at blade passage frequency, as can be seen from a comparison between Fig. A1 and Fig. A4 in Appendix A. The angle between blades on the eight-bladed rotor varies randomly between 20 and 56 degrees.

By comparison with flat plate IGV's (Fig. A10, Appendix A), the use of stacked tubular IGV's resulted in the same PWL's for all harmonics (Fig. A12, Appendix A), and the use of small-mesh honeycomb IGV's gave a considerable reduction in PWL's, particularly at the fundamental, for all rotational speeds, without significant reduction in flow (Fig. A13, Appendix A).

Comparison With Theory and the Measurements of Other Investigators

The power radiated from a fan, normalized with air weight flow, has been found to vary as the fourth to sixth power of either the relative tip speed (e. g. Ref. 13) or the mechanical tip speed. A compressor noise prediction method to be considered by the SAE is based on the mechanical tip speed. The sound power levels obtained with different blade geometries are compared with a fifth-power relative tip speed relation in Fig. 11 and with the slope of the SAE prediction curve in Fig. 12.

The main purpose of the experimental study has been to investigate the influence of rotor blade shape on discrete frequency noise generation. According to the analytical considerations (Sec. 4) the blade shape can only enter into the expression for the sound generation through its influence on the thrust and torque of the rotor. The experimental results tend to confirm this analytical hypothesis since the PWL is well correlated with air weight flow, which in turn is approximately proportional to thrust (Fig. 10).

The values of sound pressure level at a distance of 6 feet for the freely running rotor with flat plate blades and pitch angle of 30 degrees from the rotor plane have been calculated on the basis of Eq. (3). For each of the three rotational speeds of 4000, 6000, and 8000 RPM, lift and drag were determined with the following procedure:

- a) All parameters were computed at an effective radius $R_e = 5$ inches from the rotor axis.
- b) Incidence angles determined from air and pitch angles were used to compute the lift coefficient with the theoretical formula of the flat plate $C_L \approx 2\pi\alpha$. The cascade interference coefficient for comparison with single profile was taken as unity, although its value was about 1.07.

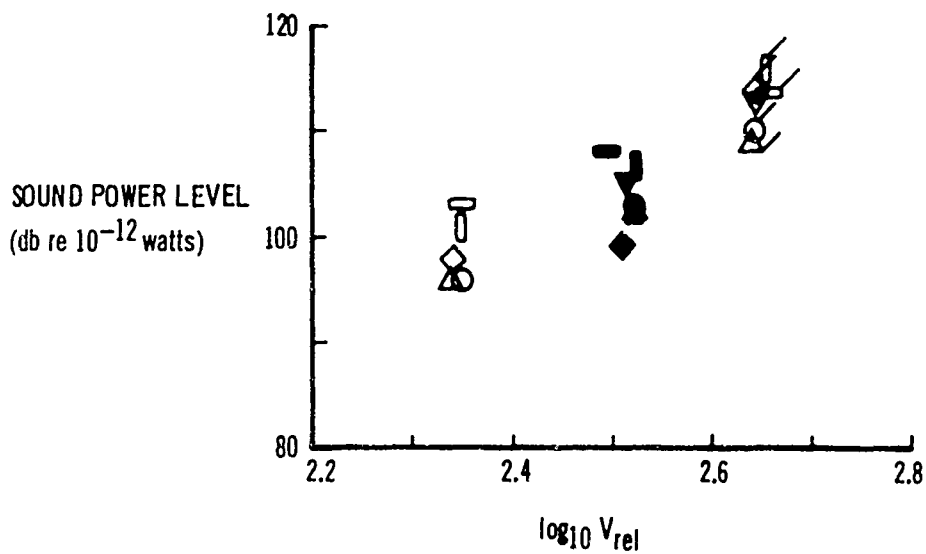
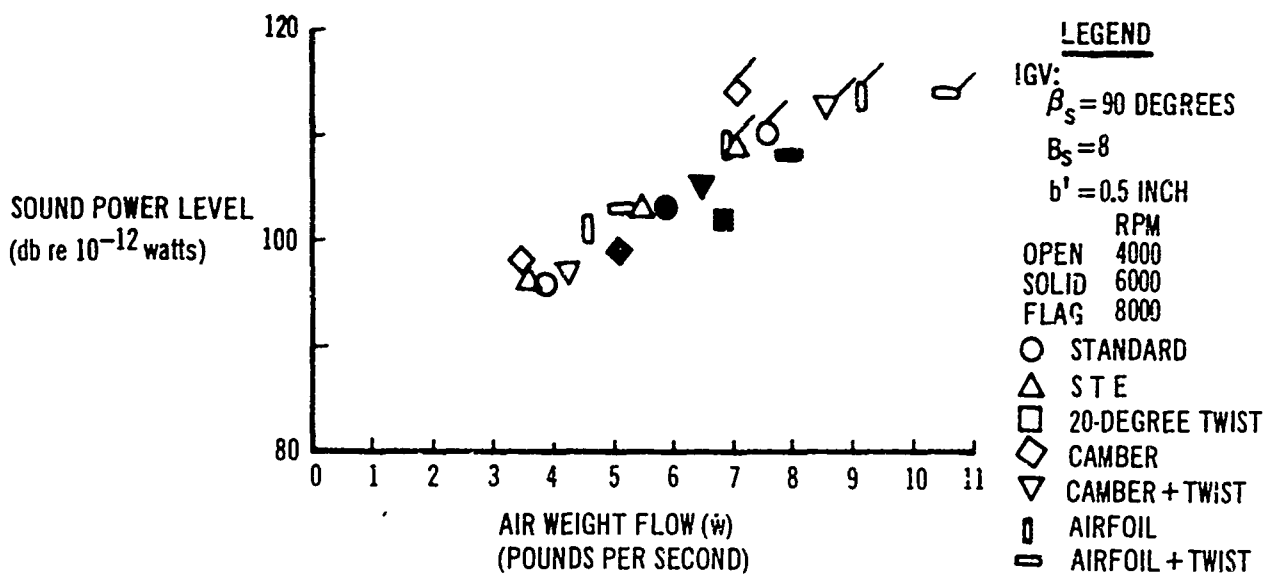
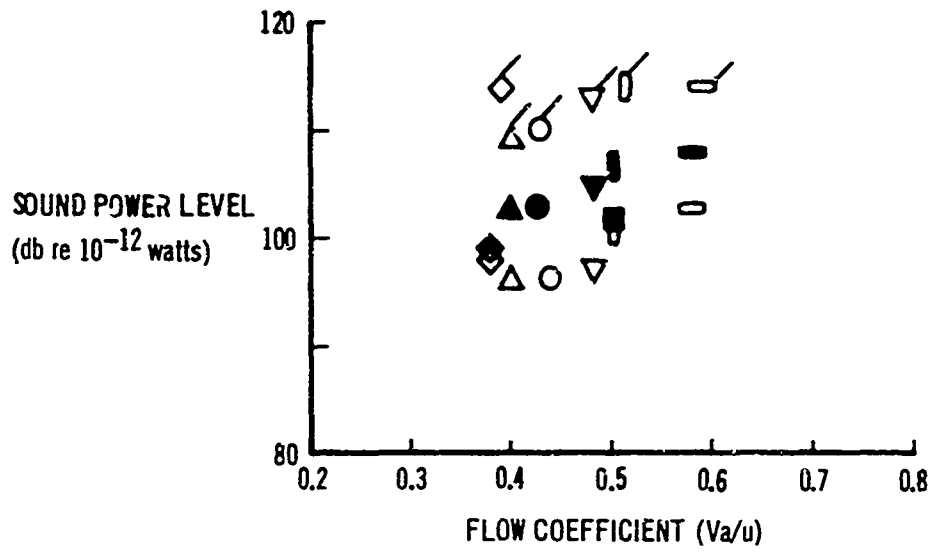


Fig. 10. Different Blade Shapes, Sound Power Level 6 Inches From Rotor ($m = 1$)

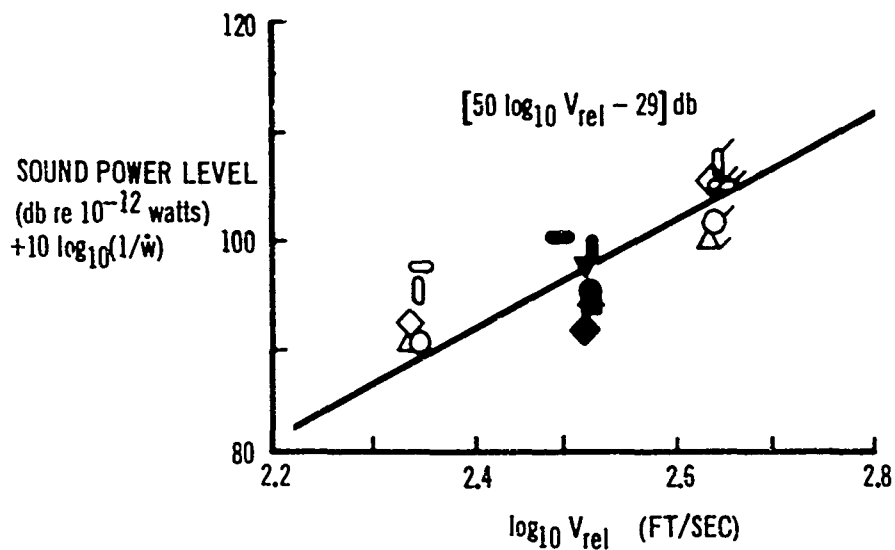


Fig. 11. Sound Power Level (Normalized With Weight Flow) Compared With V_{rel}^5

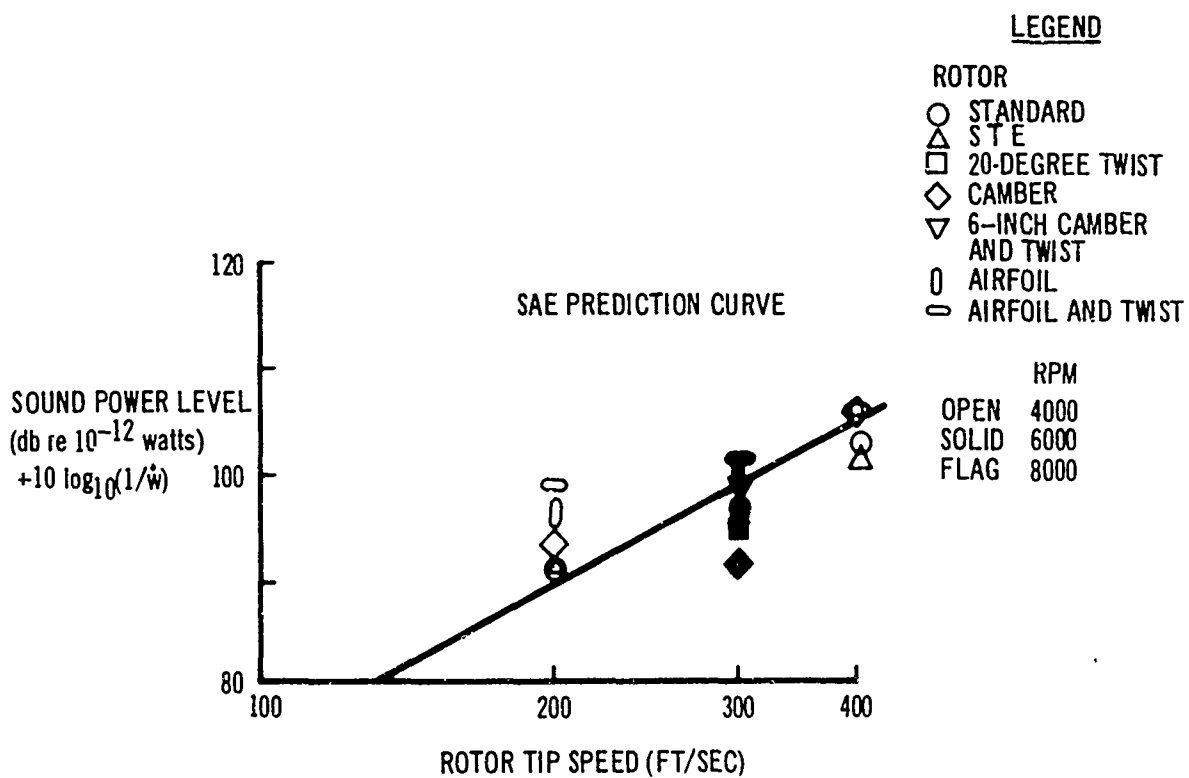


Fig. 12. Sound Power Level (Normalized With Weight Flow) Compared With Slope of Proposed SAE Prediction Curve

- c) After computing the Reynold numbers, the drag coefficient was determined from the friction coefficient of a flat plate, accounting for the mean roughness of the blade and the flat plate incidence.
- d) With the values of thrust, drag, and Mach number, the p_{rms} values were determined with Eq. (3) and from them the sound pressure levels were derived.
- e) Finally the sound power level was computed with Eq. (4).

The computed and measured data are presented in Fig. 13 for the first three harmonics. The agreement obtained between calculated and measured absolute values of the sound power level is reasonably close considering the order of magnitude approximations made in the derivation of Eq. (3). The relative levels of the three harmonics ($m = 1, 2, 3$) are approximately the same for calculated and measured values. The dependence on rotational speed follows approximately a fourth power law for the experimental values and a sixth power law for the theoretical values.

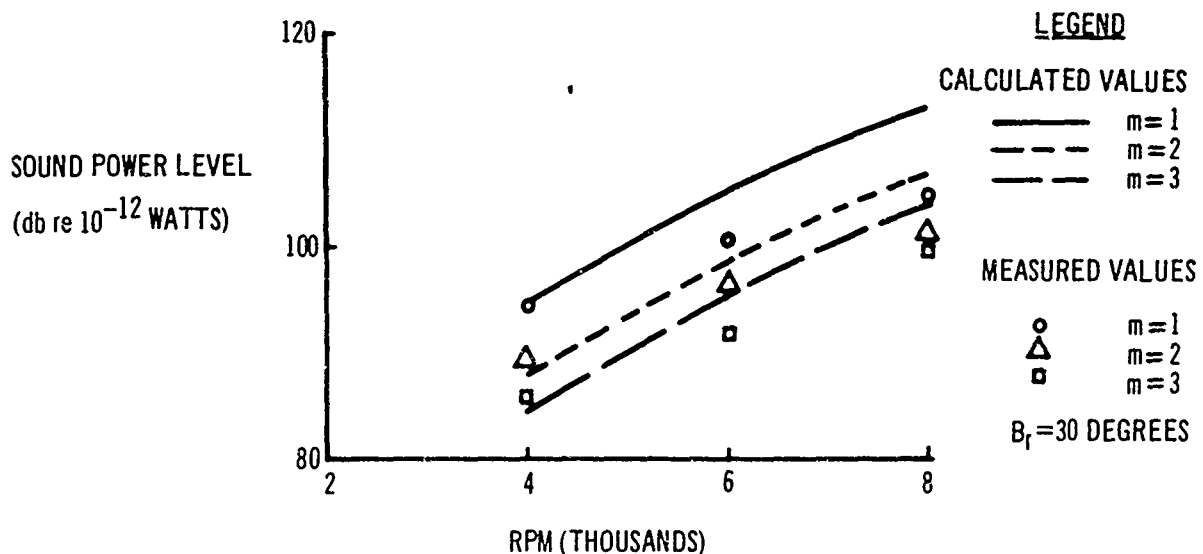


Fig. 13. Flat Blades, Rotor Alone, Rotational Speed and Sound Power Level 6 Feet From Rotor: Comparison Between Calculated and Measured Values

The effect of the IGV-rotor separation distance has been investigated by several authors (Refs. 5, 6, 14, 15). The work at Southampton University, culminating with the work of Fincher (Ref. 6), indicates that there are three effects determining the rotor-stator interaction noise: rotor lift fluctuations in the upstream stator wake, stator lift fluctuations in the potential flow field of the rotor and vice versa, and acoustic baffling of the rotor pressure fluctuation by the stator. This last effect could be accounted for by introducing a normalized separation $b'/(4c_s + 2c_r)$, where b' is the separation, and c_s and c_r are the stator and rotor blade semichords respectively. When the sound pressure level was plotted against this coefficient for different stator chords, the results generalized to a single curve. The critical separation coefficient, s_{cr} , beyond which the SPL does not decrease appreciably, is strongly dependent on other parameters. The low-speed fan of Ref. 6 gives an order of magnitude $s_{cr} = 0.04$, whereas for the transonic compressor of Ref. 14 the value is $s_{cr} = 0.4$. Since the rotor blade chord is already about the same length as

the acoustic wavelength for the transonic compressor, no baffling effect could be expected. Measurements at the low tip speeds used in this investigation do not show an obvious critical value. It can thus be inferred that the separation in these experiments has not been small enough to show the baffling effect.

The effect of stator tilting, i. e. the altering of the angle between stator trailing edge and rotor leading edge, has been investigated by Sharland (Ref. 5) and Filleul (Ref. 12). Sharland reports a 16-db difference between the maximum SPL for radial stator blades (0-degree tilt) and the minimum SPL with the stator blades tilted 60 degrees. Filleul reports a reduction of 1 db per 8-degree tilt up to 60-degree tilt of a single strut in front of the rotor. The results of Boeing's investigation for a stator with 45-degree tilt (opposite to the direction of rotor rotation) shows the following noise reduction at blade passage frequency without any reduction in weight flow:

Shaft RPM:	4000	6000	8000
db reduction:	6	8	5

This is an average of 1 db per 7-degree tilt, in close agreement with the result of Filleul (cf. Figs. A1 and A3 in Appendix A).

The effect of different pitch angles between blades up to ± 5 degrees for the rotor alone was investigated by Filleul (Ref. 12). He found no increase in noise generation for this case as compared with a rotor with equal blade pitch angles. In the Boeing experiments reported in Fig. A34 of Appendix A, with pitch angle variations of 10 and 20 degrees between rotor blades for a rotor-stator combination, a considerable increase in noise level was noted. In these experiments, some of the blades were presumably stalled.

There is a possibility that the presence of an upstream nose cone support strut or downstream flow straighteners has influenced the result of the measurements with rotor alone. Filleul (Ref. 12) reports an increase of 3 to 4 db at blade passage frequency with a single strut 1 inch downstream from the rotor, as compared with 20 db for a position 1 inch upstream from the rotor. In the Boeing study the strut had a smaller diameter and was positioned 2-1/2 inches ahead of the rotor. Measurements with and without the nose cone with strut showed little difference in noise level. Any noise from the flow straighteners, located 7-1/2 inches downstream from the rotor, must be associated with their lift, resulting from swirl in the outlet. Because of the large distance from the rotor, lift fluctuations must be small. It is therefore believed that the measured noise is genuine rotor noise.

SECTION 6

CONCLUSIONS

For the operating conditions of the fan used here:

- Sound power levels at blade passage frequency as a function of air weight flow generalized for the following blade types (Figs. 10 and A1), irrespective of tip speed:
 - Flat blades
 - Flat blades with sharp trailing edges
 - Flat blades with 20 degrees of twist
 - Cambered blades (6-inch radius of curvature)
 - Cambered blades with 20 degrees of twist
 - Airfoil blades NACA 65 - 12 (A₁₀) 10
 - Airfoil blades NACA 65 - 12 (A₁₀) 10 with 20 degrees of twist

It can thus be concluded that the blade type affects the sound generation only through its influence on the weight flow.

- Equation (3) was used to predict the sound power levels for a freely running rotor with flat blades. As shown in Fig. 13, the agreement with measured data is reasonably close and the relative levels of the harmonics are approximately the same for calculated and measured values. The dependence on rotational speed follows approximately a fourth power law for the experimental values and a sixth power law for the theoretical. Although Eq. (3) was derived on intuitive grounds, these results mark the first extension of propeller theory to include randomization of aerodynamic loads on a many-bladed rotor.

SECTION 7

RECOMMENDATIONS

As an extension of this project, a test program should be undertaken with a full-scale, two-stage compressor rig. If a turbojet were used as a power source, combustion gases of the jet could be exhausted in a plenum chamber and after some reheating be used to actuate the compressor-driving turbine. The test rig would be simpler if a turboprop were available, however. The two stages of the compressor should be designed to reflect the state of the art of present fan stages or compressor first stages and to function under realistic engine operating conditions. Two configurations should be considered: one with and the other without inlet guide vanes. Among the items to be investigated, the following are of primary importance:

- Effect of use of inlet guide vanes on the noise level emanating from the compressor inlet
- Influence of axial spacing between the stationary and moving blade rows on compressor noise generation
- Effect of the difference between the blade numbers of fixed and moving rows on noise production and transmission.

Examples of tests to be conducted on the configuration without inlet guide vanes are:

- Use in the first stage of single-row stators differing from each other in the number of blades. These changes bring about a change in the value of blade solidity if the blade chord is maintained constant; Otherwise, they produce: (a) for constant value of solidity, changes in blade chord and aspect ratio and (b) for constant axial distance between first and second rotor, changes in the values of spacing between first rotor and first stator, and between first stator and second rotor. For this reason, tests with several different stator rows must be performed to investigate separate and simultaneous effects produced by changes in the number of stator blades on both compressor performance and sound generation. The design single-row stator will employ variable geometry to correct rotor incidence and loading. Then, the compressor off-design conditions corresponding to airplane approach and landing can be better studied without the danger of introducing large perturbations because of stage stall operation.
- Replacement of the design single-row stator with a double-row stator, where the blades of the second row are displaced circumferentially one-half pitch with respect to those of the first row. In this way, the number of blades in the adjacent moving and fixed rows can differ considerably from each other, the loading on each stator blade can be decreased for the same value of stator diffusion, etc. These changes, made with the purpose of determining their effects on noise reduction, should be performed to produce little objection from the compressor designer standpoint.
- Use of rotor assembly having the alternate blades staggered at two different angles, to study the generation of subharmonics in an engine compressor. The possible combination of unequal stagger angles for adjacent blades with rotating stall to produce "buzz saw" noise should be investigated.

- Use of rotor having the stagger angles of all blades different. This experiment should contribute to the understanding of the generation of "buzz saw" noise in compressors. It could help define the relationship between rotor manufacturing tolerances and the generation of "buzz saw" noise.

Examples of some of the tests to be performed on the configuration with inlet guide vanes are the following ones, based on the use of:

- Inlet guide vane rows differing from each other in the number of their blades. For these rows the same considerations hold as those made for the stator. Here, also, the design inlet guide vanes must be of the variable-geometry type.
- Inlet guide vane assembly with air-blown vanes. Here air is injected in the flow stream through slots situated in the rear portion of the blades. The resulting beneficial effect on the vane boundary layer and wake is then studied for its relation with sound production. An alternate solution is represented by suction of the vane boundary layer.
- Inlet guide vane assembly with tilted blades instead of radial, to determine the effect of this type of blade mounting and resulting wake form on sound generation.
- Inlet guide vane assembly having vanes composed of hollow tubes. These vanes should be limited to the portion of the inlet annulus area close to the compressor outer casing, where a large percentage of the noise is produced. An alternate solution is the use of honeycomb inlet guide vanes instead of the previous ones. Both types of inlet guide vanes should be studied only to determine if some noise reduction can be obtained. If a real advantage can be gained, no major problem is anticipated in their practical application as a retractable device to be used in the approach and landing phase of aircraft flight, and eventually during takeoff.

The above facility could be used for wave propagation tests, inlet absorption lining, and other tests that are difficult to scale.

In addition, the present test rig should be used to perform certain critical experiments:

- One is suggested by the work of Sharland (Ref. 5), who inserted a ring at the periphery of a fan inlet and observed a consequent increase in overall sound power generation by a freely running rotor. This experiment should be reproduced to determine if the increase in noise due to turbulence generated by the ring is more of a broad-band than a discrete nature. Together with the above experiment, other techniques should be devised to identify the influence of inlet flow irregularities and turbulence on discrete sound generation.
- Another is related to the importance of determining by direct measurement if fluctuations in aerodynamic loads (blade thrust in particular) can be correlated with far-field sound levels.

REFERENCES

1. Richards, E.I. and Sharland I.J., "Hovercraft Noise and its Suppression," Journal of the Royal Aeronautical Society, Vol. 69, No. 654, June 1965.
2. Ernsthansen, E.W., "Der Rotierende Tragflügel als Strahlungsproblem," ZAMM, Vol. 31, No.1/2, 1951.
3. Von Gierke, H.E., "Aircraft Noise Sources," Chapter 33 of Handbook of Noise Control, edited by C.M. Harris, McGraw-Hill Book Co., New York, 1957.
4. Kemp, N.H. and Sears, W.R., "The Unsteady Forces Due to Viscous Wakes in Turbomachines," Journal of Aeronautical Science, Vol. 22, July 1955.
5. Sharland, I.J., "Sources of Noise in Axial Flow Fans," Journal of Sound and Vibration, Vol. 1, No. 3, 1964.
6. Fincher, H.M., "Fan Noise—The Effect of a Single Upstream Stator," Journal of Sound and Vibration, Vol. 3, No. 1, 1966.
7. Lawson, M.V., Basic Mechanisms of Noise Generation by Helicopters, V/STOL Aircraft and Ground Effect Machines, Wyle Labs., Res. Staff. Report # WR 65-9, May 1965. Also Journal of Sound and Vibration, Vol. 3, No. 3, 1966.
8. Lighthill, M.J., "On Sound Generated Aerodynamically. I-General Theory," Proc. Royal Society, A. 211, 1952.
9. Gutin, L., On the Sound Field of a Rotating Propeller, NACA Tech. Memo 1195.
10. Garrick, I.E., and Watkins, C.E., A Theoretical Study of the Effect of Forward Speed on the Free-Space Sound Pressure Field Around Propellers, NACA Tech. Rept. 1198, 1954.
11. Bateman, D.A., Chang, S.C., Hulse, B.T., and Large, J.B., Compressor Noise Research, FAA-ADS-31, January 1965.
12. Filleul, N. LeS., "An Investigation of Axial Flow Fan Noise," Journal of Sound and Vibration, Vol. 3, No. 2, 1966.
13. Smith, M.J.T. and House, M.E., "Engine Internal Noise—Measurement and Prediction," paper for discussion at the 76th G.T.C.C. Meeting, Bristol, Oct. 22, 1965.

REFERENCES (Continued)

14. Kilpatrick, D. A., and Reid, D. T., Transonic Compressor Noise: The Effect of Inlet Guide Vane/Rotor Spacing, A. R. C. R. & M. No. 3412, Jan. 1964.
15. Crigler, J. L. and Copeland, W. L., Noise Studies of Inlet-Guide-Vane/Rotor Interaction of a Single-Stage Axial-Flow Compressor, NASA TN D-2962, Sept. 1965.

GLOSSARY OF SYMBOLS

a	Velocity of sound
B	Number of blades
b'	Axial distance between trailing edge of the inlet guide vanes and the leading edge of rotor blades
c	Blade semichord
d	Distance of observation point from rotor disk origin
G	Drag
J_{mB}	Bessel function of the first kind with index mB
k	$\omega/a = mB\Omega/a$
m	Order of harmonic
M	Mach number based on peripheral speed at rotor effective radius, R_e
p	Fluctuating pressure
p	Pressure magnitude
p_{rms}	Root mean square pressure
PWL	Sound power level, db relative 10^{-12} watts
Q	Rotor blade torque
r	Polar coordinate
R_e	Effective rotor radius
s_0	Distance from rotor, $\sqrt{x^2 + y^2}$
SPL	Sound pressure level, db relative $0.0002 \text{ dynes/cm}^2$
t	Time in seconds
T	Thrust per blade
\bar{T}	Total thrust
u	Blade circumferential velocity $R_e\Omega$ at effective radius
V_a	Air axial velocity

GLOSSARY OF SYMBOLS (Continued)

V_{rel}	Air velocity relative to rotor blade at the blade tip
\dot{w}	Air weight flow, pounds per second
x	Axial distance of observation point from rotor
y	Radial distance of observation point from the rotor axis
α	Blade angle of attack
β	Blade pitch angle, taken from rotor plane
ρ	Fluid density
θ	Polar coordinate, angle from rotor rotational axis
ω	Frequency of m^{th} harmonic, $mB\Omega$
ω_1	Fundamental blade passage frequency, $B\Omega$
Ω	Angular velocity in radians per second

Subscripts

r	rotor
s	stator or guide vane

ACKNOWLEDGMENTS

Mr. Bruce T. Hulse served as Project Leader during the experimental phase of the study program. Mr. Dave Bateman assisted with design of the apparatus and conducted the experiments.

APPENDIX A
SOUND LEVEL DATA

APPENDIX A

ILLUSTRATIONS

<u>Figure</u>		<u>Page</u>
A1	Different Blade Shapes, Sound Power Level 6 Feet From Rotor ($m = 1$)	A-4
A2	Twisted Rotor Blades, Sound Power Level 6 Feet From Rotor ($m = 1$)	A-5
A3	Tilted Stator Blades, Twisted Rotor: Sound Power Level 6 Feet From Rotor ($m = 1$)	A-6
A4	Irregular IGV Angular Spacing, Sound Power Level 6 Feet From Rotor ($m = 1$)	A-7
A5	Airfoil Blades, Sound Power Level 6 Inches From Rotor ($m = 1$)	A-8
A6	Airfoil Blades, Sound Power Level 6 Feet From Rotor ($m = 1$)	A-9
A7	Airfoil Blades With Twist, Sound Power Level 6 Inches From Rotor ($m = 1$)	A-10
A8	Airfoil Blades With Twist, Sound Power Level 6 Feet From Rotor ($m = 1$)	A-11
A9	Different Blade Shapes, Rotational Speed and Sound Power Level 6 Inches From Rotor	A-12
A10	Different Blade Shapes, Rotational Speed and Sound Power Level 6 Feet From Rotor	A-13
A11	Rotor Blades With 20-Degree Twist, Rotational Speed and Sound Power Level 6 Feet From Rotor	A-14
A12	Tubular IGV, Rotational Speed and Sound Power Level 6 Feet From Rotor	A-15
A13	Honeycomb IGV (3/16-Inch Cell), Rotational Speed and Sound Power Level 6 Feet From Rotor	A-16
A14	Airfoil Blade With Twist, Sound Power Level and Rotational Speed	A-17
A15	Different IGV Numbers: Flow Coefficient, Weight Flow, Sound Power Level 6 Feet From Rotor, and Rotational Speed	A-18
A16	Tilted IGV's: Flow Coefficient, Weight Flow, Sound Power Level 6 Feet From Rotor, and Rotational Speed	A-19
A17	Irregular IGV Angular Spacing: Flow Coefficient, Weight Flow, Sound Power Level 6 Feet From Rotor, and Rotational Speed	A-20
A18	Rotor 6-Inch Camber, 20-Degree Twist, $\beta_s = 45$ Degrees: Flow Coefficient, Weight Flow, Sound Power Level 6 Inches From Rotor, and Rotational Speed	A-21
A19	Rotor 6-Inch Camber, 20-Degree Twist, $\beta_s = 60$ Degrees: Flow Coefficient, Weight Flow, Sound Power Level 6 Inches From Rotor, and Rotational Speed	A-22

ILLUSTRATIONS (Continued)

<u>Figure</u>		<u>Page</u>
A20	Rotor 6-Inch Camber, 20-Degree Twist, $\beta_s = 90$ Degrees: Flow Coefficient, Weight Flow, Sound Power Level 6 Inches From Rotor, and Rotational Speed	A-23
A21	Airfoil Rotor Blades: Flow Coefficient, Weight Flow, Sound Power Level, and Rotational Speed	A-24
A22	Tubular IGV: Relative Tip Speed, Flow Coefficient, Weight Flow, and Rotational Speed	A-25
A23	Honeycomb IGV (3/16-Inch Cell): Relative Tip Speed, Flow Coefficient, Weight Flow, and Rotational Speed	A-26
A24	Airfoil Rotor Blades With 20-Degree Twist: Flow Coefficient, Weight Flow, Sound Power Level, and Rotational Speed	A-27
A25	Flat Rotor Blades, Different β_s : Sound Power Level 6 Inches From Rotor, and IGV-Rotor Spacing	A-28
A26	Flat Rotor Blades, Different β_s : Sound Power Level 6 Feet From Rotor, and IGV-Rotor Spacing	A-29
A27	Rotor Blades With 6-Inch Camber, 20-Degree Twist: Sound Power Level 6 Inches From Rotor and IGV-Rotor Spacing	A-30
A28	Rotor Blades With 6-Inch Camber, 20-Degree Twist: Sound Power Level 6 Feet From Rotor and IGV-Rotor Spacing	A-31
A29	Airfoil Blades, Straight and Twisted: Sound Power Level 6 Feet From Rotor and IGV-Rotor Spacing	A-32
A30	Tubular IGV, Sound Power Level 6 Inches From Rotor and IGV-Rotor Spacing	A-33
A31	Tubular IGV, Sound Power Level 6 Feet From Rotor and IGV-Rotor Spacing	A-34
A32	Honeycomb IGV (3/16-Inch Cell), Sound Power Level 6 Inches From Rotor and IGV-Rotor Spacing	A-35
A33	Honeycomb IGV (3/16-Inch Cell), Sound Power Level 6 Feet From Rotor and IGV-Rotor Spacing	A-36
A34	Alternate Rotor Blade Angles Equal, Sound Pressure Level and Frequency	A-37

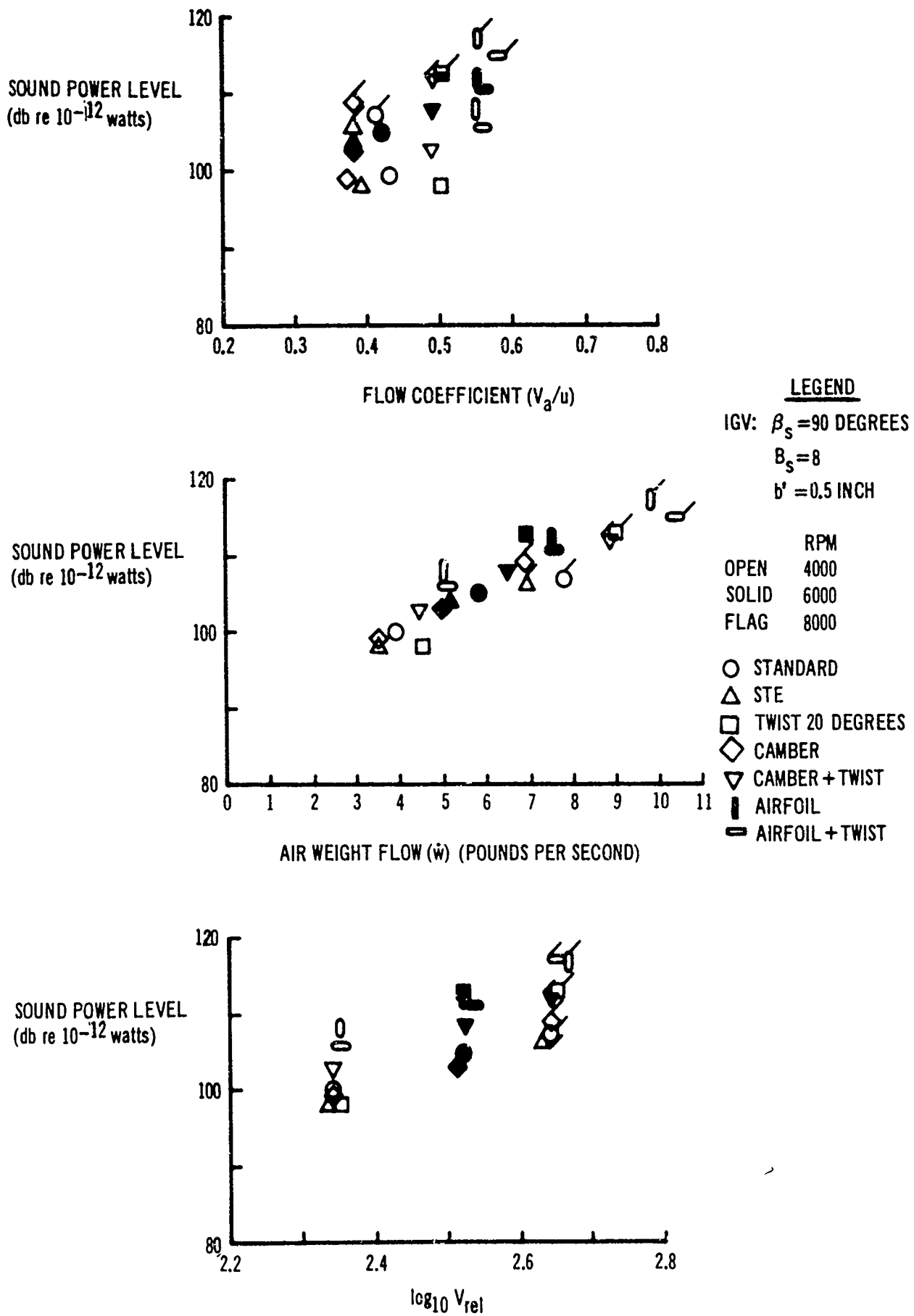
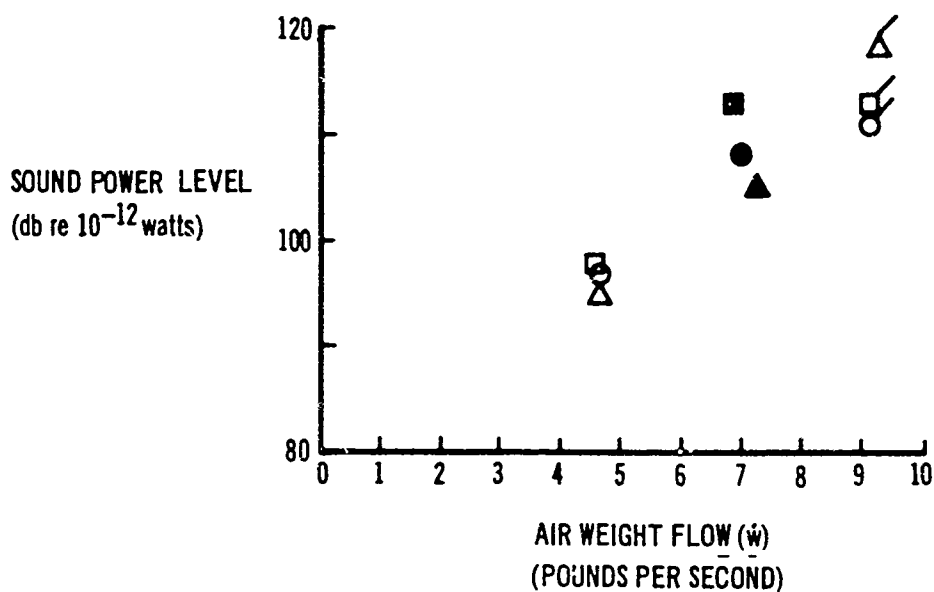
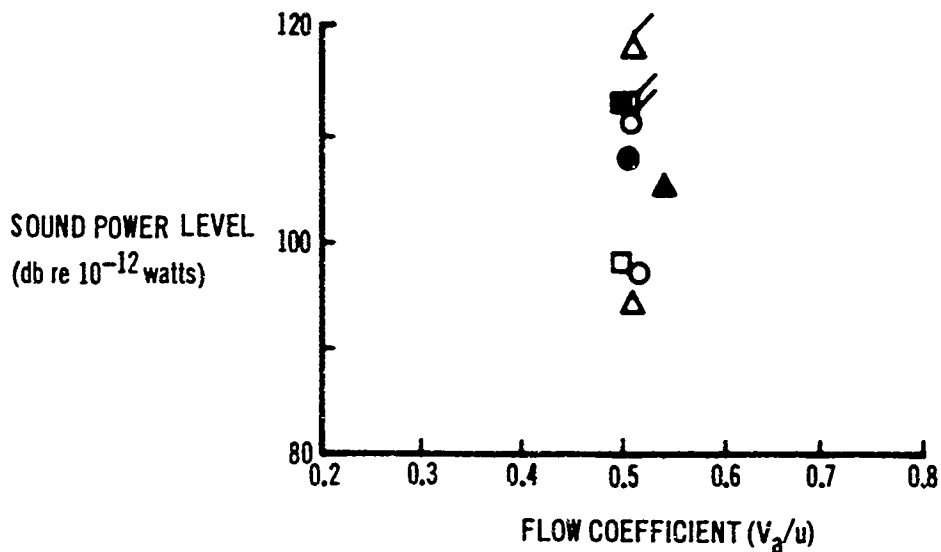


Fig. A1. Different Blade Shapes, Sound Power Level 6 Feet From Rotor ($m = 1$)



LEGEND

IGV:

$\beta_s = 90$ DEGREES

$B_s = 3$ ○

5 ▲

7 □

$b' = 0.5$ INCH

RPM

OPEN 4000

SOLID 6000

FLAG 8000

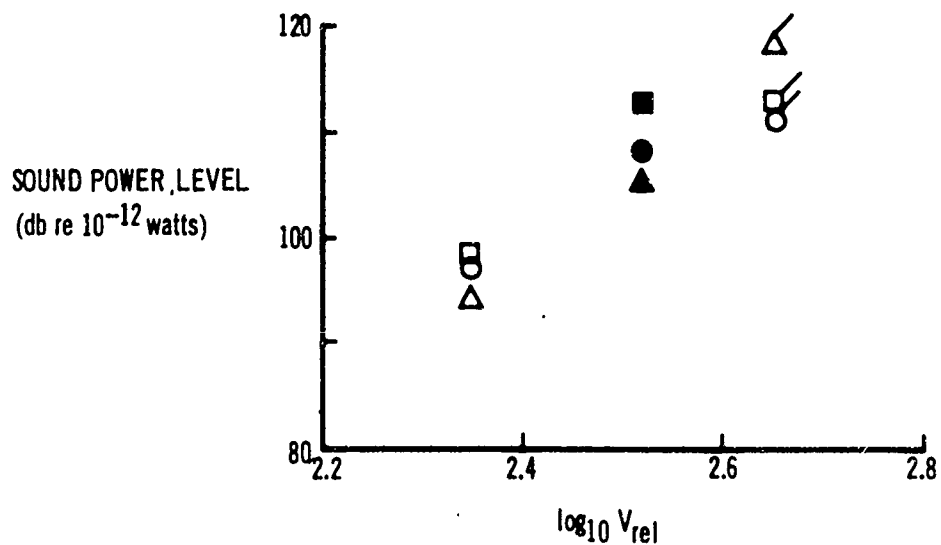
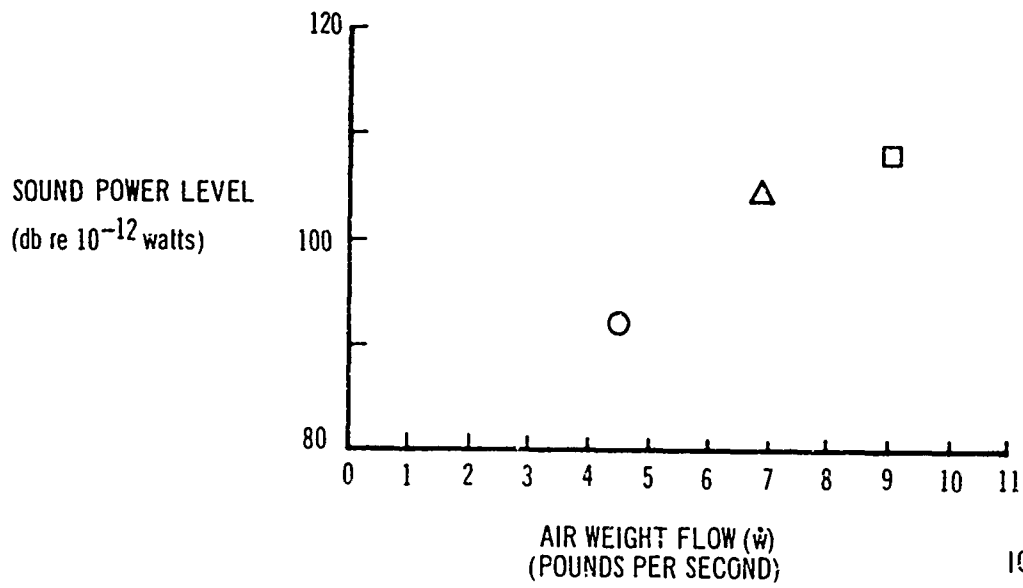
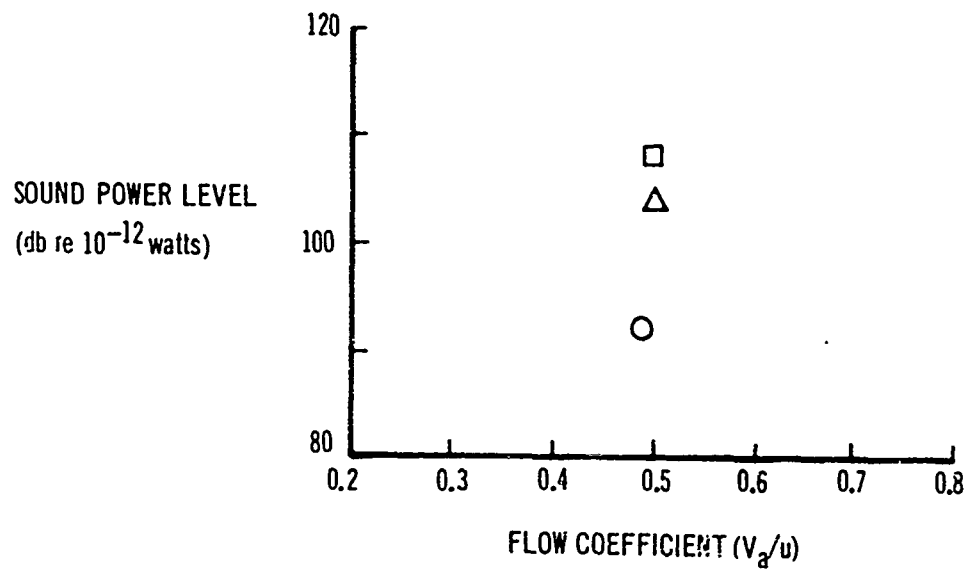


Fig. A2. Twisted Rotor Blades, Sound Power Level 6 Feet From Rotor ($m = 1$)



LEGEND

IGV:

$\beta_s = 90$ DEGREES

$B_s = 8$

$b' = 0.5$ INCH

RPM

○ 4000

△ 6000

□ 8000

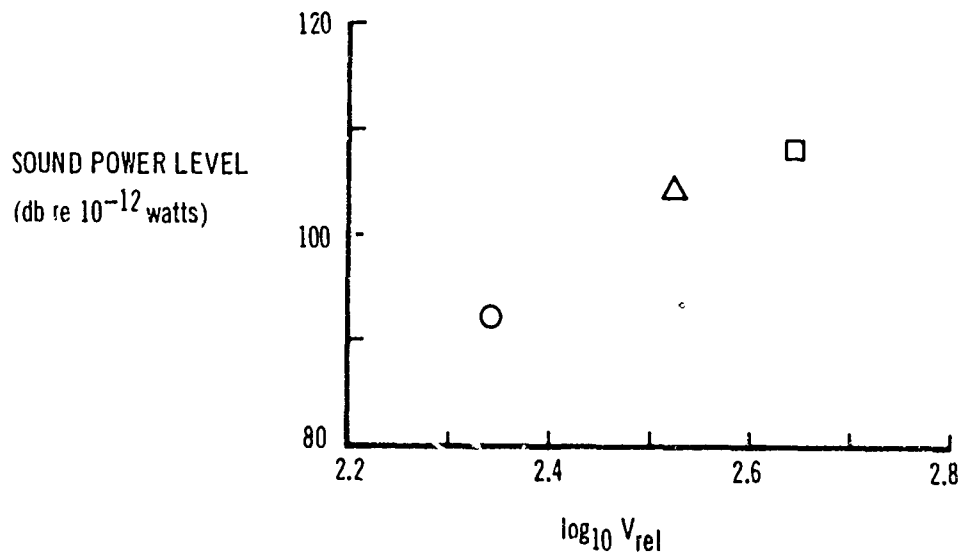
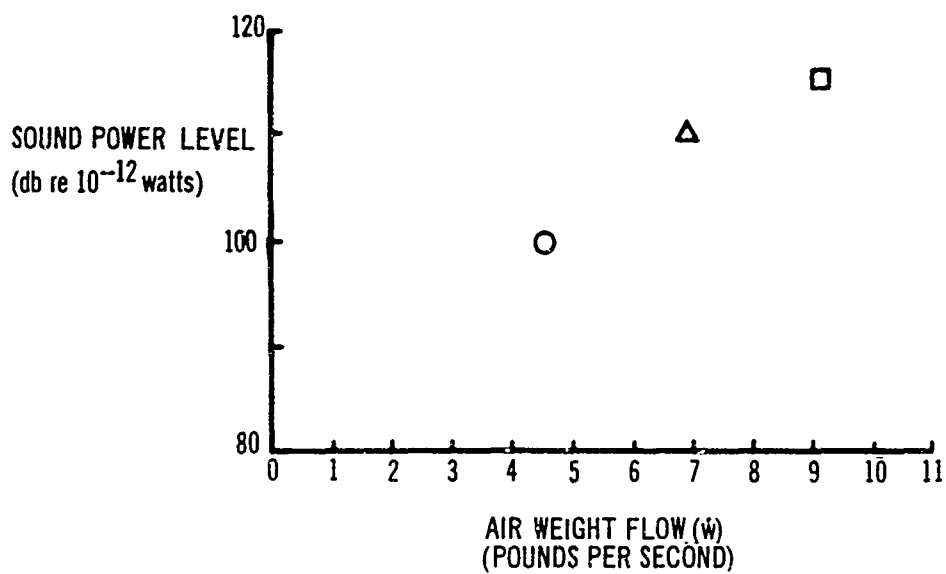
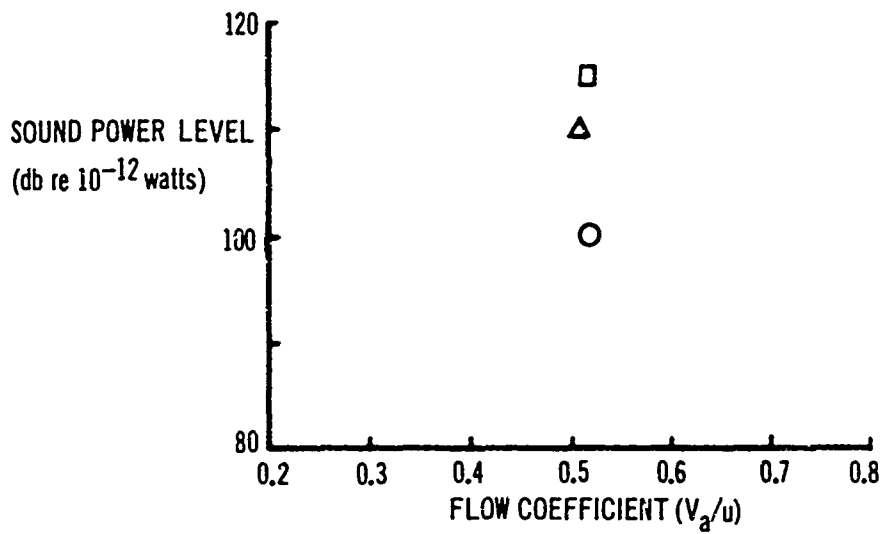


Fig. A3. Tilted Stator Blades, Twisted Rotor: Sound Power Level vs Flow Coefficient (m = 1)



LEGEND

IGV:
 $\beta_s = 90$ DEGREES
 $B_s = 8$
 $b' = 0.5$ INCH

RPM
 ○ 4000
 △ 6000
 □ 8000

ROTOR:
 STE 10-DEGREE TWIST

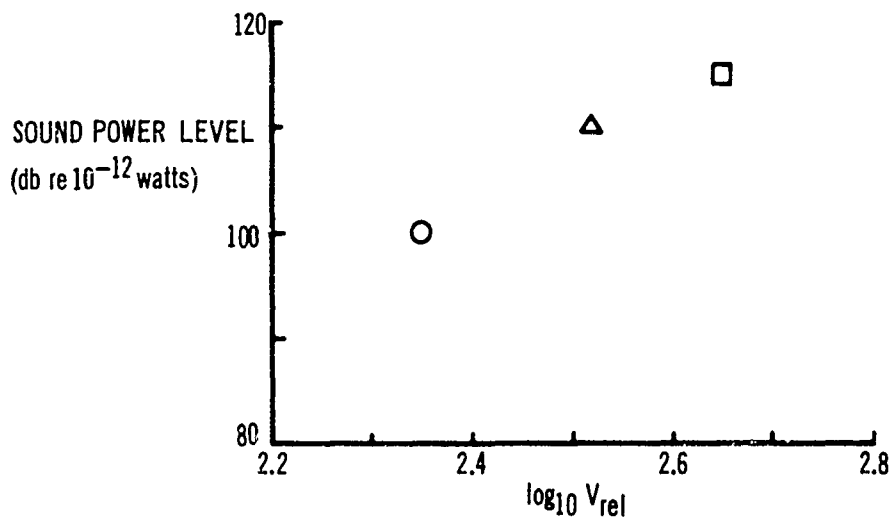
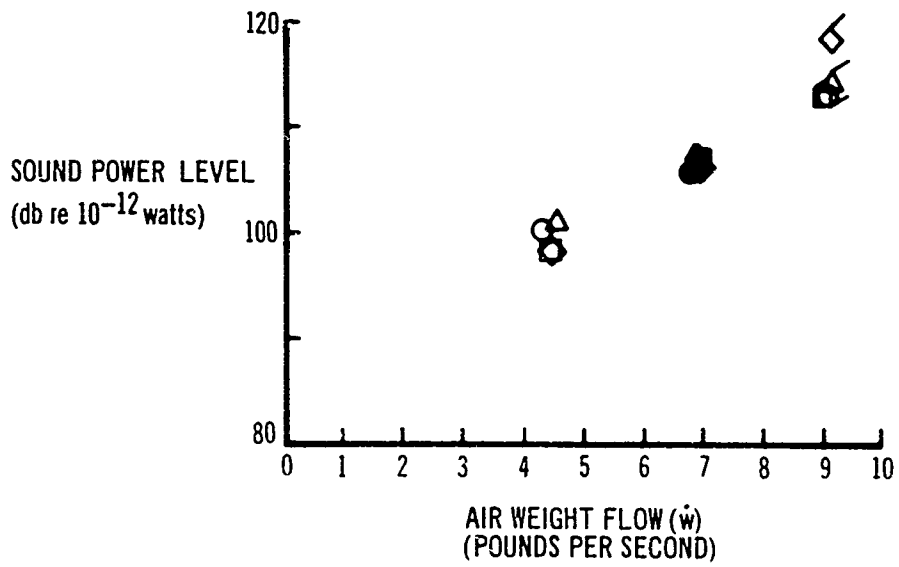
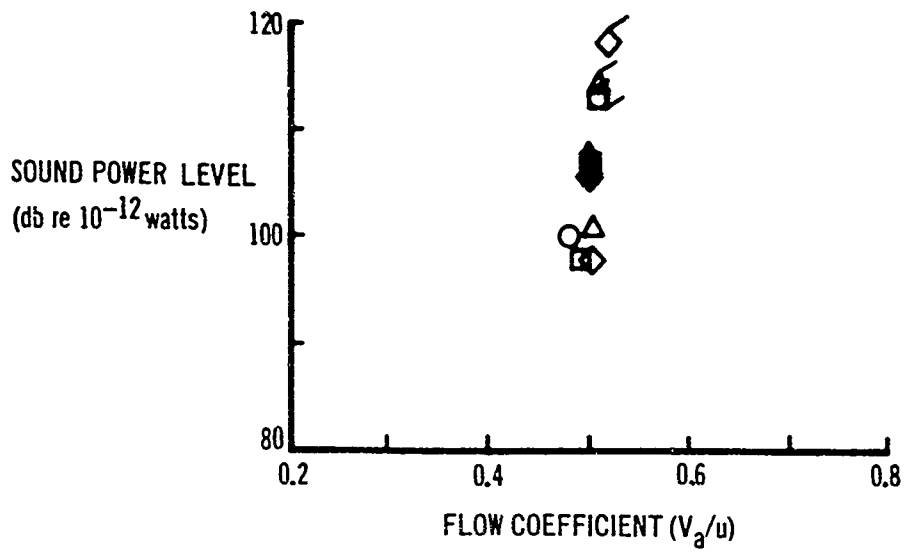


Fig. A4. Irregular IGV Angular Spacing, Sound Power Level 6 Feet From Rotor ($m = 1$)



LEGEND

RPM
 OPEN 4000
 SOLID 6000
 FLAG 8000

IGV-ROTOR SPACING
 b' (INCHES)
 ○ 0.2
 △ 0.5
 □ 1.0
 ◇ 2.0

IGV :
 $B_s = 90$ DEGREES
 $\beta_s = 8$

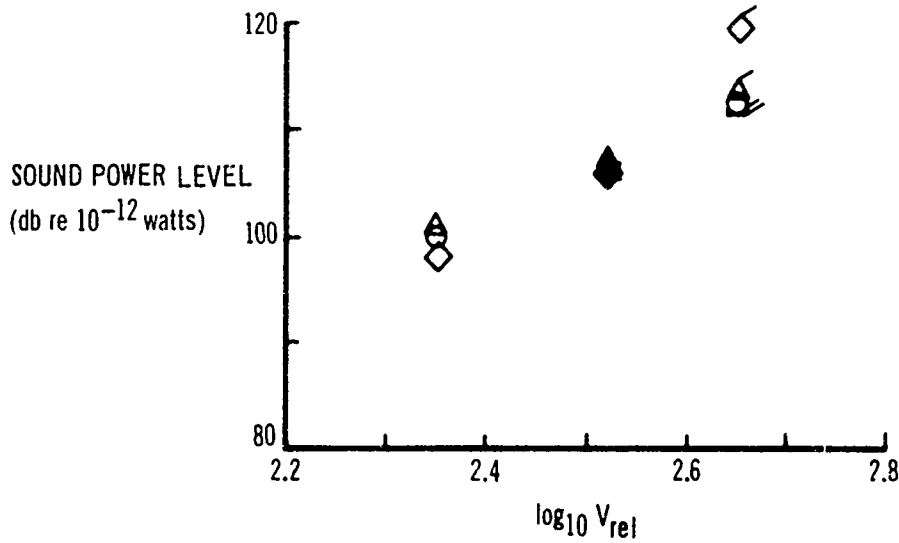
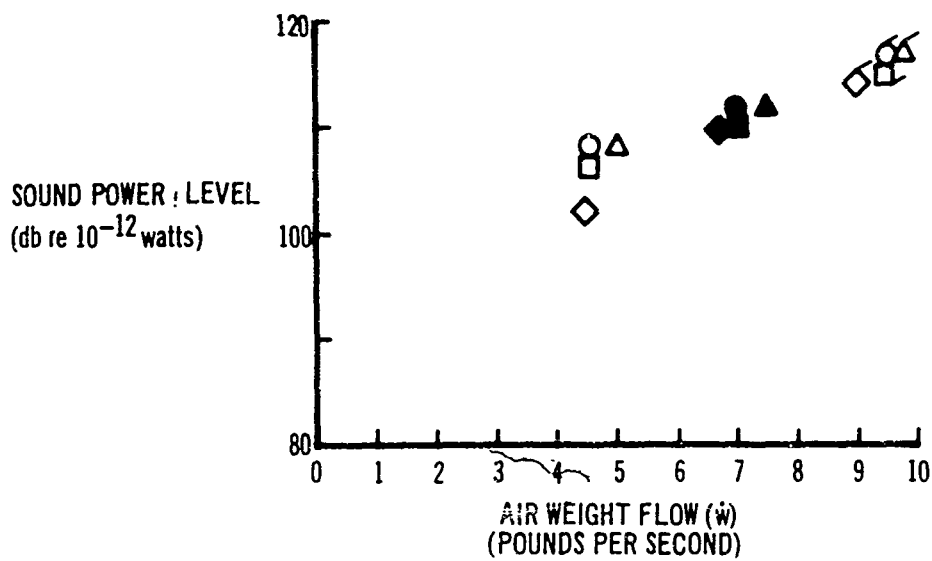
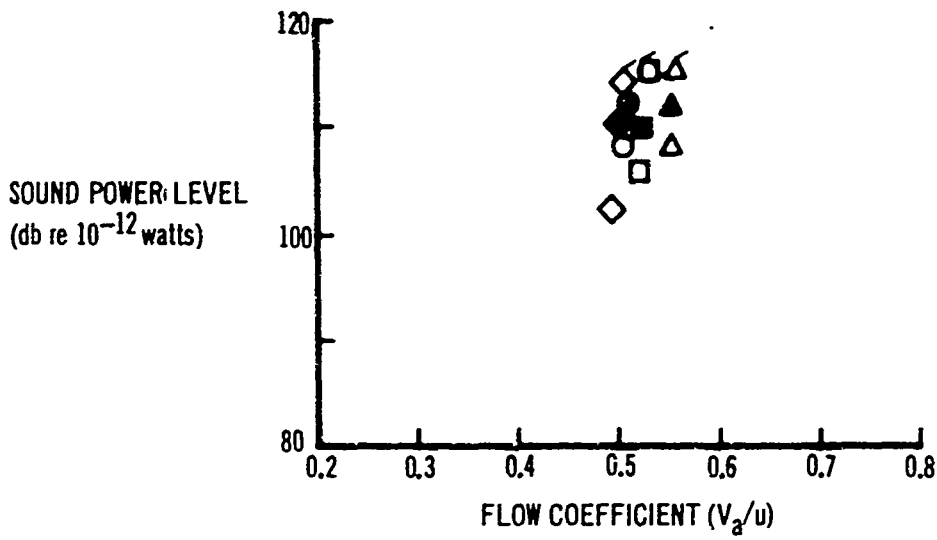


Fig. A5. Airfoil Blades, Sound Power Level 6 Inches From Rotor ($m = 1$)



LEGEND

RPM
 OPEN 4000
 SOLID 6000
 FLAG 8000

IGV-ROTOR SPACING:

b' (INCHES)
 ○ 0.2
 △ 0.5
 □ 1.0
 ◇ 2.0

IGV:
 $\beta_s = 90$ DEGREES
 $B_s = 8$

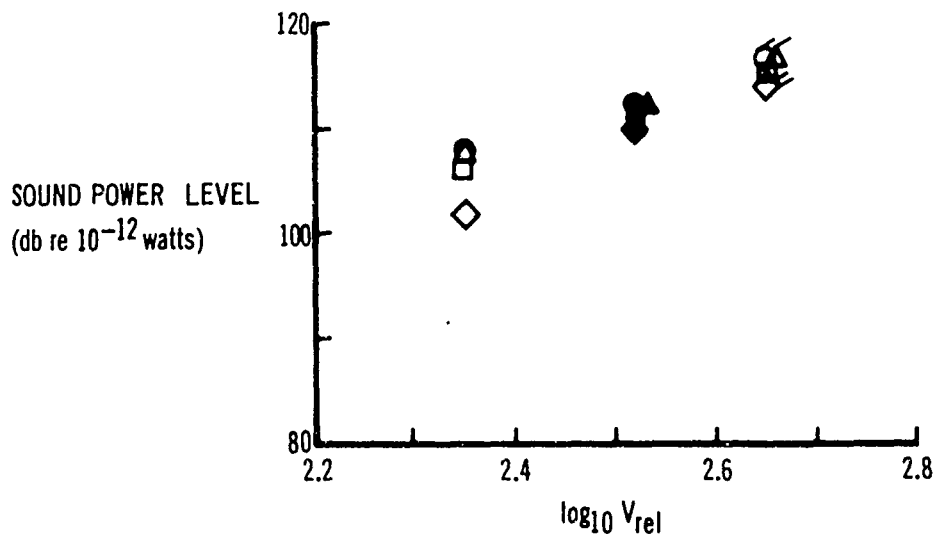


Fig. A6. Airfoil Blades, Sound Power Level 6 Feet From Rotor ($m = 1$)

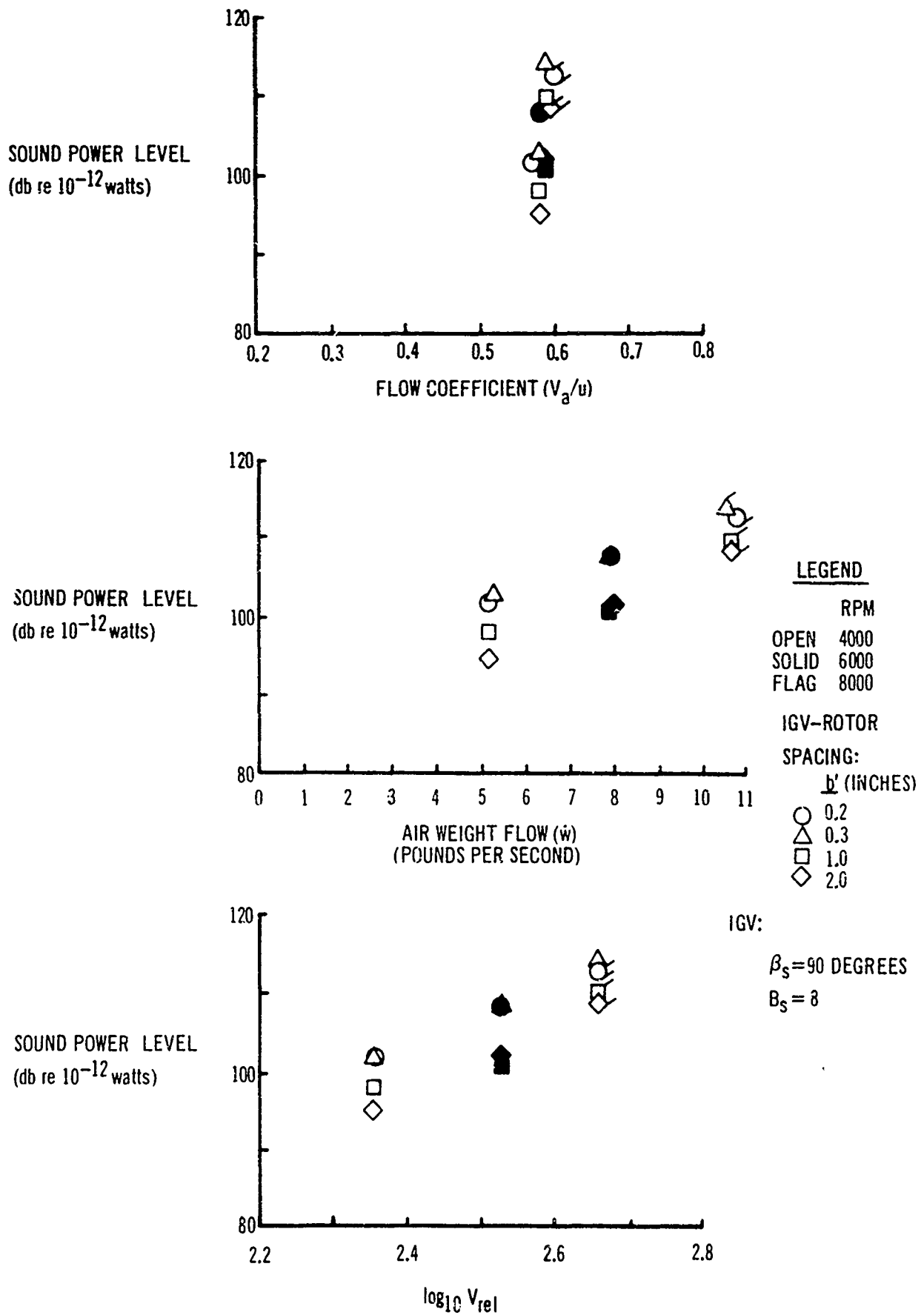


Fig. A7. Airfoil Blades With Twist, Sound Power Level 6 Inches From Rotor ($m = 1$)

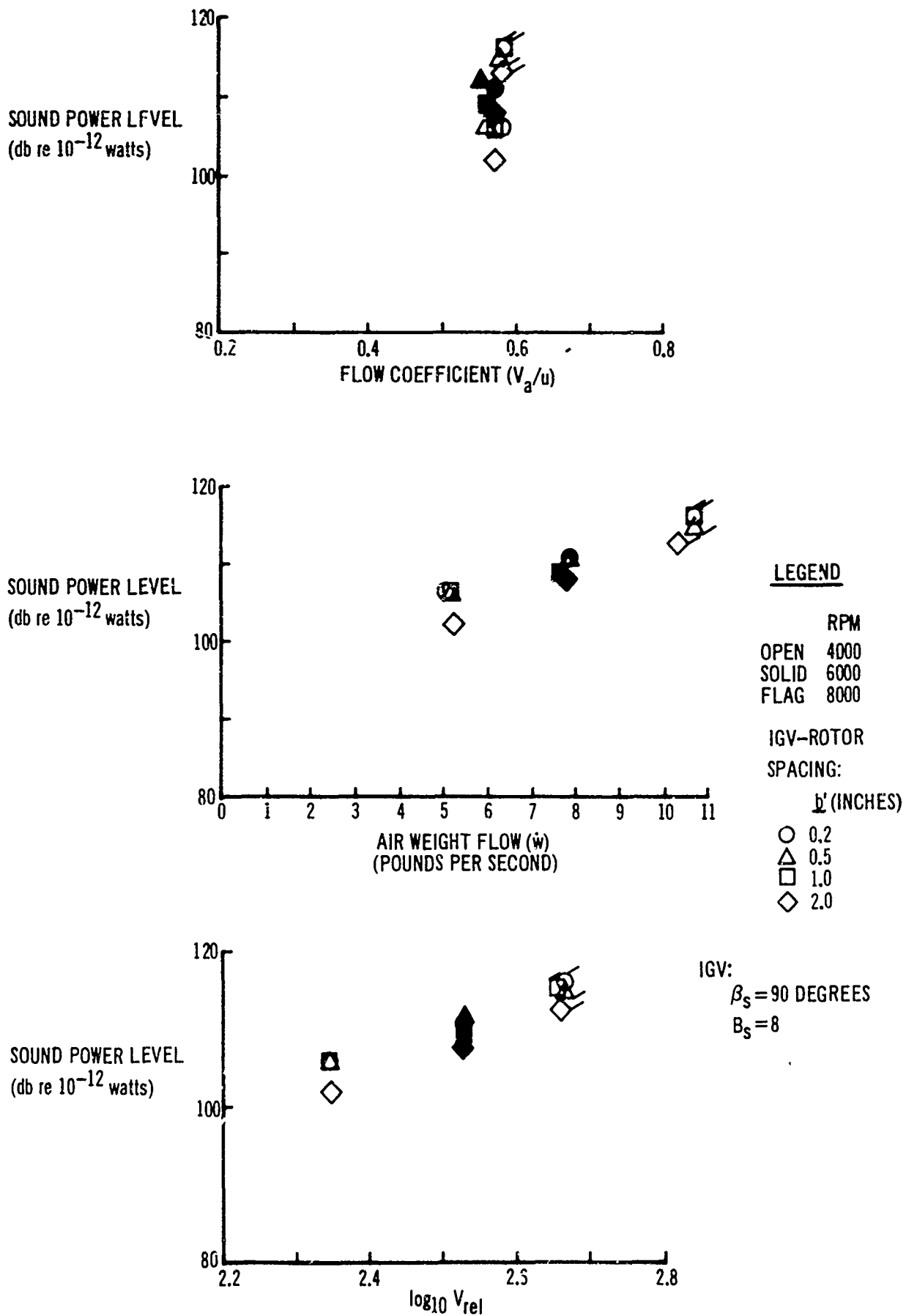


Fig. A8. Airfoil Blades With Twist, Sound Power Level 6 Feet From Rotor ($m = 1$)

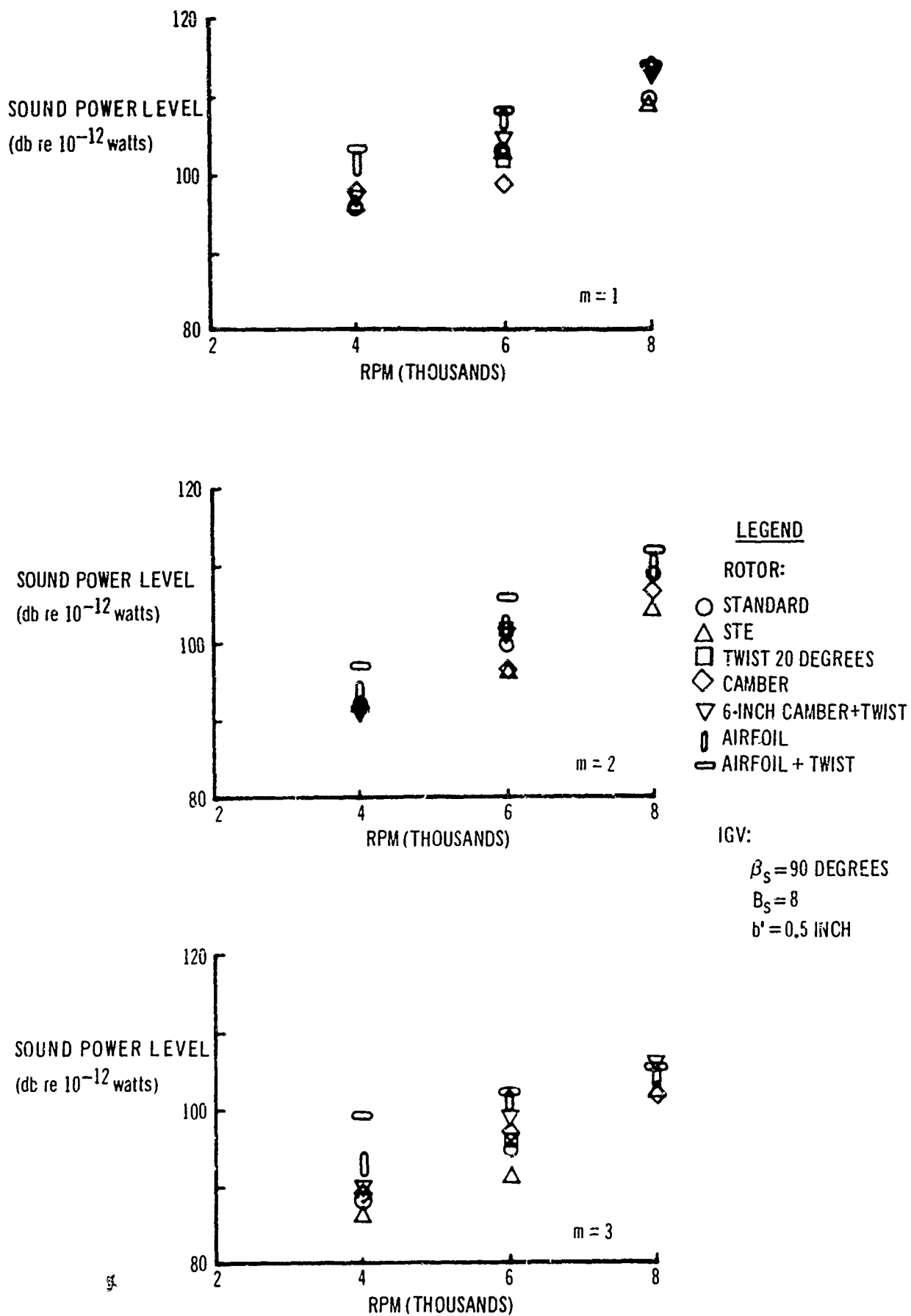
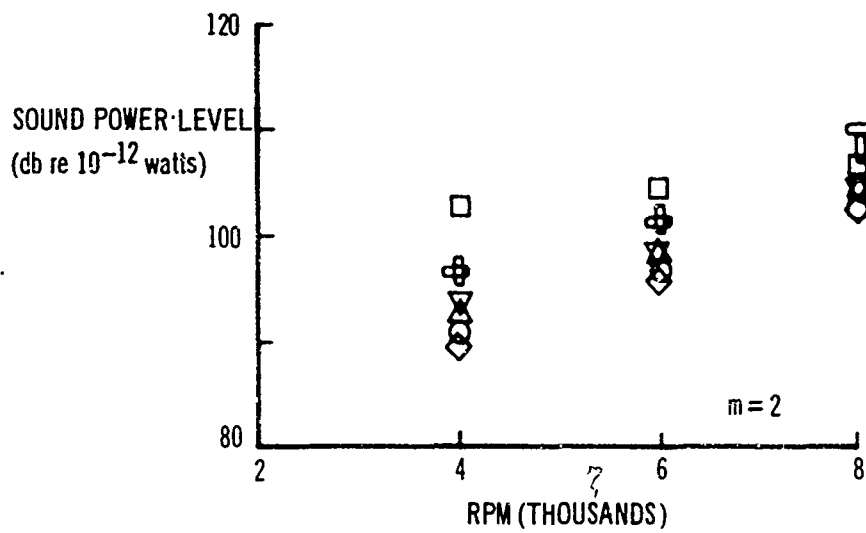
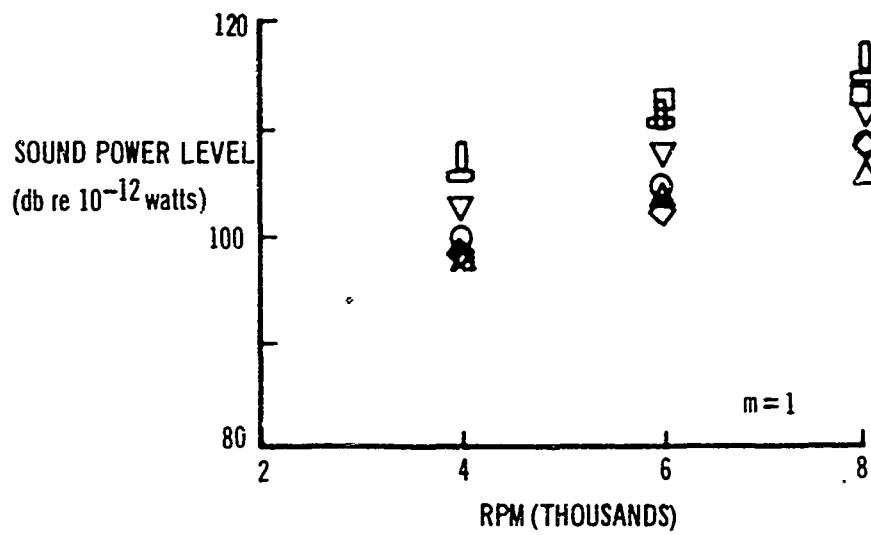


Fig. A9. Different Blade Shapes, Rotational Speed and Sound Power Level 6 Inches From Rotor



LEGEND

IGV:

$\beta_s = 90$ DEGREES
 $B_s = 8$
 $b' = 0.5$ INCH

ROTOR:

- STANDARD
- △ STE
- TWIST 20 DEGREES
- ◇ CAMBER
- ▽ 3-INCH CAMBER + TWIST
- ◊ AIR FOIL
- ◌ AIRFOIL + TWIST

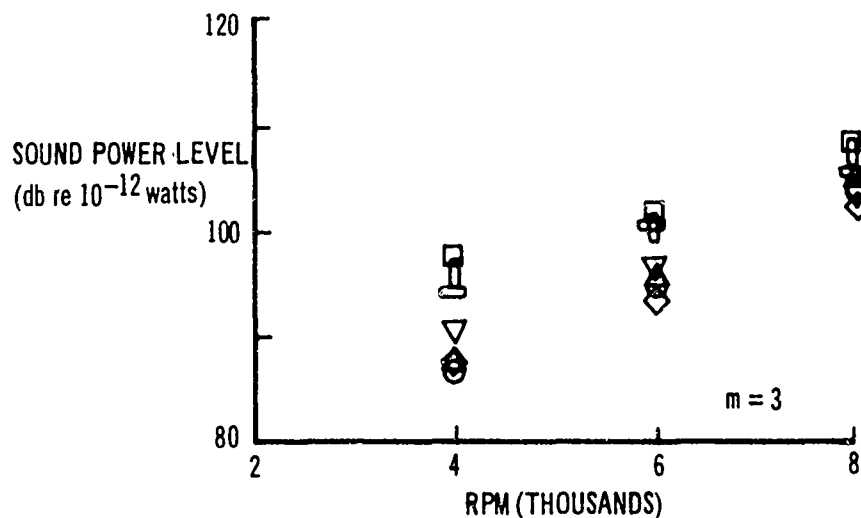


Fig. A10. Different Blade Shapes, Rotational Speed and Sound Power Level 6 Feet From Rotor

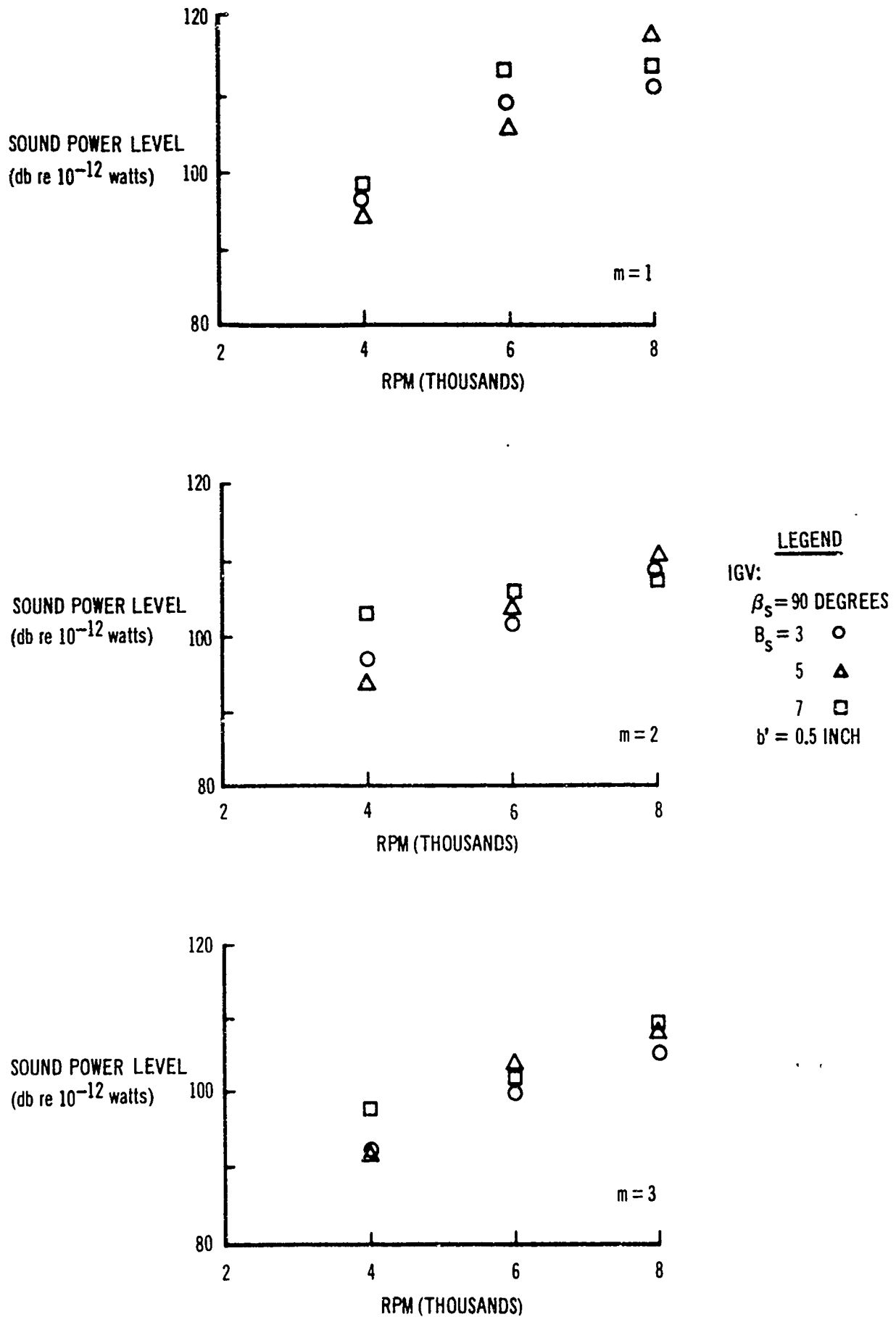


Fig. A11. Rotor Blades With 20-Degree Twist, Rotational Speed and Sound Power Level 6 Feet From Rotor

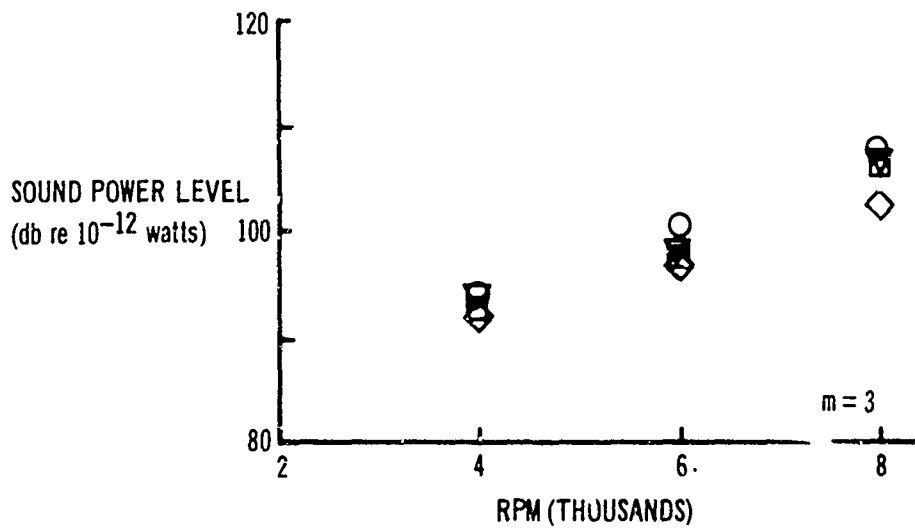
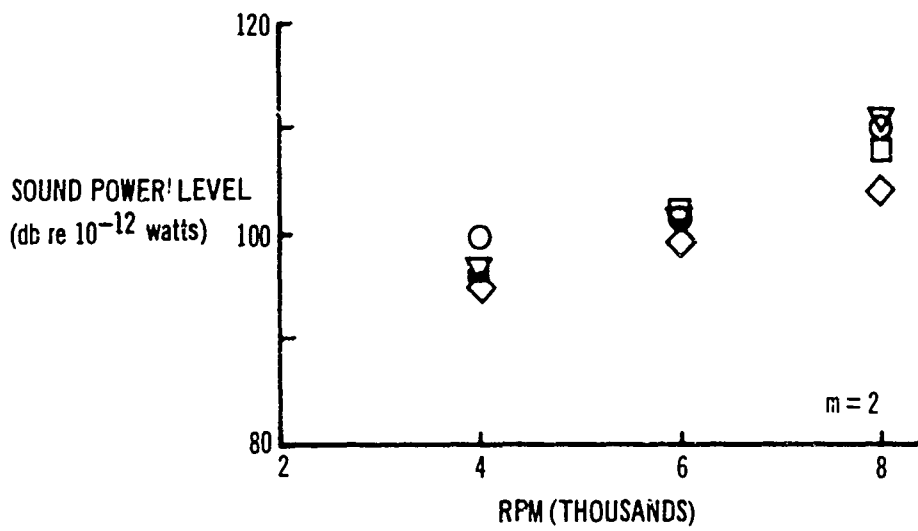
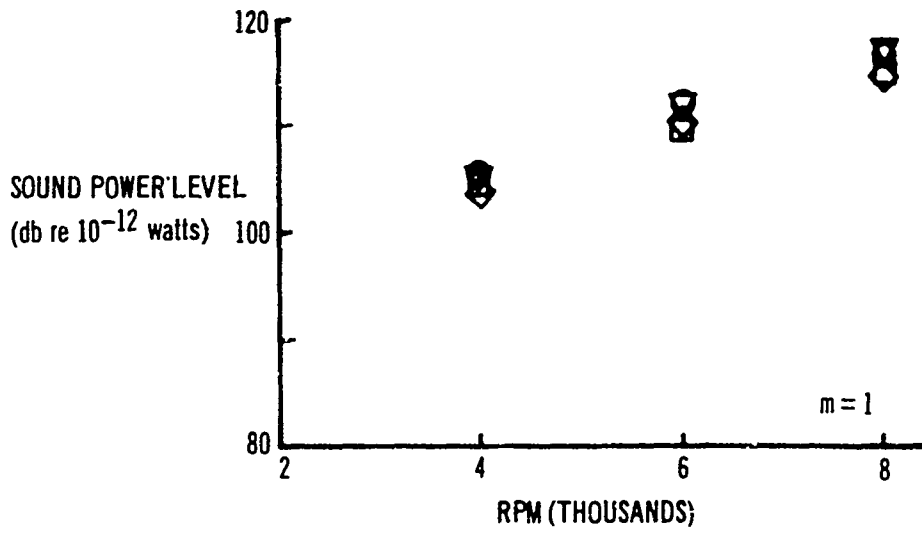


Fig. A12. Tubular IGV, Rotational Speed and Sound Power Level 6 Feet From Rotor

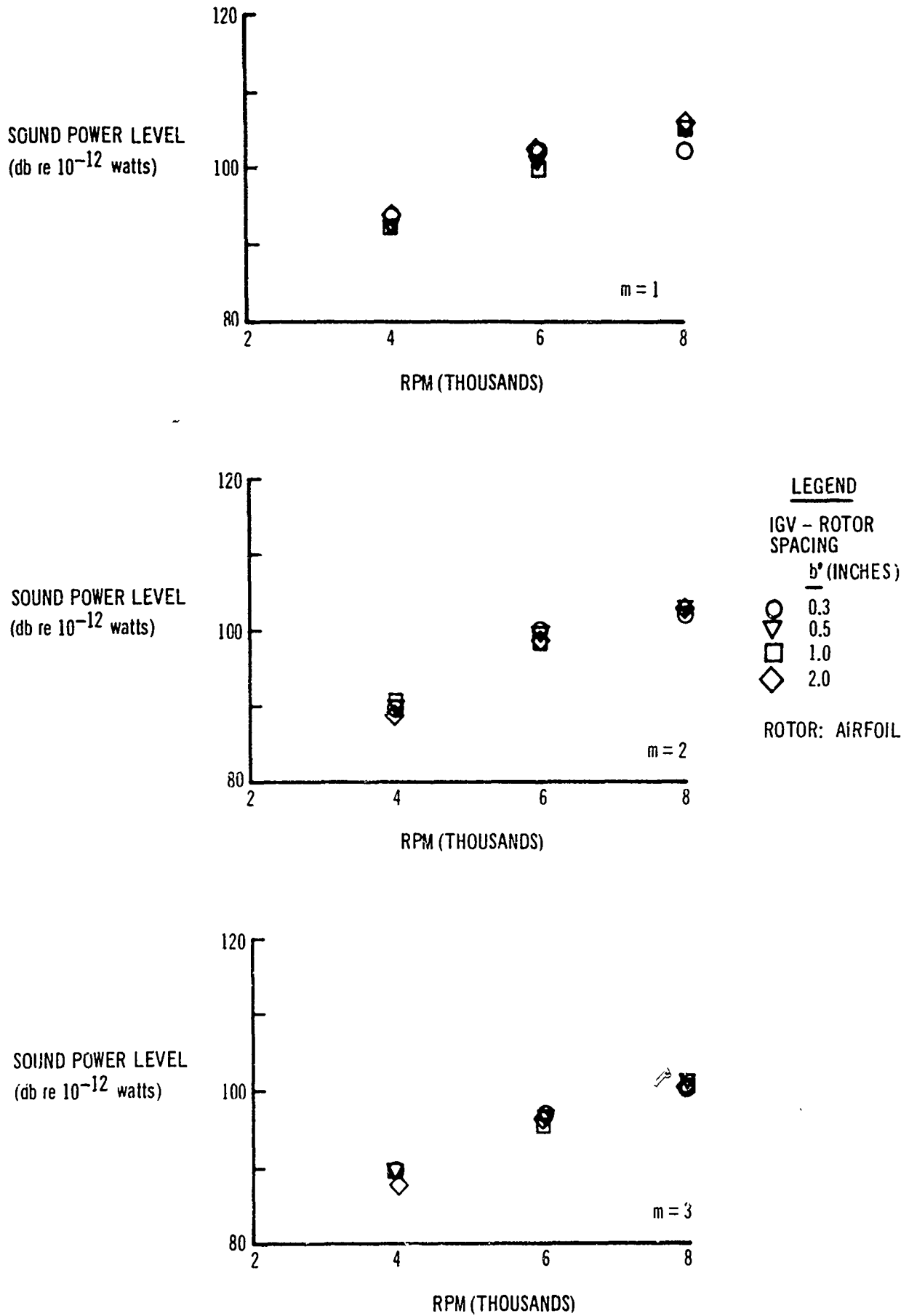
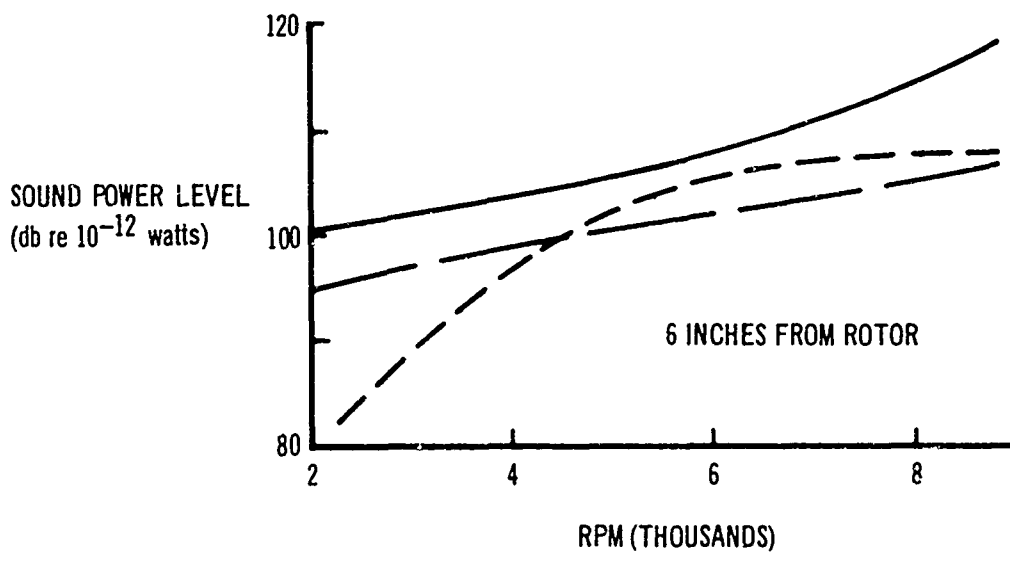
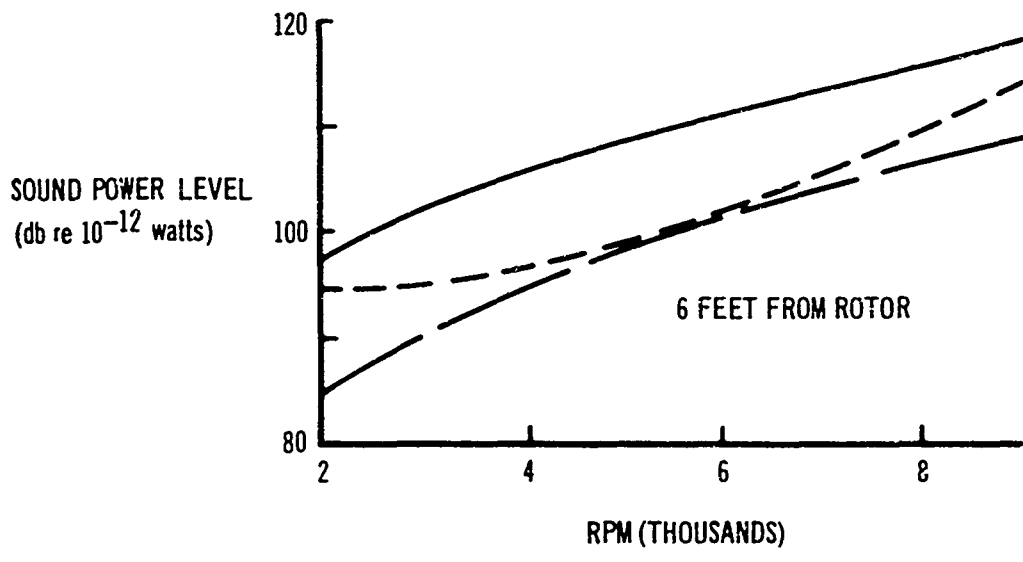


Fig. A13. Honeycomb IG (3/16-Inch Cell), Rotational Speed and Sound Power Level 6 Feet From Rotor



LEGEND

- IGV:
 $\beta_s = 90$ DEGREES
 $B_s = 8$
 $b' = 0.5$ INCH
 ——— m=1
 - - - m=2
 - · - m=3

Fig. A14. Airfoil Blade With Twist, Sound Power Level and Rotational Speed

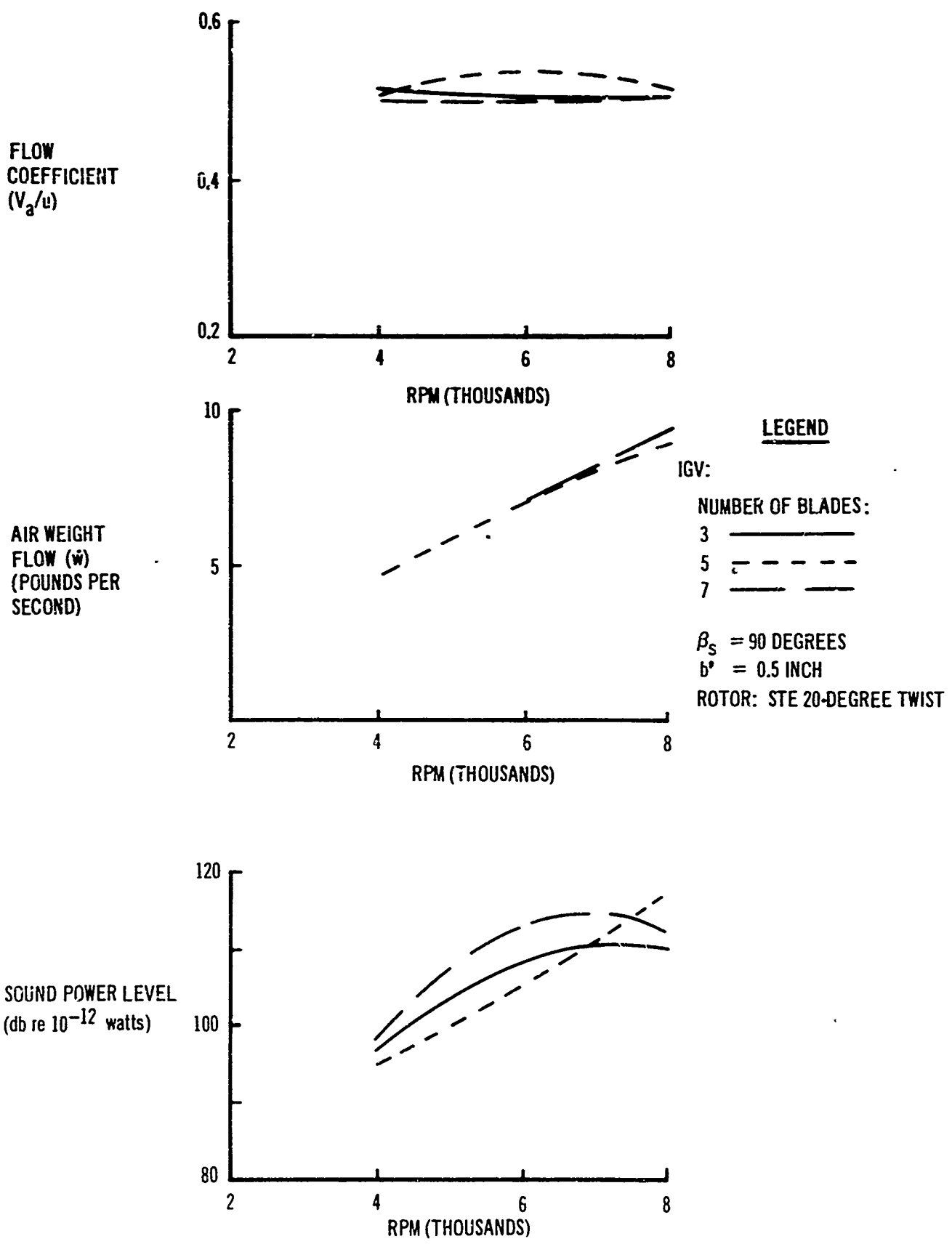
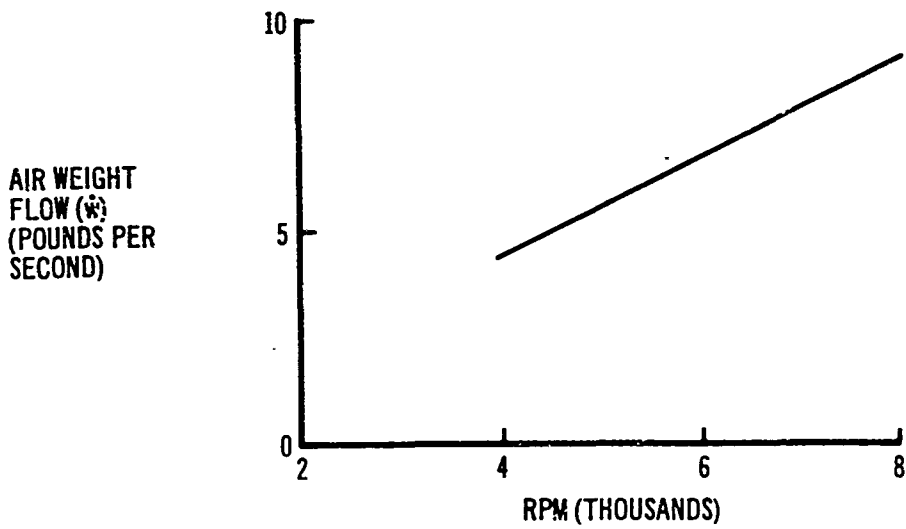
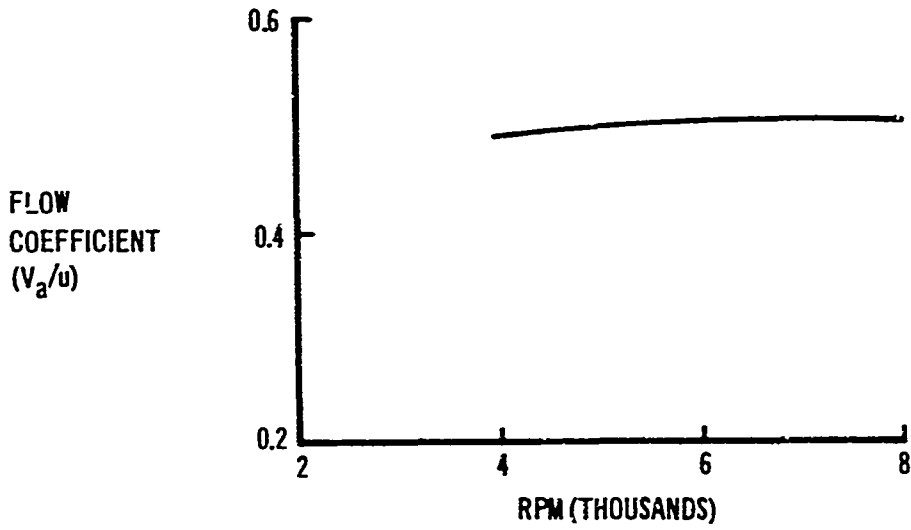


Fig. A15. Different IGV Numbers: Flow Coefficient, Weight Flow, Sound Power Level 6 Feet From Rotor, and Rotational Speed



LEGEND

IGV:
 $\beta_s = 90$ DEGREES
 $B_s = 8$
 $b' = 0.5$ INCH
 ROTOR:
 STE 20-DEGREE TWIST

— m = 1
 - - - m = 2
 - · - m = 3

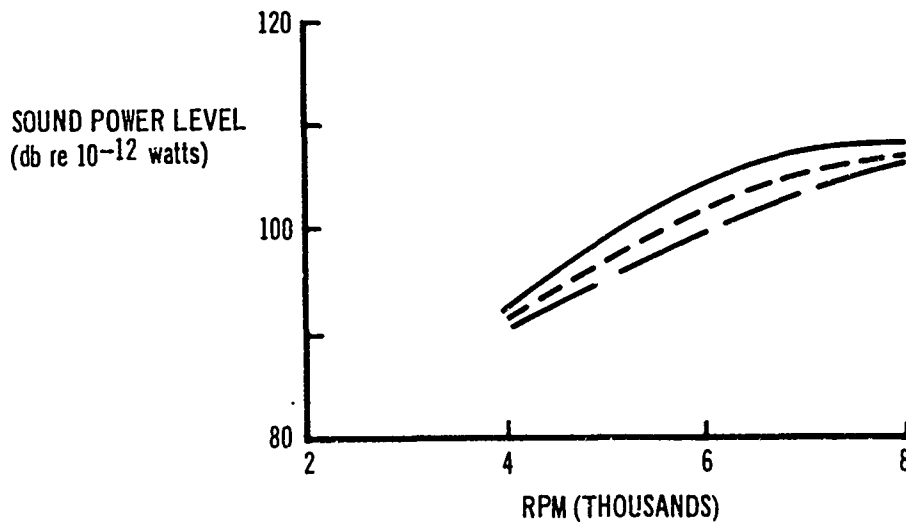


Fig. A16. Tilted IGV's: Flow Coefficient, Weight Flow, Sound Power Level 6 Feet From Rotor, and Rotational Speed

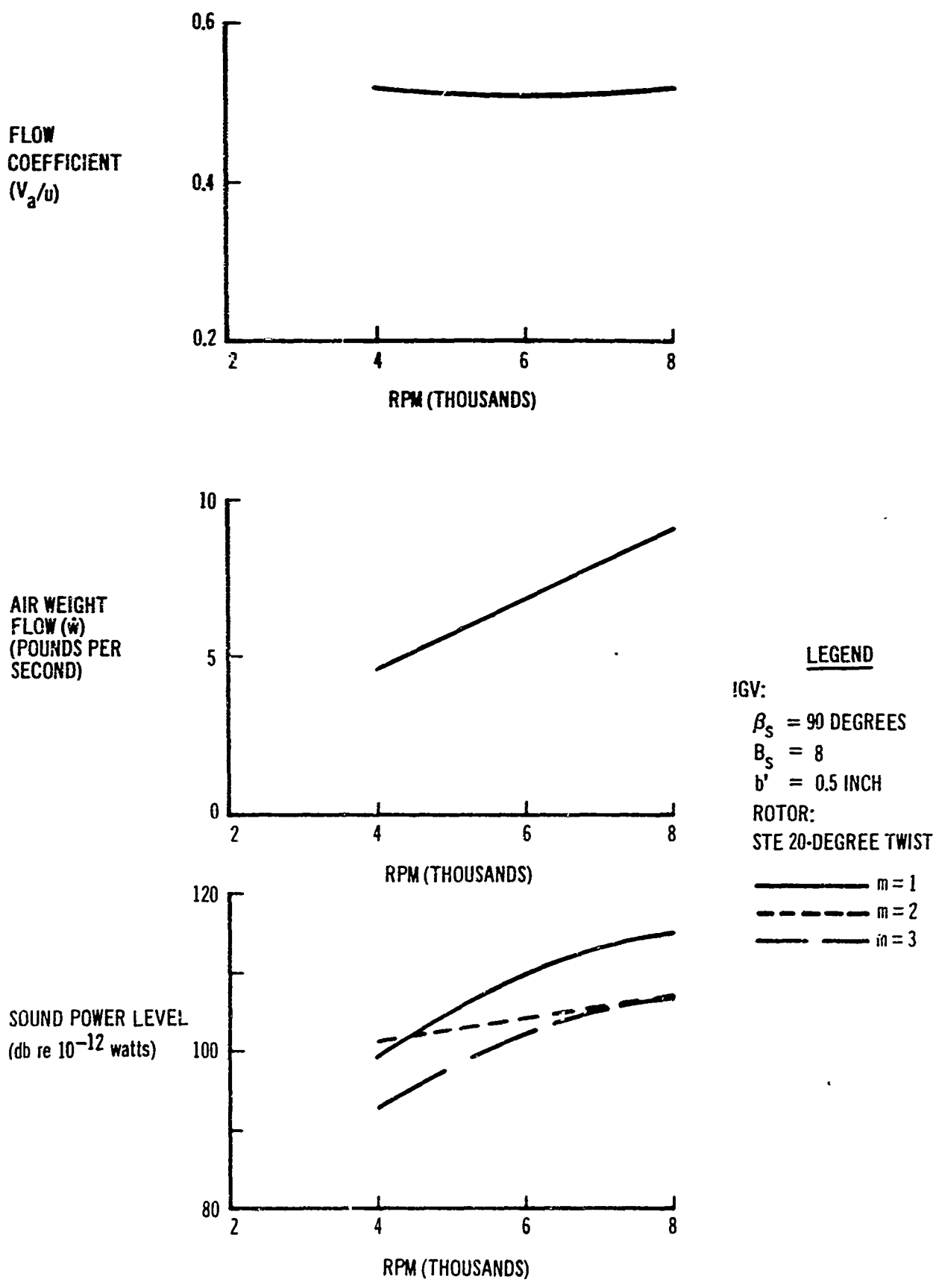


Fig. A17. Irregular IGV Angular Spacing: Flow Coefficient, Weight Flow, Sound Power Level 6 Feet From Rotor, and Rotational Speed

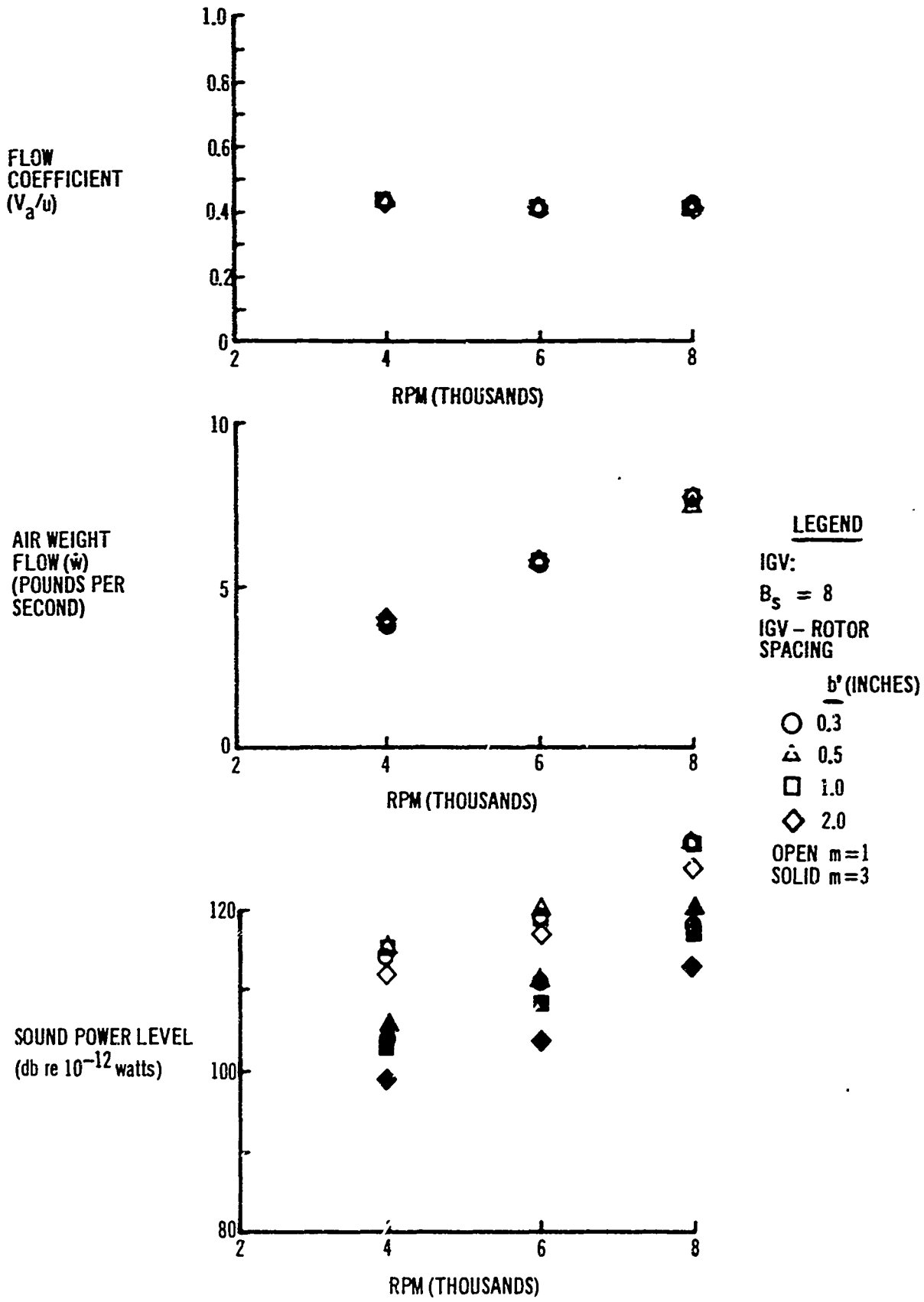


Fig. A18. Rotor 6-Inch Camber, 20-Degree Twist, $\beta_s = 45$ Degrees: Flow Coefficient, Weight Flow, Sound Power Level 6 Inches From Rotor, and Rotational Speed

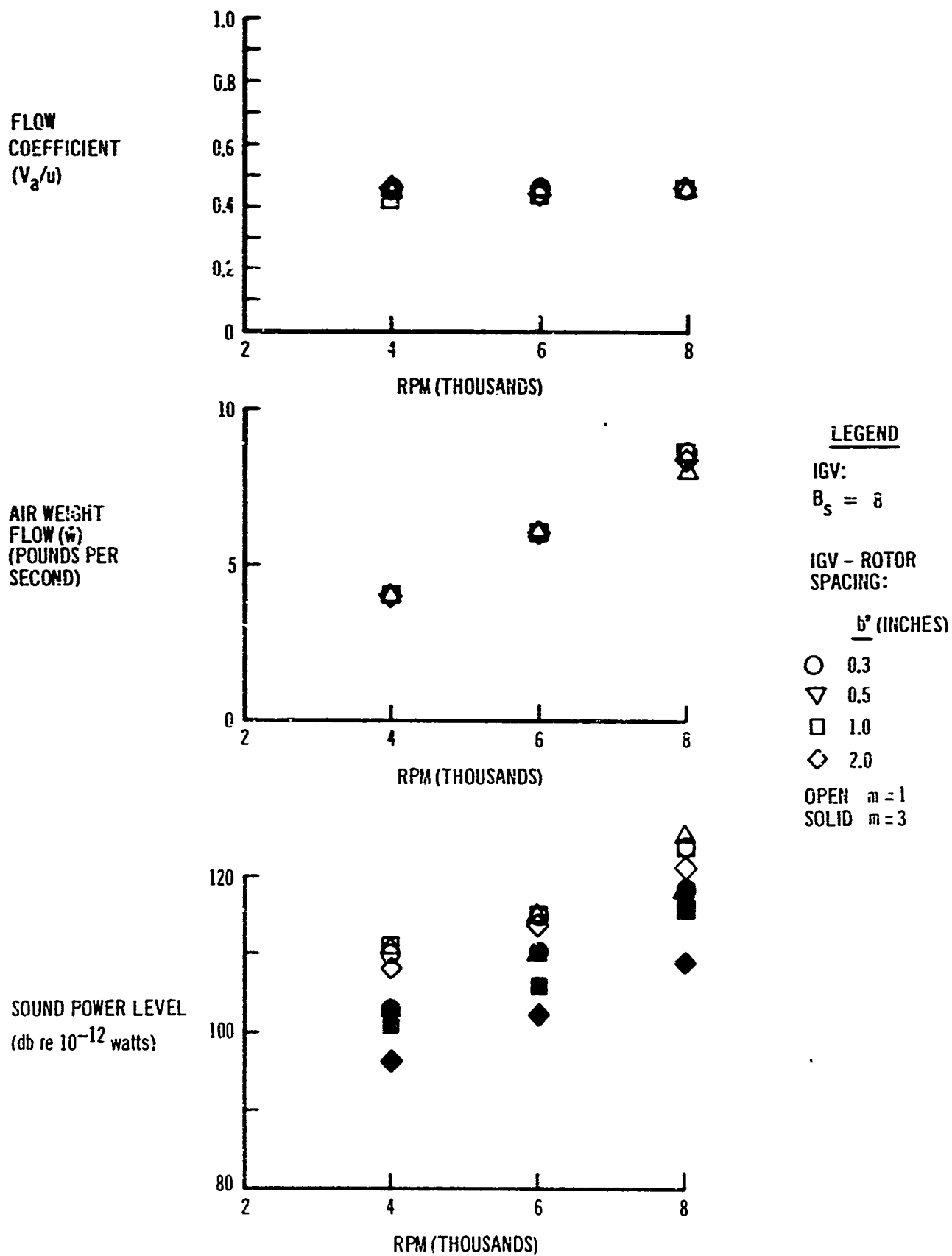


Fig. A19. Rotor 6-Inch Camber, 20-Degree Twist, $\beta_s = 60$ Degrees: Flow Coefficient, Weight Flow, Sound Power Level 6 Inches From Rotor, and Rotational Speed

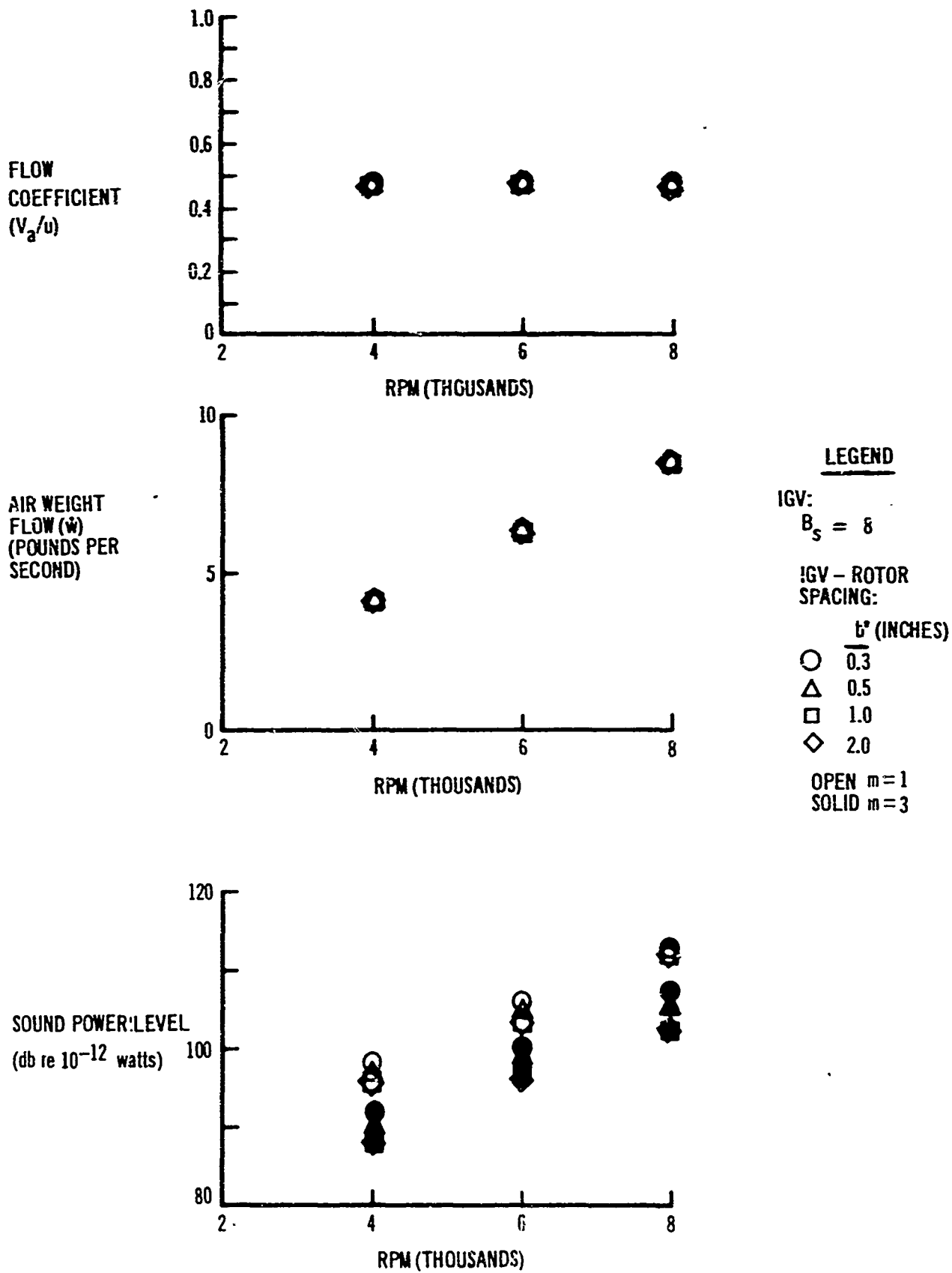


Fig. A20. Rotor 6-Inch Camber, 20-Degree Twist, $\beta_s = 90$ Degrees: Flow Coefficient, Weight Flow, Sound Power Level 6 Inches From Rotor, and Rotational Speed

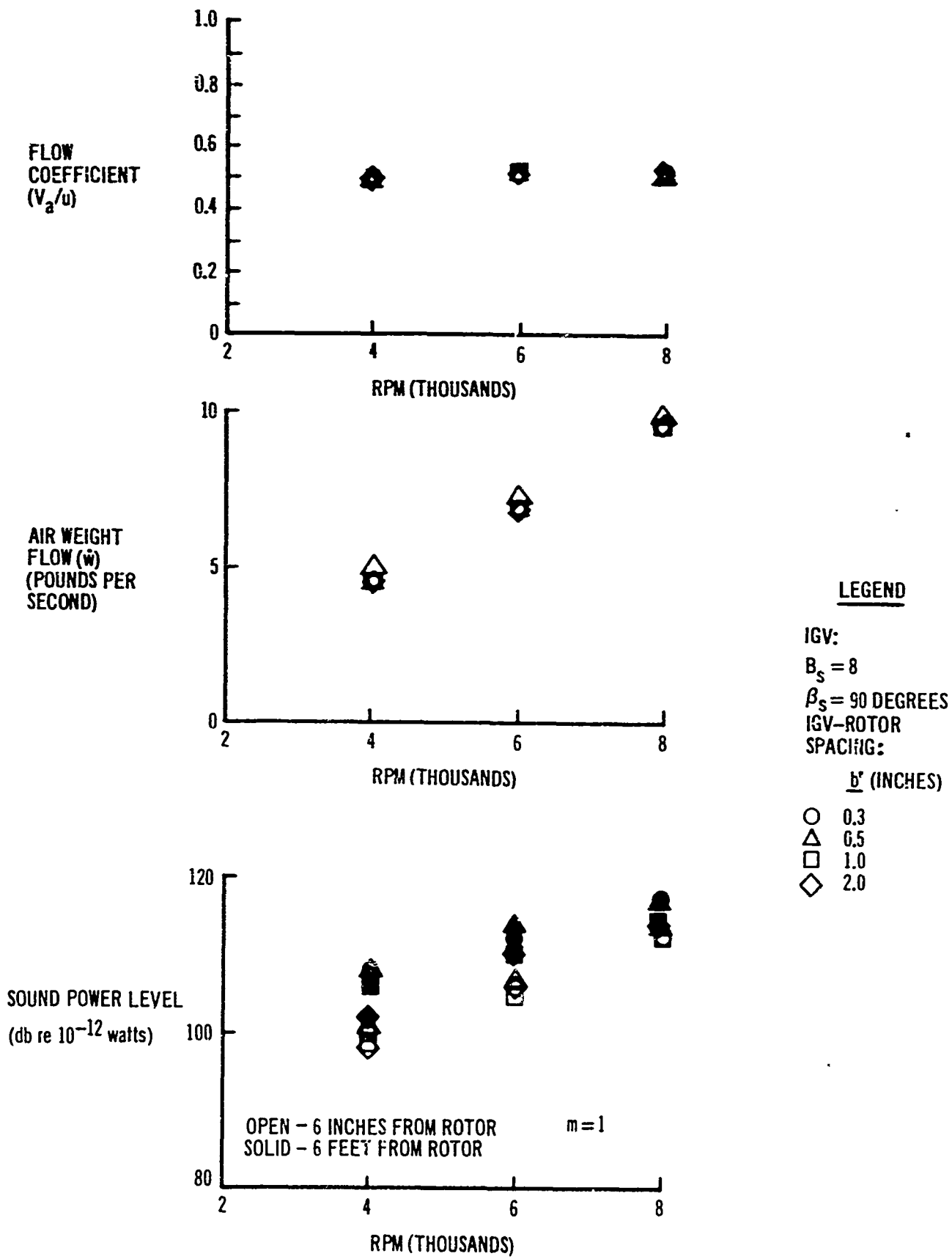
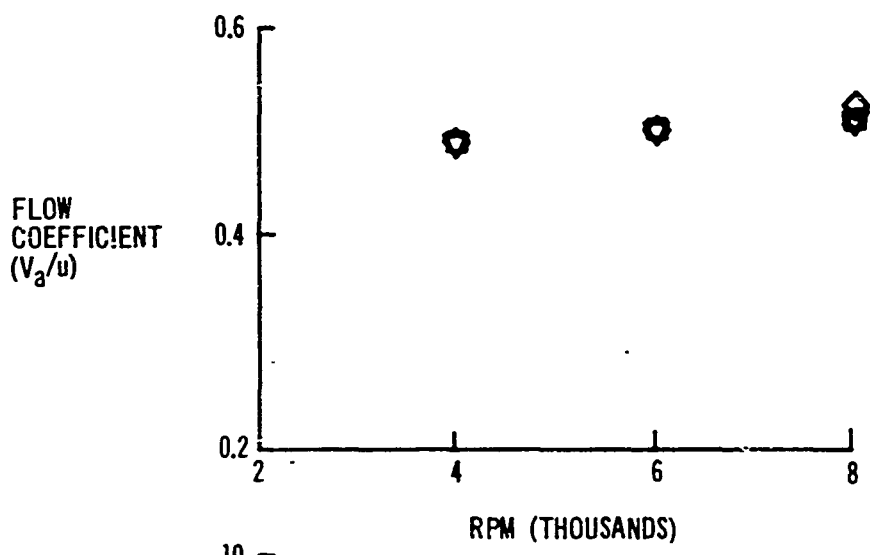
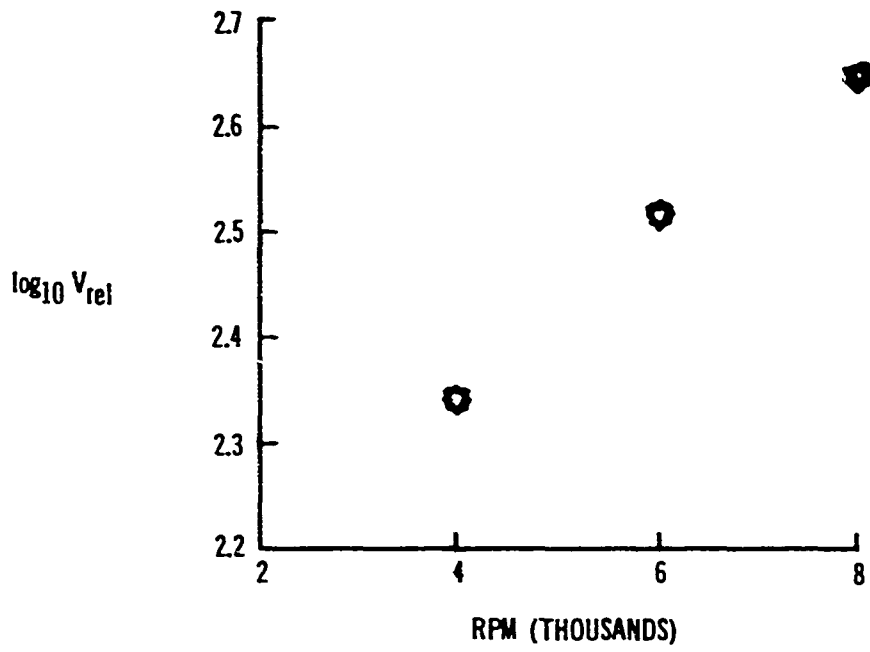


Fig. A21. Airfoil Rotor Blades: Flow Coefficient, Weight Flow, Sound Power Level, and Rotational Speed



LEGEND

ROTOR: AIRFOIL BLADES
 IGV:
 B_s = 8
 β_s = 90 DEGREES

IGV - ROTOR SPACING:
 b' (INCHES)
 ○ 0.3
 ▼ 0.5
 □ 1.0
 ◇ 2.0

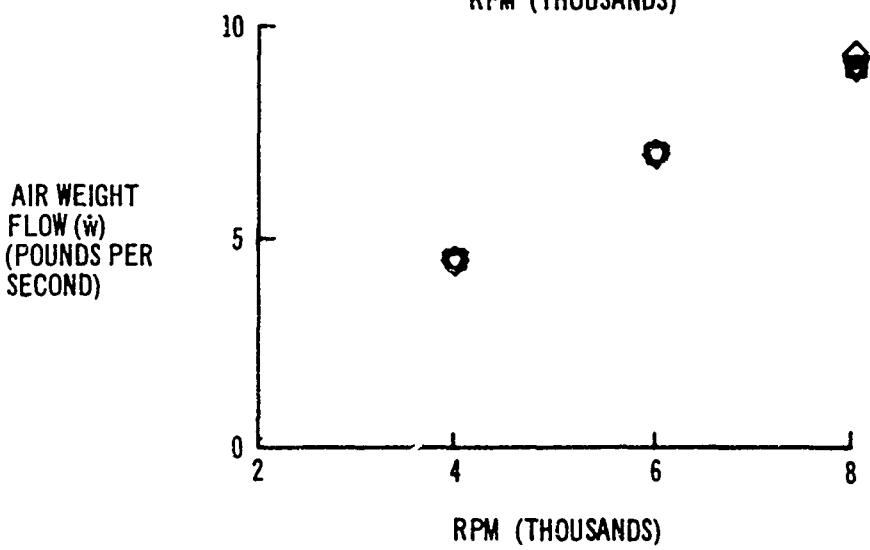


Fig. A22. Tubular IGV; Relative Tip Speed, Flow Coefficient, Weight Flow, and Rotational Speed

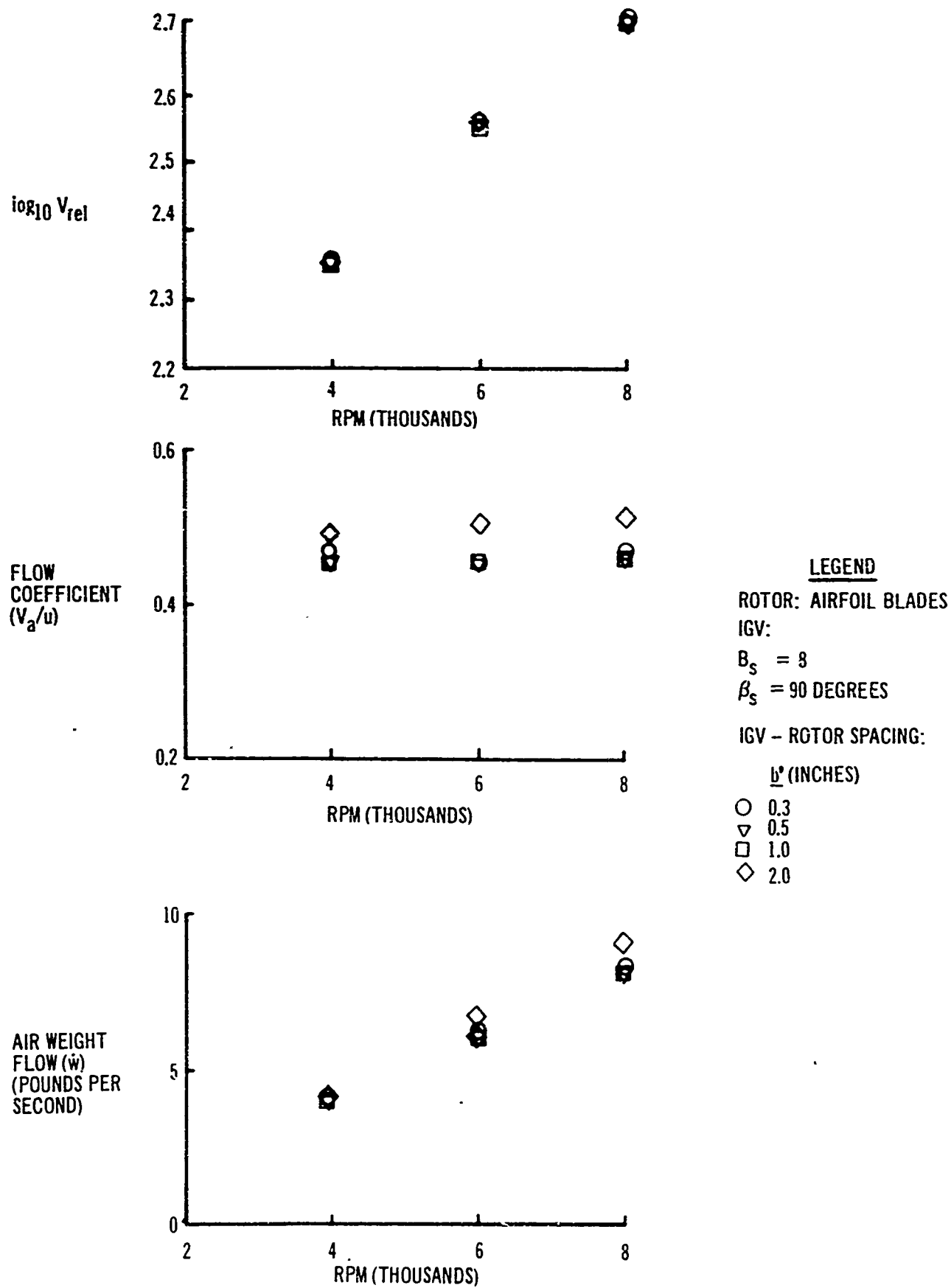


Fig. A23. Honeycomb IGV (3/16-Inch Cell): Relative Tip Speed, Flow Coefficient, Weight Flow, and Rotational Speed

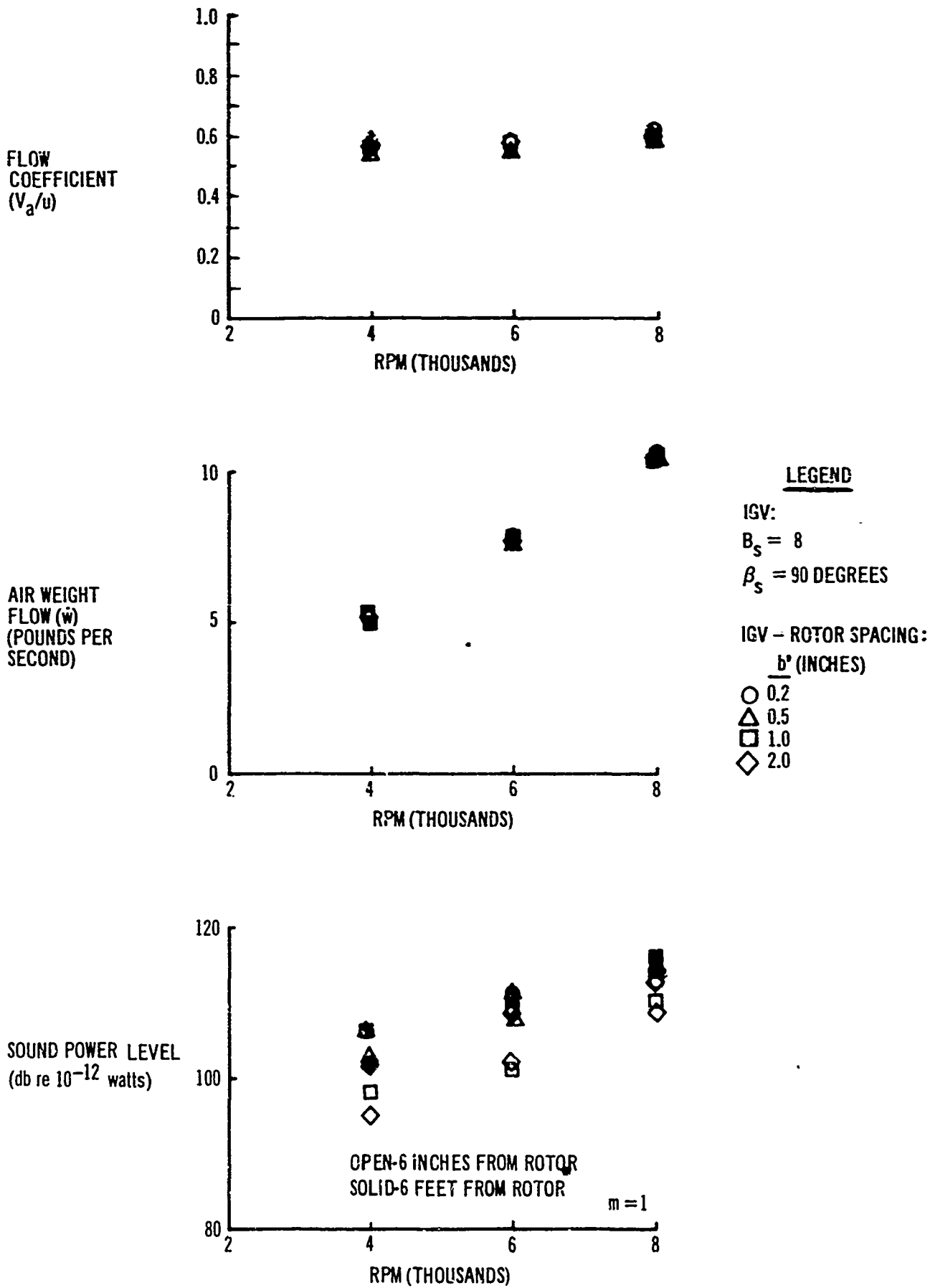


Fig. A24. Airfoil Rotor Blades With 20-Degree Twist: Flow Coefficient, Weight Flow, Sound Power Level, and Rotational Speed

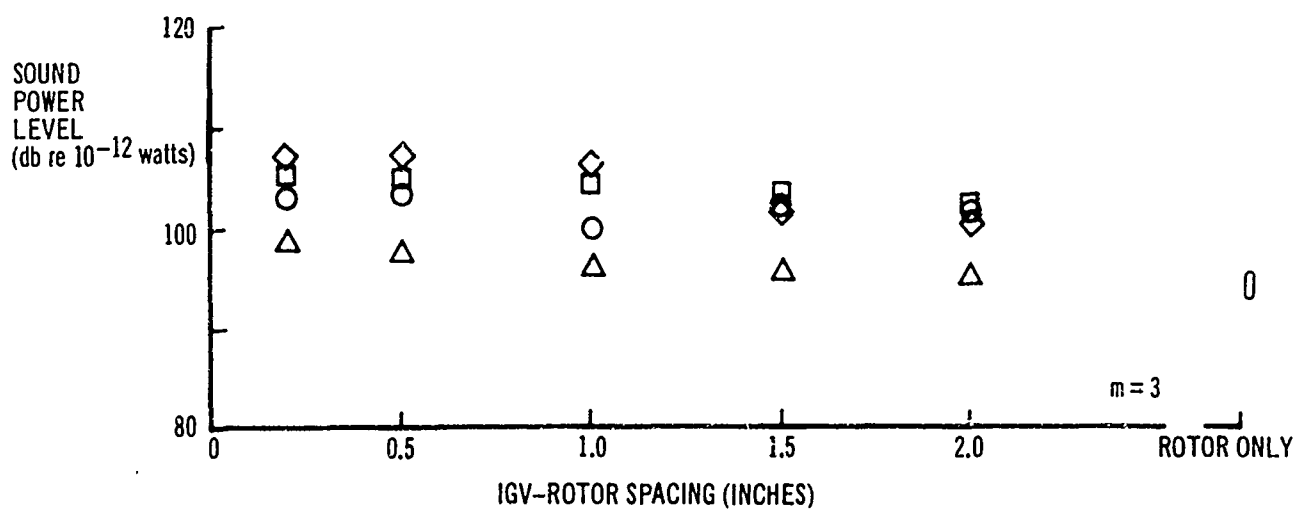
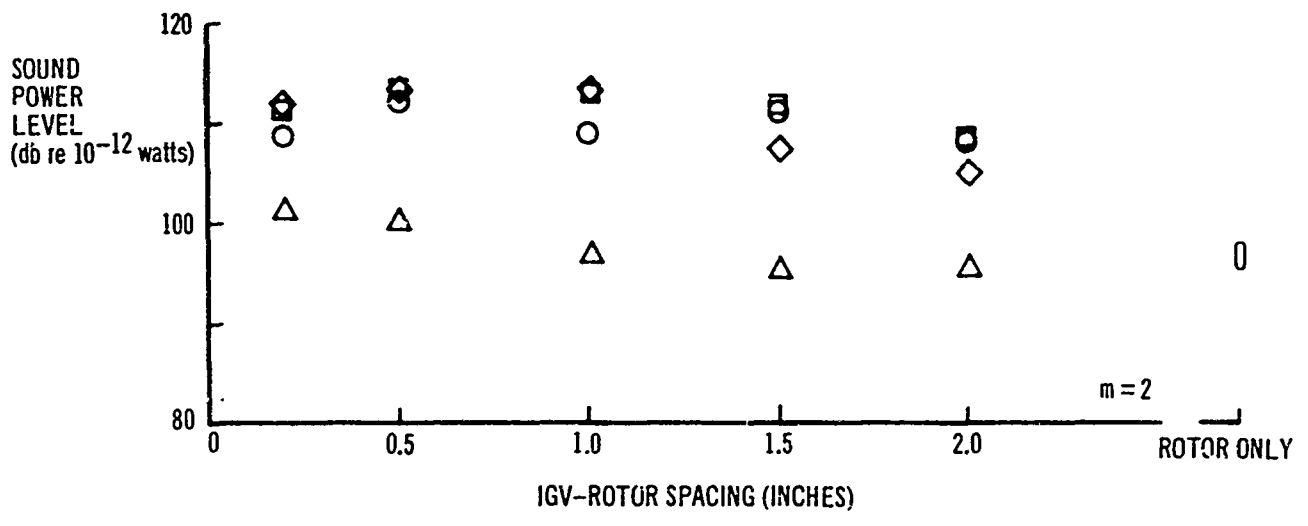
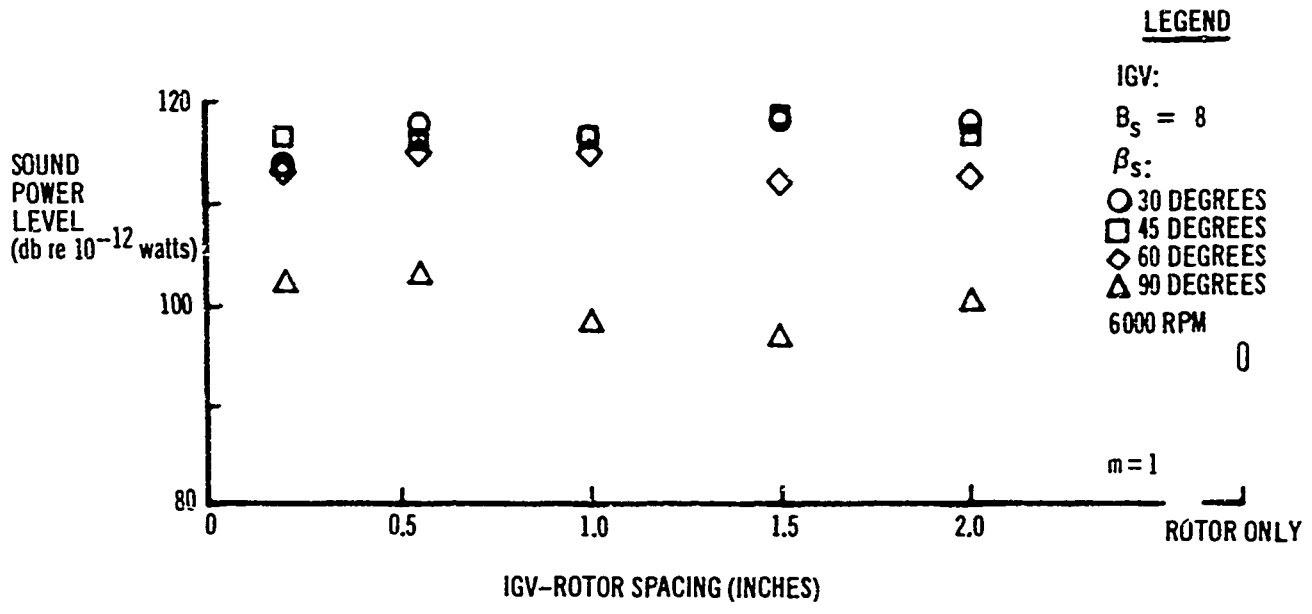


Fig. A25. Flat Rotor Blades, Different β_s ; Sound Power Level 6 Inches From Rotor and IGV-Rotor Spacing

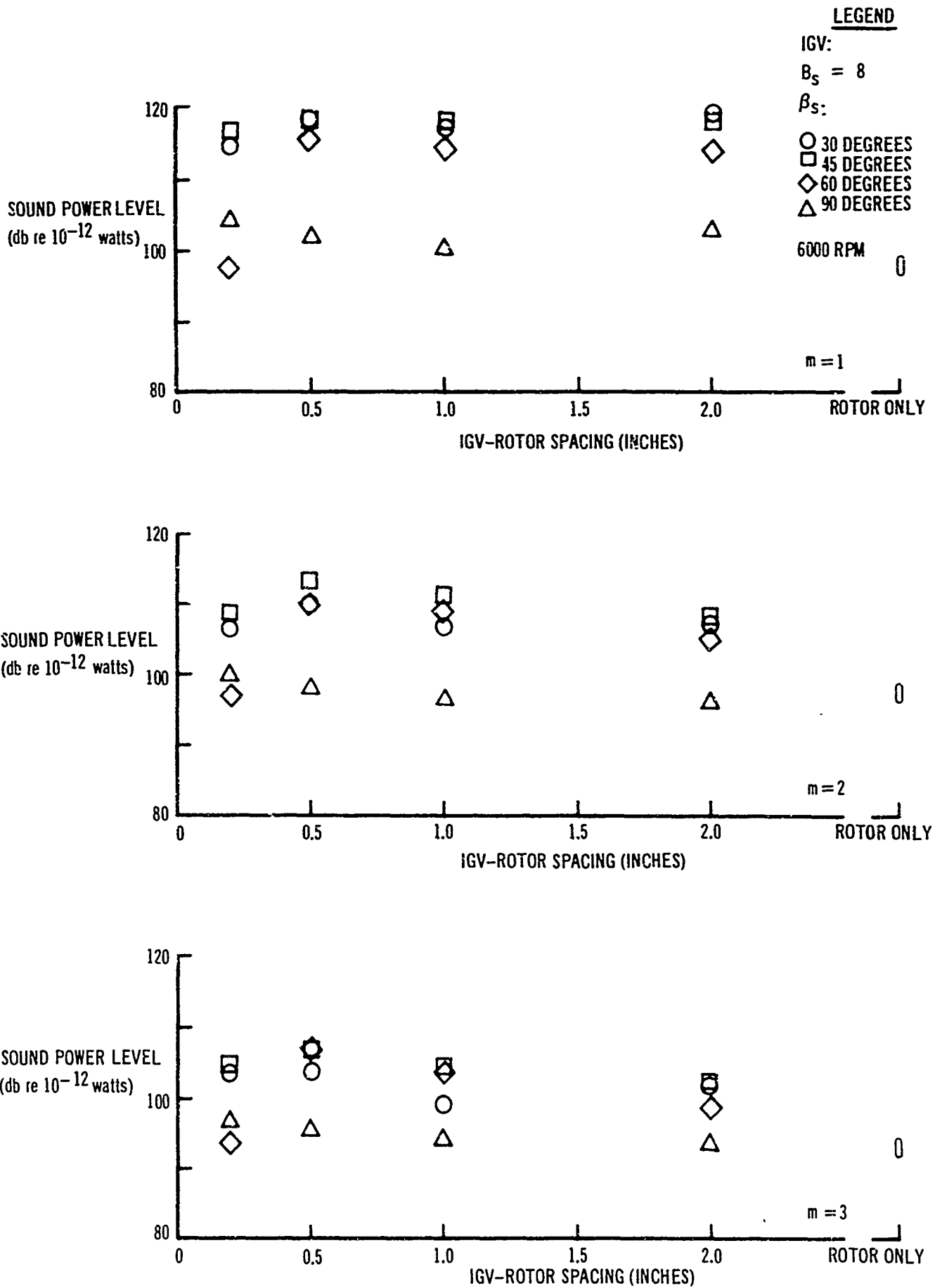
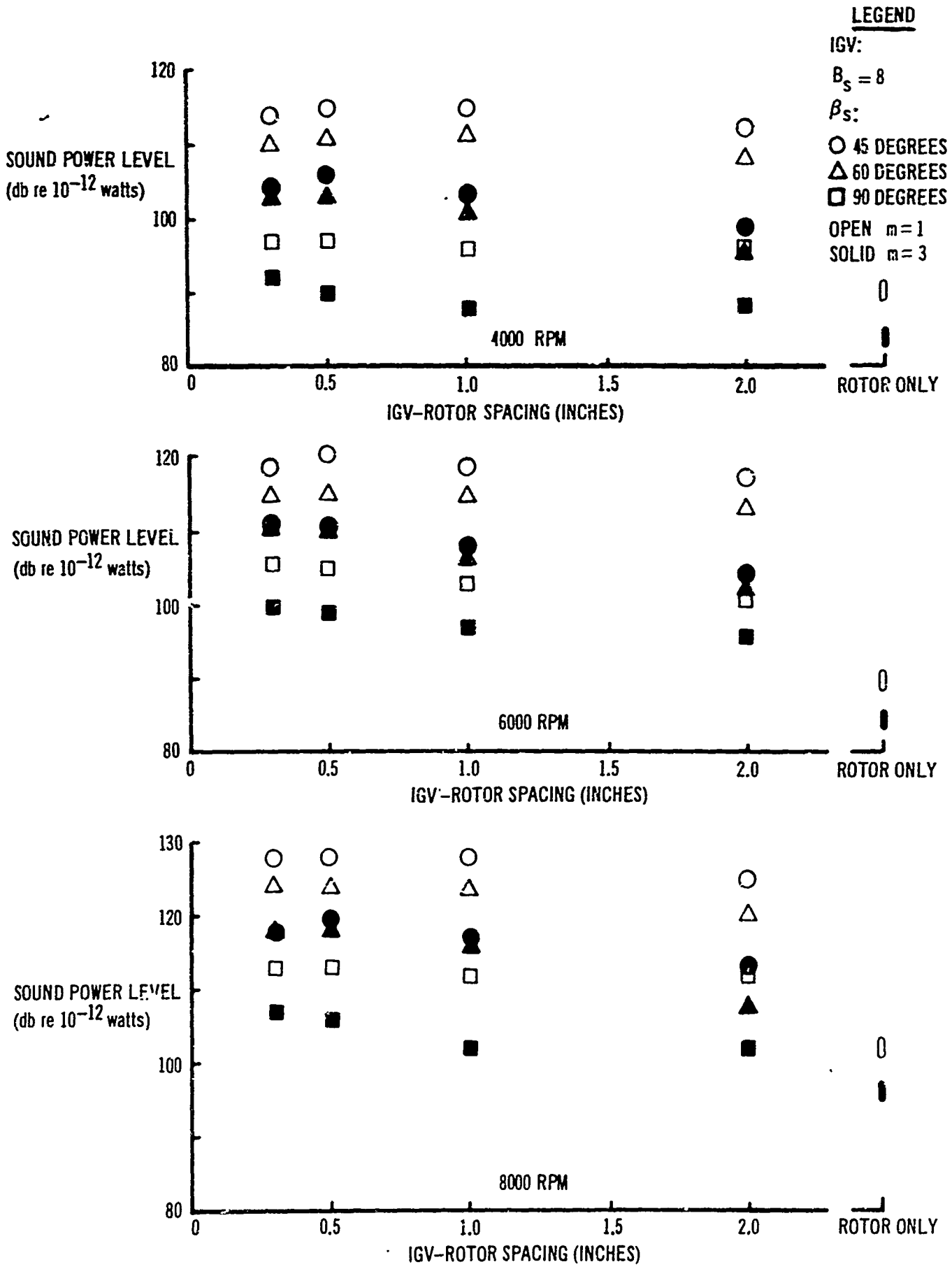


Fig. A26. Flat Rotor Blades, Different β_s ; Sound Power Level 6 Feet From Rotor and IGV-Rotor Spacing



**Fig. A27. Rotor Blades With 6-Inch Camber, 20-Degree Twist:
 Sound Power Level 6 Inches From Rotor and IGV-Rotor Spacing**

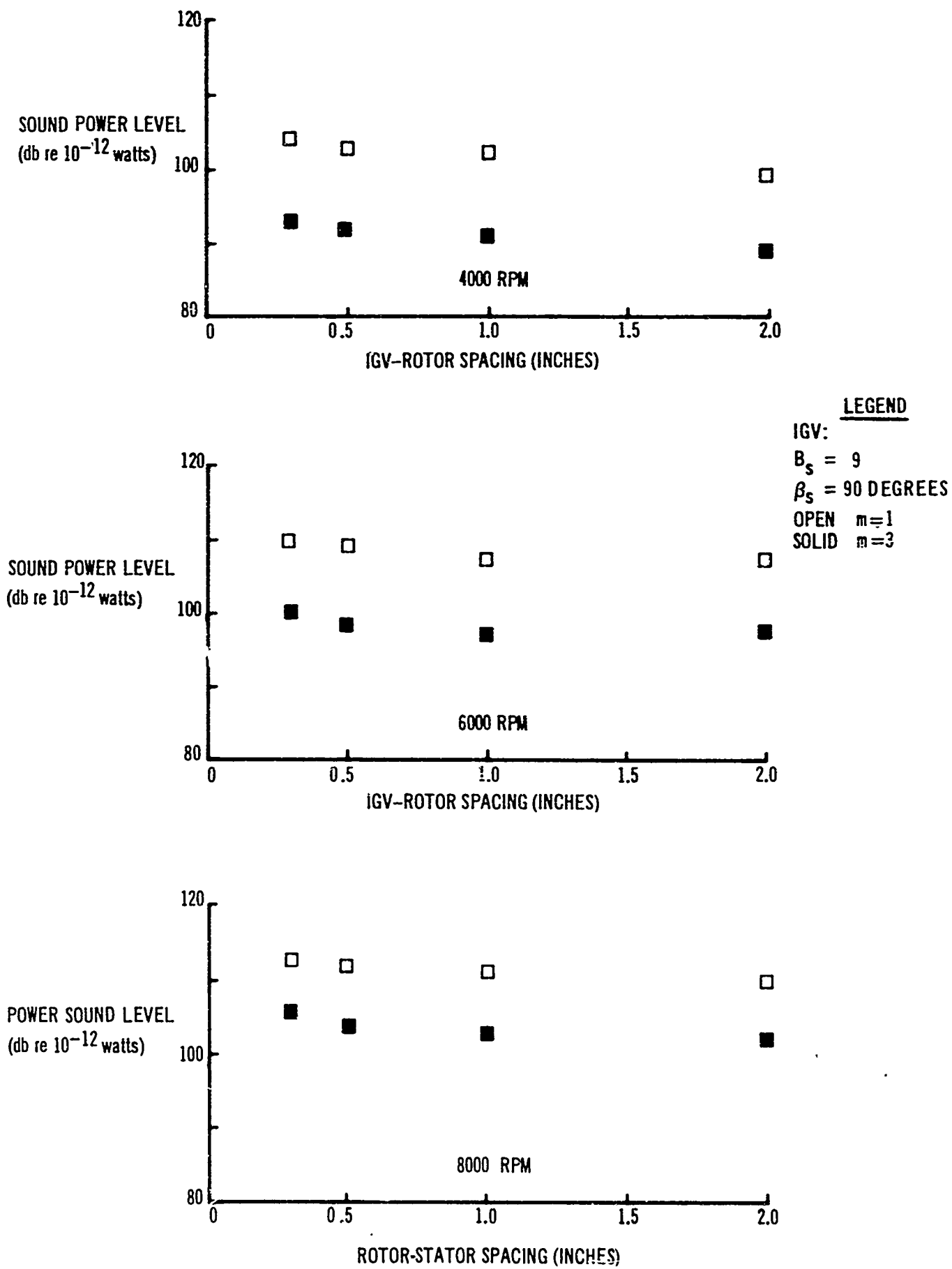


Fig. A28. Rotor Blades With 6-Inch Camber, 20-Degree Twist:
 Sound Power Level 6 Feet From Rotor and IGV-Rotor Spacing

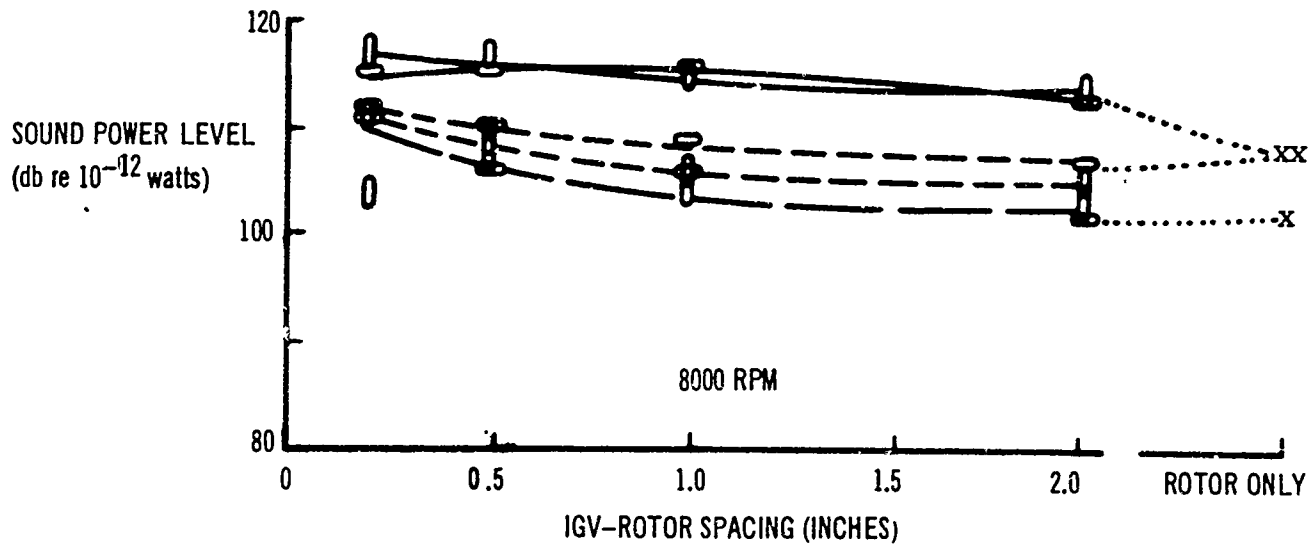
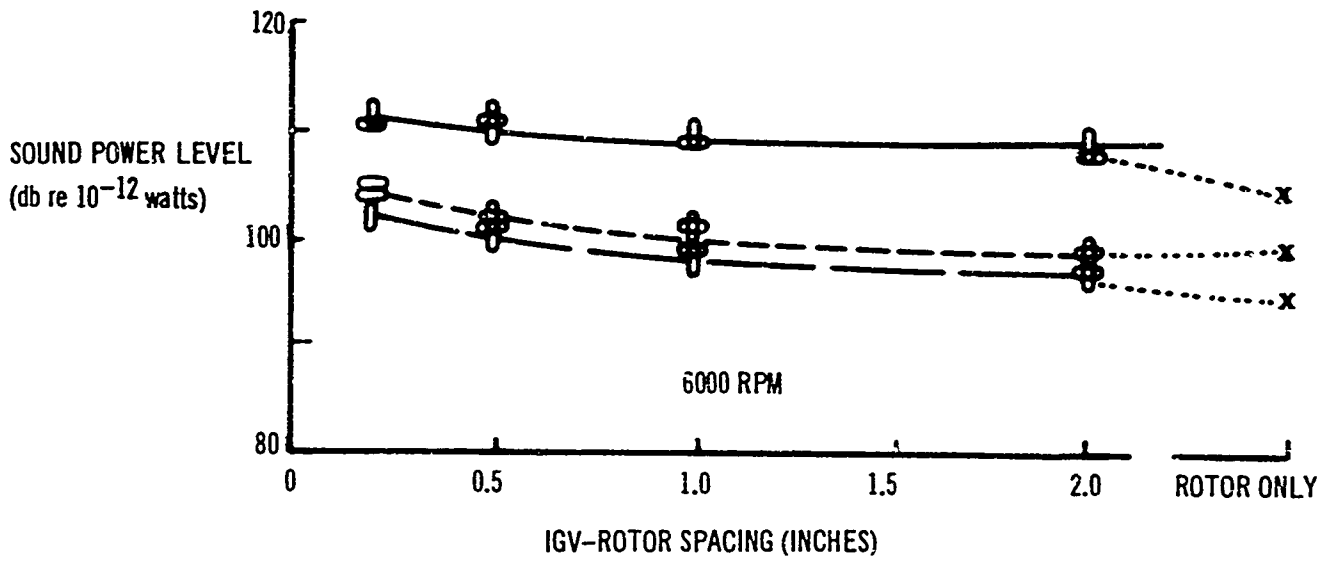
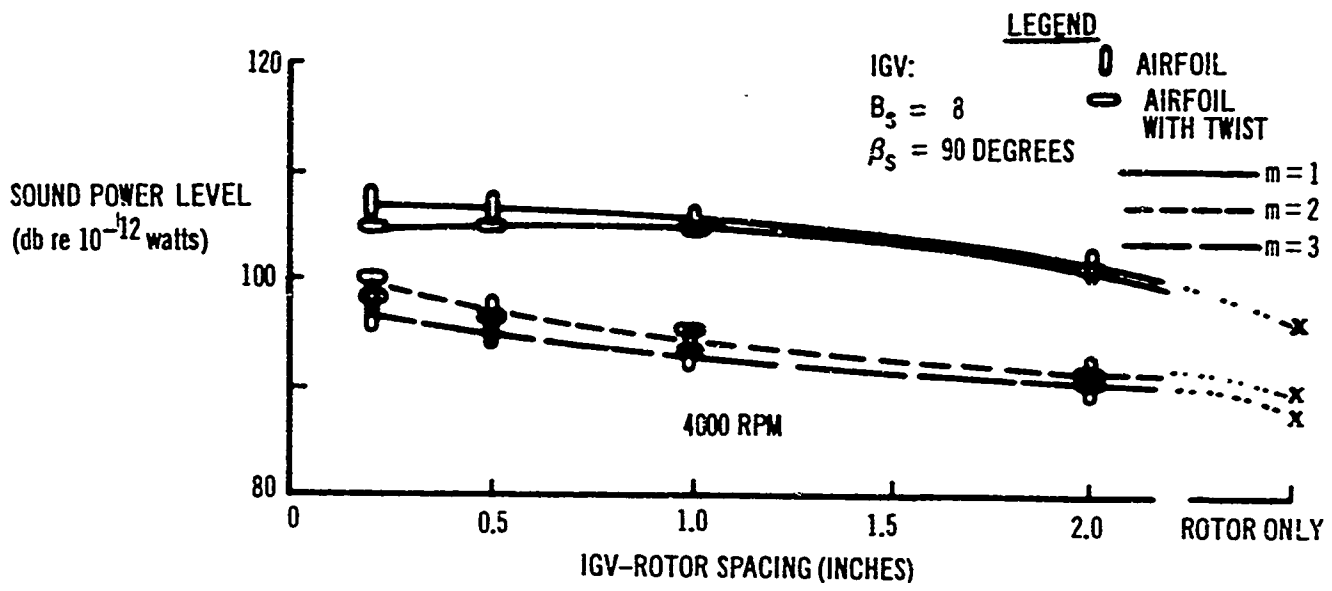


Fig. A29. Airfoil Blades, Straight and Twisted:
Sound Power Level 6 Feet From Rotor and IGV-Rotor Spacing
 A-32

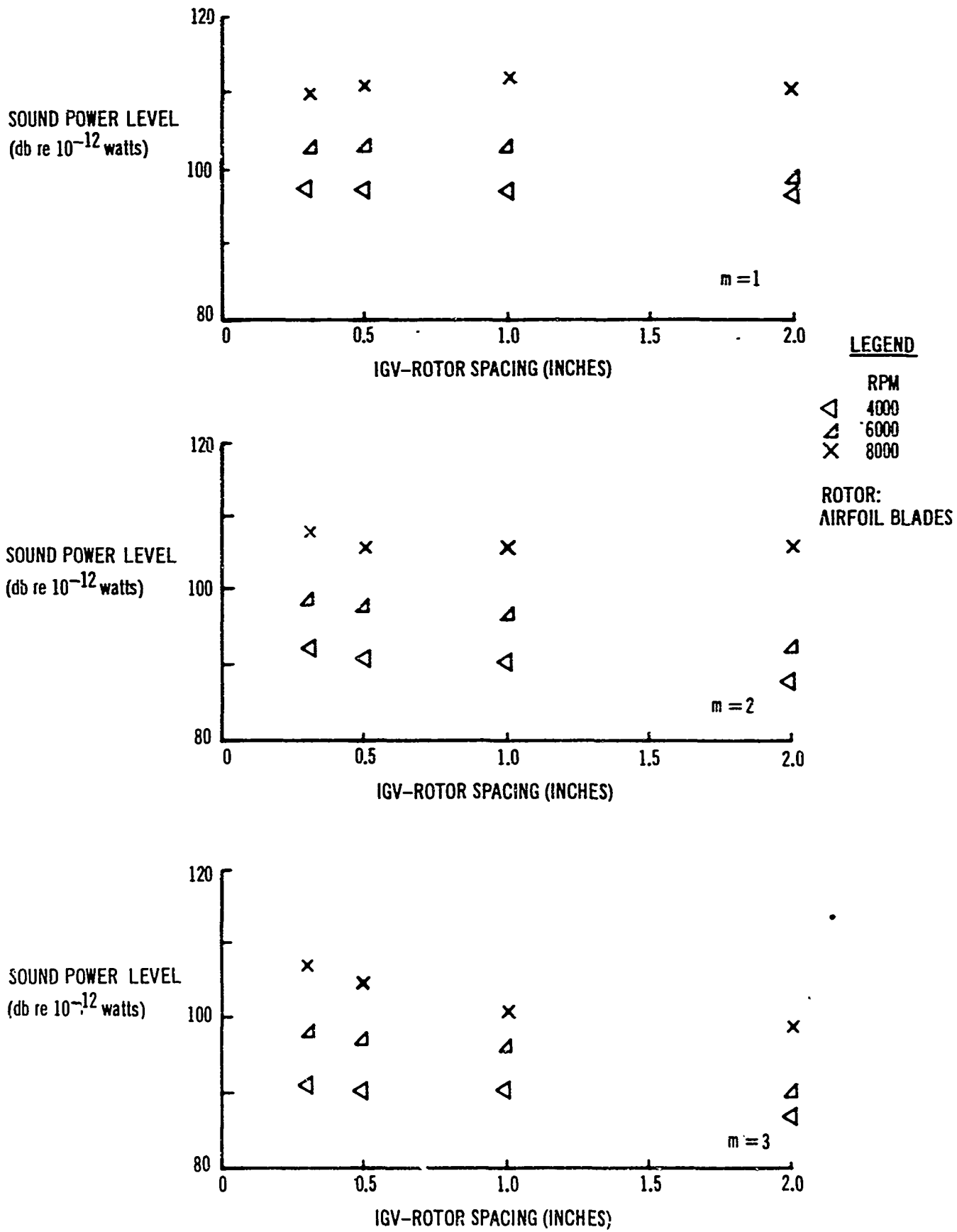


Fig. A30. Tubular IGV, Sound Power Level 6 Inches From Rotor and IGV-Rotor Spacing

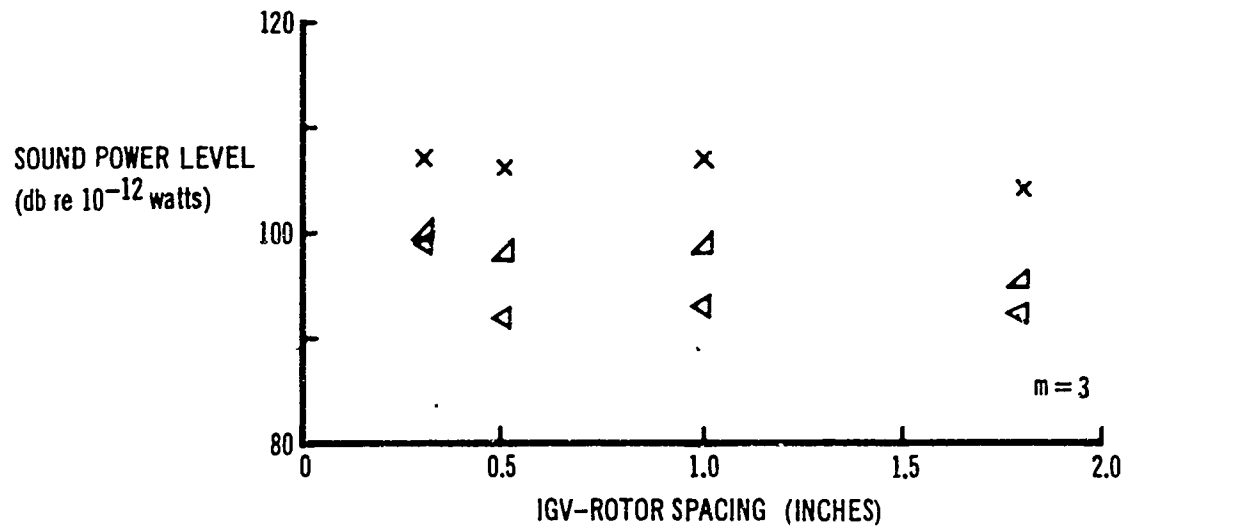
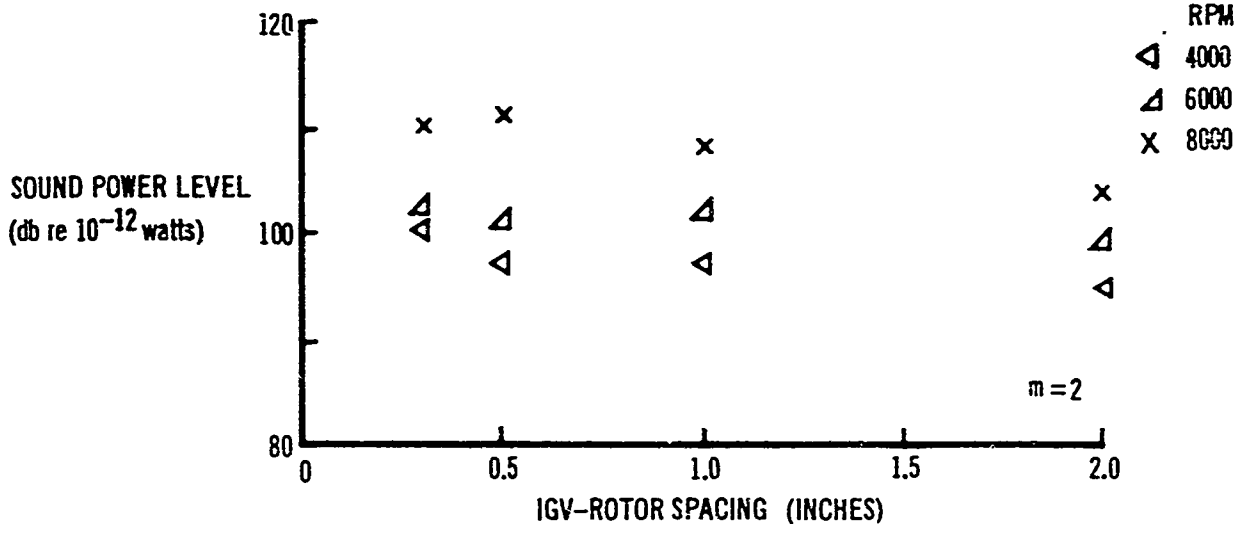
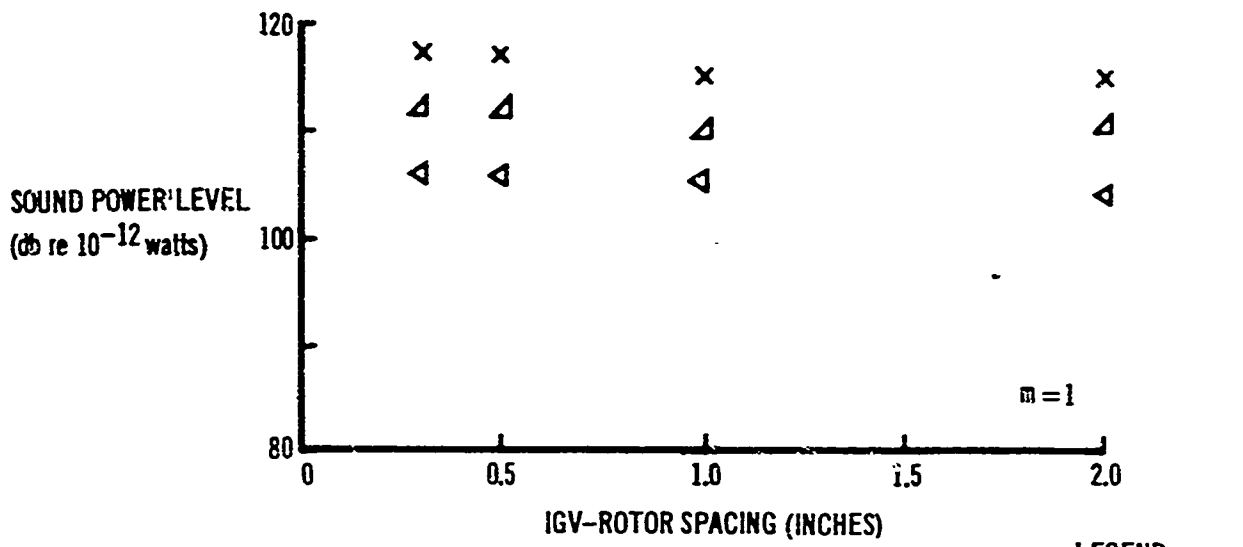
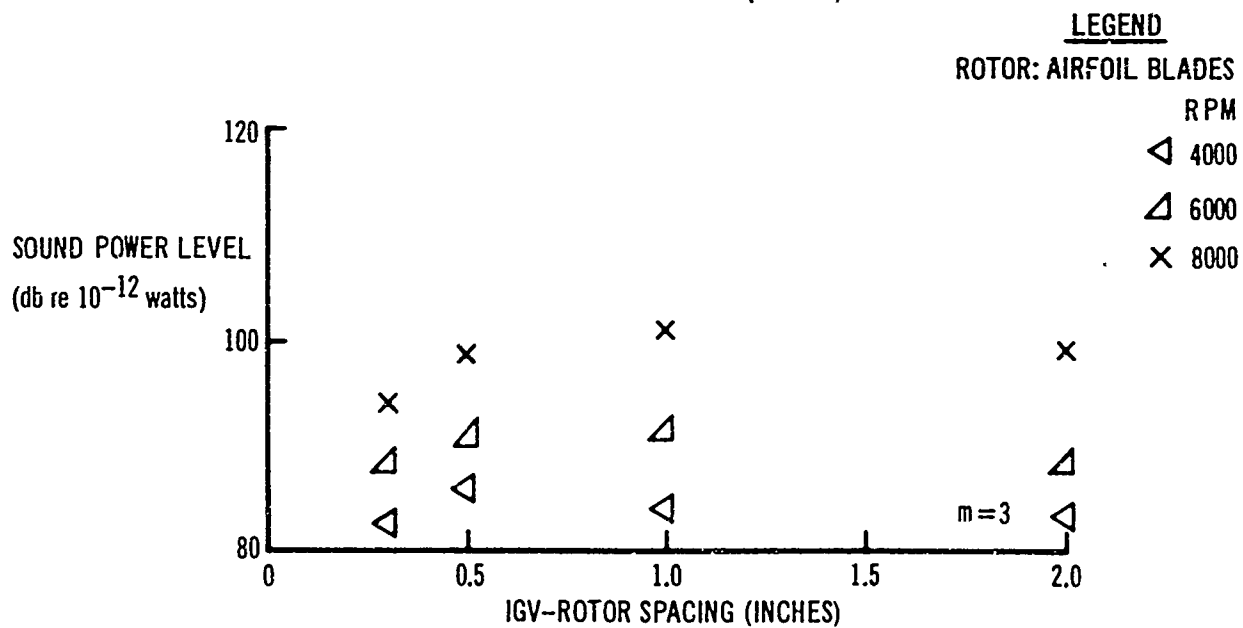
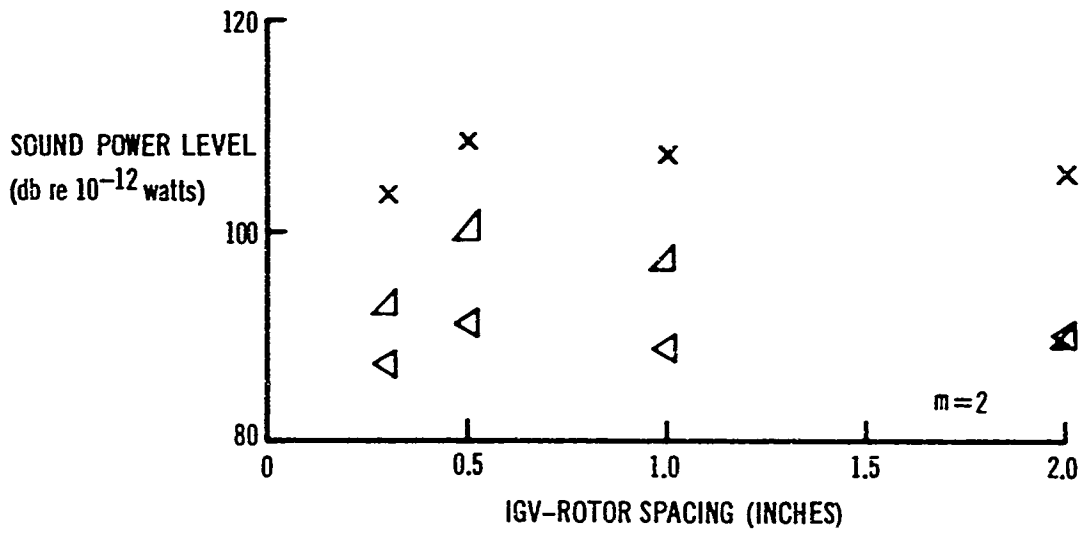
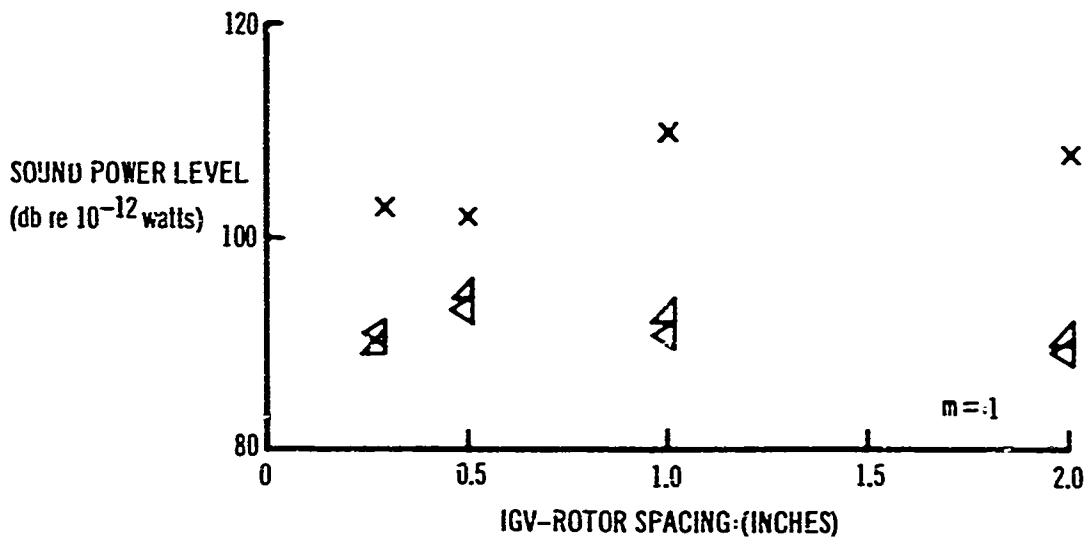


Fig. A31. Tubular IGV, Sound Power Level 6 Feet From Rotor and IGV-Rotor Spacing



LEGEND
 ROTOR: AIRFOIL BLADES
 RPM
 ◁ 4000
 △ 6000
 × 8000

Fig. A32. Honeycomb IGV (3/16-Inch Cell), Sound Power Level 6 Inches From Rotor and IGV-Rotor Spacing

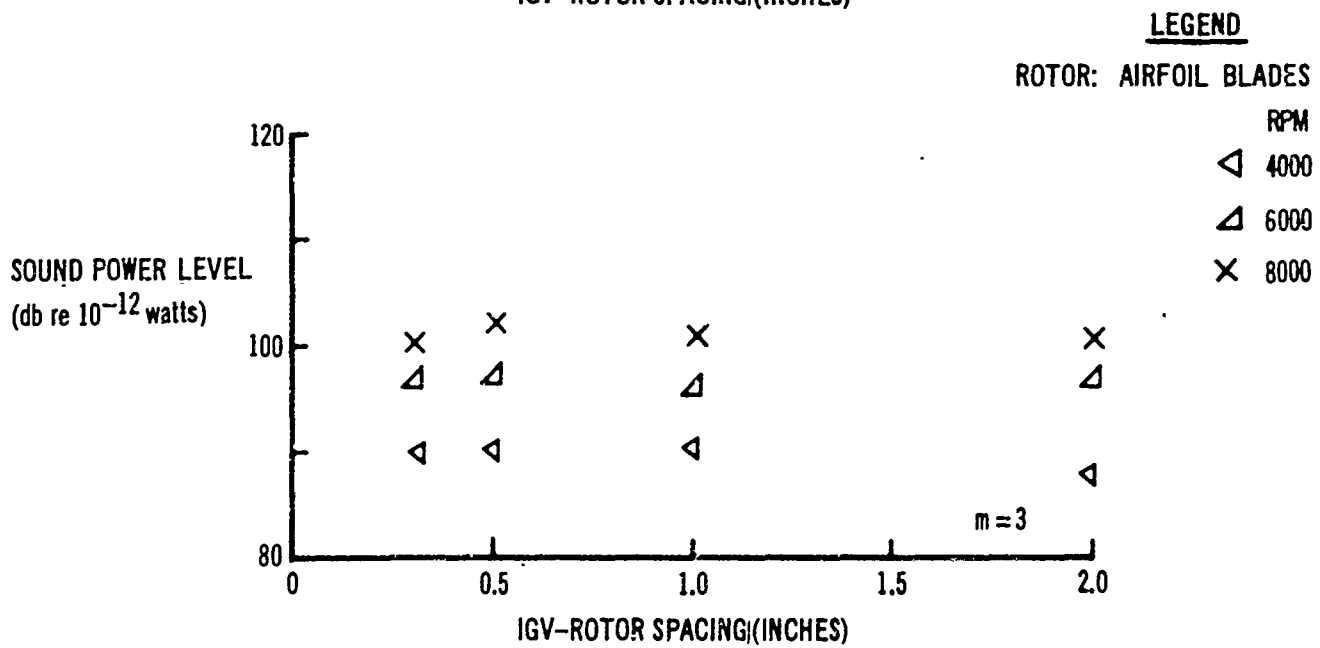
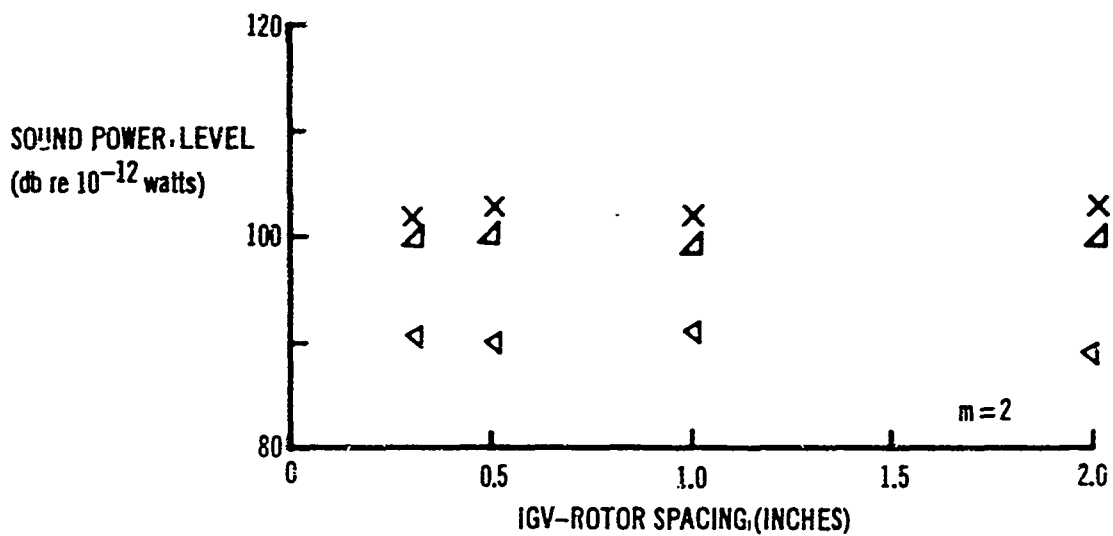
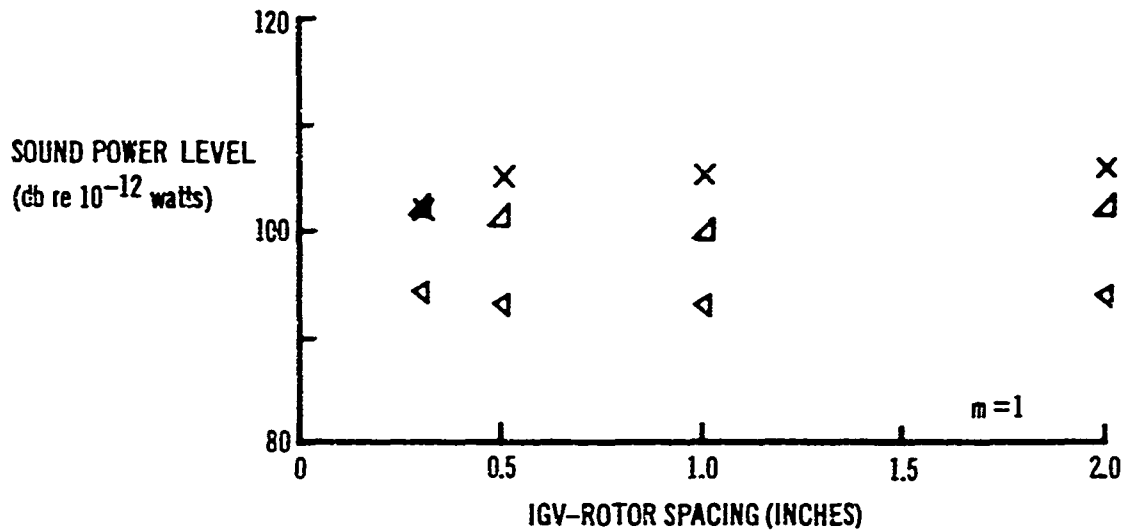


Fig. A33. Honeycomb IGV (3/16-Inch Cell), Sound Power Level 6 Feet From Rotor and IGV-Rotor Spacing

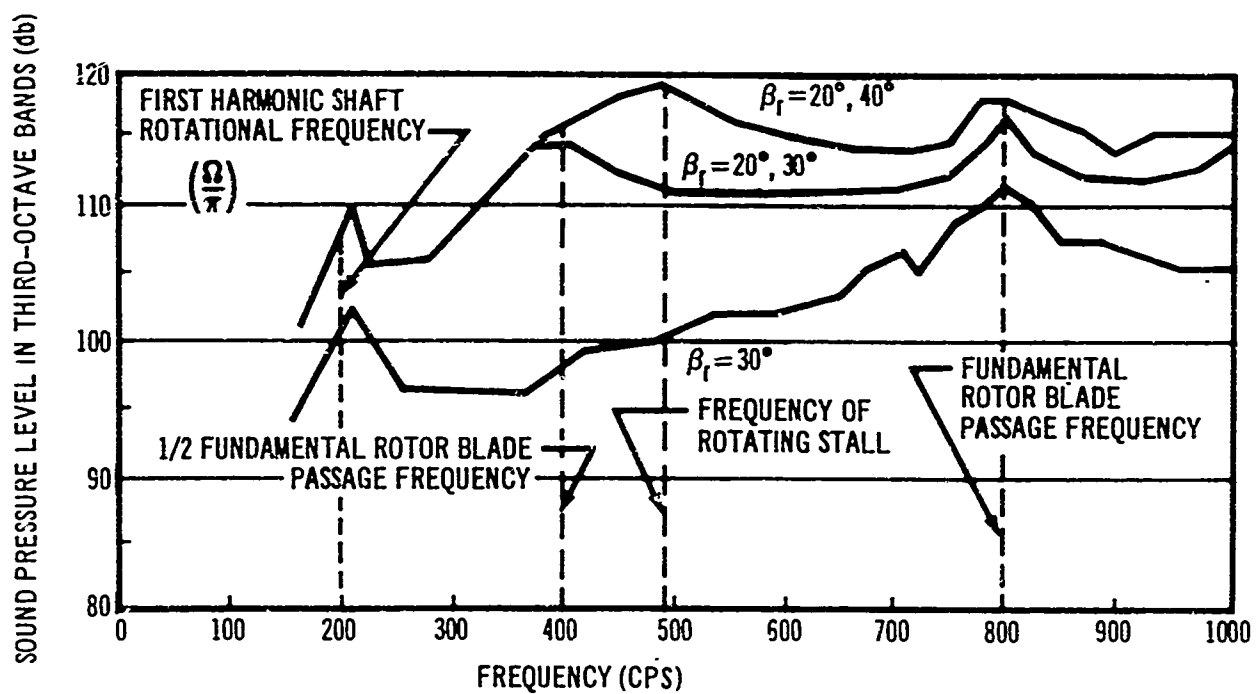


Fig. A34. Alternate Rotor Blade Angles Equal, Sound Pressure Level and Frequency

APPENDIX B

FAR-FIELD NOISE FROM JET-ENGINE COMPRESSORS

Introduction to Analysis

Starting with the work of Gutin (Ref. 9) in 1936, there have been several analyses of the far-field noise resulting from aircraft propellers or jet-engine compressors. The most complete treatment of aircraft propeller noise appears to be that of Garrick and Watkins (Ref. 10) in 1954, in which they found good agreement between their analytical results and experiments.

In principle, their results should also be applicable to a compressor, if proper account is taken of the duct sound propagation characteristics, since the number of blades—a parameter in their final formula—can be made arbitrarily large. However, the formula indicates a rapid decrease in the sound intensity level as the number of blades is increased, which does not occur in an engine. In fact, the Gutin-Garrick-Watkins formula may be written

$$|p| = \frac{m\omega_1}{2\pi a s_0} \left| \bar{T} \frac{x}{s_0} - Q \frac{Ba}{\omega_1 R_e^2} \right| J_{mB} \left(\frac{kyR_e}{s_0} \right) \quad (1)$$

For a rotor, the argument of the Bessel function J_{mB} is of less than unity in magnitude, so that the order of magnitude of J_{mB} is

$$\frac{1}{(mB)!} \cdot \left(\frac{m\omega_1 y R_e}{2a s_0} \right)^{mB} \quad (2)$$

which decreases very rapidly as mB increases. For the case of a practical rotor, with B large, this formula would predict an almost inaudible sound level. Moreover, Eq. (1) requires $p = 0$ for $y = 0$, and again this is not always observed.

One task of the present investigation has been to determine the reason for this discrepancy and to attempt to derive a more realistic expression for the far-field sound intensity for this case. The first possibility to be considered was that the derivation of Eq. (1), as given by Gutin et al., is not applicable to the case of large B . The derivation in question terminates with the determination of the first term of an asymptotic approximation to a more accurate expression, so that the calculation of the second approximation seemed appropriate. This was done, and the results appear in the second part of this appendix. It was concluded that the approximation leading to Eq. (1) remained valid even for the case of large B .

The next topic to be investigated was that of the validity of the derivation leading to the more exact Gutin result [to which Eq. (1) is the first approximation]. The Gutin-Garrick derivation is rather intricate. It involves a Fourier decomposition of the pressure distribution over a compressor blade, and

it is not clear how the nature of the distribution interacts with the spatial locations of the compressor blades. An alternative derivation of Eq. (1) has been given by Lawson (Ref. 3), but this derivation seems rather difficult to interpret because of unclear manipulations involving retarded values of singularity functions. Moreover, the final result obtained by Lawson [his Eq. (21)] appears to require p to vanish (for thrust, but no drag) as R_e approaches zero, whereas the result should approach the nonzero pressure resulting from a concentrated stationary force at the origin.

It therefore seemed useful to reexamine the derivation of the far-field pressure formula, concentrating on the effect of a large number of blades. This derivation is carried out below. The effect of a duct head of the rotor is not considered.

Acoustic Field of Force Singularities

We begin with a brief derivation of the pressure field resulting from an impulse applied in the x -direction at time zero, at the origin of a Cartesian coordinate system. The equations of motion are

$$\begin{aligned} \rho_0 \frac{\partial u_j}{\partial t} &= \delta_{j1} \delta(x) \delta(y) \delta(z) \delta(t) - p_{,j} \\ \frac{\partial \rho}{\partial t} + \rho_0 u_{k,k} &= 0 \\ p &= a^2 \rho \end{aligned} \tag{3}$$

where

- ρ_0 = base density
- ρ = fluctuation in density
- p = fluctuation in pressure
- a = velocity of sound
- u_k = velocity component fluid in direction of k -axis
- δ_{jk} = Kronecker delta (zero, unless j and k are same index)
- $,k$ = $\frac{\partial}{\partial k}$
- $\delta(x)$ = delta function (concentrated unit area impulse at $x = 0$; thus

$$\int_{-\infty}^{\infty} f(\xi) \delta(x - \xi) d\xi = f(x)$$

Here and in the future, a repeated index indicates summation from 1 to 3; thus

$$u_{k,k} = \frac{\partial u_1}{\partial x_1} + \frac{\partial u_2}{\partial x_2} + \frac{\partial u_3}{\partial x_3}$$

Take Fourier transforms in each of x_1, x_2, x_3 , and a Laplace transform in time, to give

$$P = \frac{i\lambda_1}{(2\pi)^{3/2} \left[\lambda_j \lambda_j + \frac{s^2}{a^2} \right]}$$

where P is the Fourier-Laplace transform of p . Inverting with respect to the space variables, we obtain

$$\bar{P} = \int_0^\infty e^{-st} p(x_1, x_2, x_3, t) dt = \frac{1}{(2\pi)^3} \frac{\partial}{\partial x} \iiint_{-\infty}^{\infty} \frac{\exp[-i \lambda_k x_k]}{\lambda_j \lambda_j + \frac{s^2}{a^2}} d\lambda_1 d\lambda_2 d\lambda_3$$

Rotation of coordinates in the λ_j variables leads to

$$\bar{P} = -\frac{1}{(2\pi)^2} \frac{\partial}{\partial x} \int_0^\infty \int_0^\pi \frac{\exp[-i rd \cos\theta]}{r^2 + \frac{s^2}{a^2}} dr r^2 \sin\theta d\theta$$

where d is the distance of the observation point from the origin. Thus

$$\begin{aligned} \bar{P} &= -\frac{1}{(2\pi)^2} \frac{\partial}{\partial x} \int_{-\infty}^{\infty} \frac{r \sin(rd)}{d \left[r^2 + \frac{s^2}{a^2} \right]} dr \\ &= -\frac{1}{4\pi} \frac{\partial}{\partial x} \left(\frac{\exp[-sd/a]}{d} \right) \\ &= -\frac{1}{4\pi} \frac{\partial}{\partial x} \left[\frac{1}{d} \delta \left(t - \frac{d}{a} \right) \right] \end{aligned} \quad (4)$$

two special cases may be noted. First, let a force $F \sin \Omega t$ be applied at the origin in the x direction. Then

$$\begin{aligned}
 p &= -\frac{1}{4\pi} \frac{\partial}{\partial x} \int \frac{F \sin \Omega \tau \cdot \delta \left(t - \tau - \frac{d}{a} \right)}{d} d\tau \\
 &= -\frac{F}{4\pi} \frac{\partial}{\partial x} \left[\frac{\sin \Omega \left(t - \frac{d}{a} \right)}{d} \right]
 \end{aligned} \tag{5}$$

Second, let the force F (in the x -direction) move with uniform velocity V along the x -axis. Then

$$\begin{aligned}
 p &= -\frac{F}{4\pi} \frac{\partial}{\partial x} \int_{-\infty}^{\infty} \frac{d\tau}{\sqrt{(x - V\tau)^2 + y^2 + z^2}} \delta \left(t - \tau - \frac{r}{a} \right) \\
 &= -\frac{F}{4\pi} \frac{\partial}{\partial x} \left[\frac{1}{r + \frac{(x - Vt)(-V)}{a}} \right]
 \end{aligned}$$

where

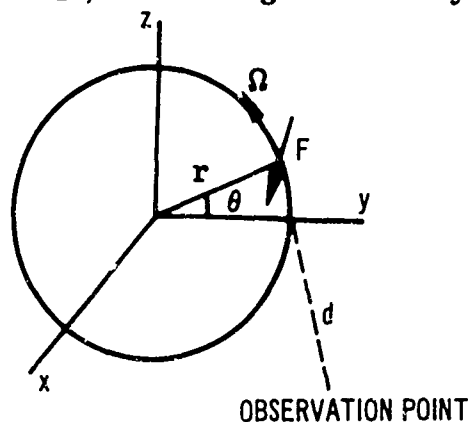
$$r = \left(1 - \frac{V^2}{a^2} \right)^{-1} \left[(x - Vt) \frac{V}{a} + \sqrt{(x - Vt)^2 + \left(1 - \frac{V^2}{a^2} \right) (y^2 + z^2)} \right]$$

Thus,

$$p = \left(\frac{F}{4\pi} \right) \frac{x - Vt}{\left[(x - Vt)^2 + \left(1 - \frac{V^2}{a^2} \right) (y^2 + z^2) \right]^{3/2}} \tag{6}$$

Pressure Field Due to Rotor

We now use Eq. (5) to derive the pressure field resulting from the rotational motion of a single concentrated force. Consider the case in which a concentrated force F , in the direction of the positive x -axis, rotates around the x -axis, at radial distance r , with an angular velocity Ω .



In the time interval τ to $\tau + d\tau$, a concentrated impulse of amount $Fd\tau$ is applied at the point $(0, r \cos \Omega\tau, r \sin \Omega\tau)$. The corresponding pressure, as seen at the observation point $(x, y, 0)$, is

$$dp = -\frac{1}{4\pi} \frac{\partial}{\partial x} \left[\frac{Fd\tau}{d} \delta \left(t - \tau - \frac{d}{a} \right) \right] \quad (7)$$

Consequently,

$$p = -\frac{1}{4\pi} \frac{\partial}{\partial x} \int_{-\infty}^{\infty} \frac{F \delta \left[t - \tau - \frac{1}{a} \sqrt{x^2 + (y - r \cos \Omega\tau)^2 + (r \sin \Omega\tau)^2} \right]}{\sqrt{x^2 + (y - r \cos \Omega\tau)^2 + (r \sin \Omega\tau)^2}} d\tau \quad (8)$$

Let

$$\tau + \frac{1}{a} \sqrt{x^2 + y^2 + r^2 - 2yr \cos \Omega\tau} = \xi$$

so that

$$d\tau \left[1 + \frac{yr \Omega \sin \Omega\tau}{a \sqrt{x^2 + y^2 + r^2 - 2yr \cos \Omega\tau}} \right] = d\xi$$

Then

$$p = -\frac{F}{4\pi} \frac{\partial}{\partial x} \left[\frac{1}{\sqrt{x^2 + y^2 + r^2 - 2yr \cos \Omega\tau} + \frac{1}{a} yr \Omega \sin \Omega\tau} \right] \quad (9)$$

where $\tau = \tau(t)$ via

$$\tau + \frac{1}{a} \sqrt{x^2 + y^2 + r^2 - 2yr \cos \Omega\tau} = t \quad (10)$$

Carrying out the differentiation, we obtain

$$p = \frac{F}{4\pi} \frac{\frac{x + yr\Omega\tau_x \sin\Omega\tau}{\sqrt{x^2 + y^2 + r^2 - 2yr \cos\Omega\tau}} + \frac{yr\Omega^2\tau_x}{a} \cos\Omega\tau}{\left[\sqrt{x^2 + y^2 + r^2 - 2yr \cos\Omega\tau} + \frac{1}{a} yr\Omega \sin\Omega\tau \right]^2} \quad (11)$$

But differentiation of Eq. (10) yields

$$\tau_x + \frac{x + yr\Omega\tau_x \sin\Omega\tau}{a \sqrt{x^2 + y^2 + r^2 - 2yr \cos\Omega\tau}} = 0$$

so that Eq. (11) becomes

$$p = \frac{F}{4\pi} \cdot \frac{a\tau_x \left[\frac{yr\Omega^2}{a^2} \cos\Omega\tau - 1 \right]}{\left[\sqrt{x^2 + y^2 + r^2 - 2yr \cos\Omega\tau} + \frac{yr \Omega \sin\Omega\tau}{a} \right]^2}$$

$$= \frac{Fx}{4\pi} \cdot \frac{1 - \frac{yr\Omega^2}{a^2} \cos\Omega\tau}{\left[\sqrt{x^2 + y^2 + r^2 - 2yr \cos\Omega\tau} + \frac{yr \Omega \sin\Omega\tau}{a} \right]^3} \quad (12)$$

where Eq. (10) provides the relationship between τ and t .

To compute the n^{th} harmonic of this signal, define $\theta = \Omega\tau$.
Then

$$a_n + ib_n = \frac{1}{\pi} \int_0^{2\pi} p(\Omega\tau) \cdot e^{i n\theta} d\theta \quad (13)$$

where $p(\Omega\tau)$ is given by Eq. (12), and where $\theta(\tau)$, from Eq. (10), may be written

$$\theta = \Omega\tau + \frac{\Omega}{a} \sqrt{x^2 + y^2 + r^2 - 2yr \cos \Omega\tau}$$

Thus Eq. (13) becomes

$$a_n + ib_n = \frac{1}{\pi} \int_0^{2\pi} p(\Omega\tau) \cdot e^{i n \left[\Omega\tau + \frac{\Omega}{a} \sqrt{x^2 + y^2 + r^2 - 2yr \cos \Omega\tau} \right]} d\left(\frac{d\theta}{d(\Omega\tau)}\right) d(\Omega\tau) \quad (14)$$

where we have used the fact that the τ -period is the same as the t -period.

Equation (14) is exact. If we now carry out a far-distance approximation, in which the product yr is considered small compared with

$$D^2 = x^2 + y^2 + r^2$$

we can write

$$\sqrt{x^2 + y^2 + r^2 - 2yr \cos \Omega\tau} = D \sqrt{1 - \frac{2yr}{D^2} \cos \Omega\tau} \cong D \left[1 - \frac{yr}{D^2} \cos \Omega\tau \right]$$

All the terms in Eq. (14) may then be expanded via the binomial theorem, and the result computed in terms of conventional Bessel integrals; the resulting formulas turn out to be comparable to those obtained by Gutin, Garrick and Watkins, and Lowson. In fact, we can see at once that we will encounter integrals of the form

$$\frac{1}{\pi} \int_0^{2\pi} e^{i \left[n\theta - \frac{n\Omega yr}{aD} \cos \theta \right]} d\theta = J_n \left(\frac{n\Omega yr}{aD} \right) \quad (15)$$

just as obtained by Gutin et al.

The preceding derivation makes it clearer, however, that (a) the details of the pressure distribution introduced rather arbitrarily by Garrick and Watkins play little or no role in the far-field approximation, and (b) the rather intricate resolution into radiative and nonradiative terms carried out by Lowson is unnecessary.

The conclusion is that the extremely rapid decay of the far-field noise with the increasing number of blades (note that for B blades, the lowest harmonic that can occur is the Bth harmonic of a single blade signal; all lower harmonics cancel) is a valid theoretical result.

SECOND APPROXIMATION TO THE GUTIN FAR-FIELD FORMULA FOR SOUND PRESSURE

Gutin (Ref. 9) and Garrick and Watkins (Ref. 10) have given formulas for the far-field sound intensity of rotating propeller blades based on an "effective ring" approximation. In this report, these results (for B = m = 1) have been used as the basis for the prediction of far-field compressor noise. In order to establish the region of validity of the far-field results, the second approximation to both p_Q and p_T is determined here. The first approximation should be valid when the second approximation is relatively small.

Garrick and Watkins give the following expressions for sound pressure due to thrust and torque forces (for m = B = 1).

$$p_Q = \frac{e^{i\Omega t} Q_i}{4\pi^2 R_c^2} \int_0^{2\pi} e^{-i \left[\theta + h(1-w)^{1/2} \right]} \frac{d\theta}{s_o(1-w)^{1/2}} \quad (16)$$

$$p_T = \frac{-c^{i\Omega t}}{4\pi^2} \int_0^{2\pi} T \left[\frac{ikx}{s_o^2(1-w)} + \frac{x}{s_o^3(1-w)^{3/2}} \right] e^{-i \left[\theta + h(1-w)^{1/2} \right]} d\theta \quad (17)$$

where

$$s_o = \left(x^2 + y^2 + R_c^2 \right)^{1/2}, \quad w = b \cos \theta, \quad h = \Omega s_o / a, \quad \text{and } b = 2yR_c / s_o^2.$$

Since $|\cos \theta| \leq 1$, w will be small when b is small. Since b is small for the far field, the first approximation to these integrals for far-field conditions is obtained by retaining in the integrand only the lowest order terms in b. This procedure was invoked by Gutin and by Garrick and Watkins, and their results were referred to earlier in this report. To obtain the next approximation,

appropriate succeeding terms are retained in the expression of the integrand, and the integration subsequently performed. Accordingly, the expression for p_Q and p_T takes the following form:

$$p_Q = \frac{e^{i\Omega t}}{4\pi^2} \frac{Qie^{-ih}}{R_e^2 s_o} \int_0^{2\pi} e^{-i\left(\theta - \frac{hb}{2} \cos \theta\right)} \left(1 + \frac{b^2 \cos \theta}{2} + \frac{ihb^2 \cos^2 \theta}{8}\right) d\theta \quad (18)$$

$$p_T = \frac{-e^{i\Omega t}}{4\pi^2} \frac{Txe^{-ih}}{s_o^2} \int_0^{2\pi} \left[\left(ik + \frac{1}{s_o}\right) + ikb \cos \theta + \frac{ikihb^2 \cos^2 \theta}{8} \right] e^{-i\left(\theta - \frac{hb \cos \theta}{2}\right)} d\theta \quad (19)$$

The required integrations may be performed by making use of the relation

$$\int_0^{2\pi} e^{i(\lambda \cos \theta - n\theta)} d\theta = 2\pi i^n J_n(\lambda) \quad (20)$$

The following expressions, obtained by differentiating Eq. (20) with respect to λ , are also used in the integration.

$$\int_0^{2\pi} \cos \theta e^{i(\lambda \cos \theta - n\theta)} d\theta = 2\pi i^{n+1} J'_n(\lambda) \quad (21)$$

$$\int_0^{2\pi} \cos^2 \theta e^{i(\lambda \cos \theta - n\theta)} d\theta = 2\pi i^n J''_n(\lambda) \quad (22)$$

Using these formulas to perform the integration, we obtain the following expressions for $|p_T|$ and $|p_Q|$:

$$|p_T| = \frac{T_x k J_1\left(\frac{hb}{2}\right)}{2\pi s_o^2} \left\{ 1 + \left[\frac{1}{h} + \frac{b J_1'\left(\frac{hb}{2}\right)}{J_1\left(\frac{hb}{2}\right)} + \frac{hb^2 J_1''\left(\frac{hb}{2}\right)}{8 J_1\left(\frac{hb}{2}\right)} \right]^2 \right\}^{1/2} \quad (23)$$

$$|p_Q| = \frac{Q J_1\left(\frac{hb}{2}\right)}{2\pi R_e^2 s_o} \left\{ 1 + \frac{\left| \frac{b}{2} J_1'\left(\frac{hb}{2}\right) + \frac{hb^2}{8} J_1''\left(\frac{hb}{2}\right) \right|^2}{J_1\left(\frac{hb}{2}\right)} \right\}^{1/2} \quad (24)$$

The first factor in each of these expressions corresponds to the far-field first approximation referred to in the main body of the report. The terms in brackets represent the next approximation, and both of these quantities tend to unity as s_o becomes sufficiently large. For the conditions considered here, the SPL difference between the first and second approximation is less than 1 dB.

This indicates that the use of the far-field first approximation under these conditions is satisfactory.

APPENDIX C

MEASUREMENT APPARATUS

Equipment and instrumentation used for this project are similar to those described in FAA Technical Report ADS-31. A schematic sketch of the single-stage model compressor is shown in Fig. C1. The compressor is separated from the driving air turbine by a 5-foot shaft to allow installation of the turbine outside the test cell, so it could be acoustically isolated from the cell by a brick wall. The pitot rake for making air flow measurements and the tachometer probe for measuring rotor shaft rotational speed may be seen in the figure. The compressor inlet duct is 12 inches in diameter and the hub diameter is 4 inches.

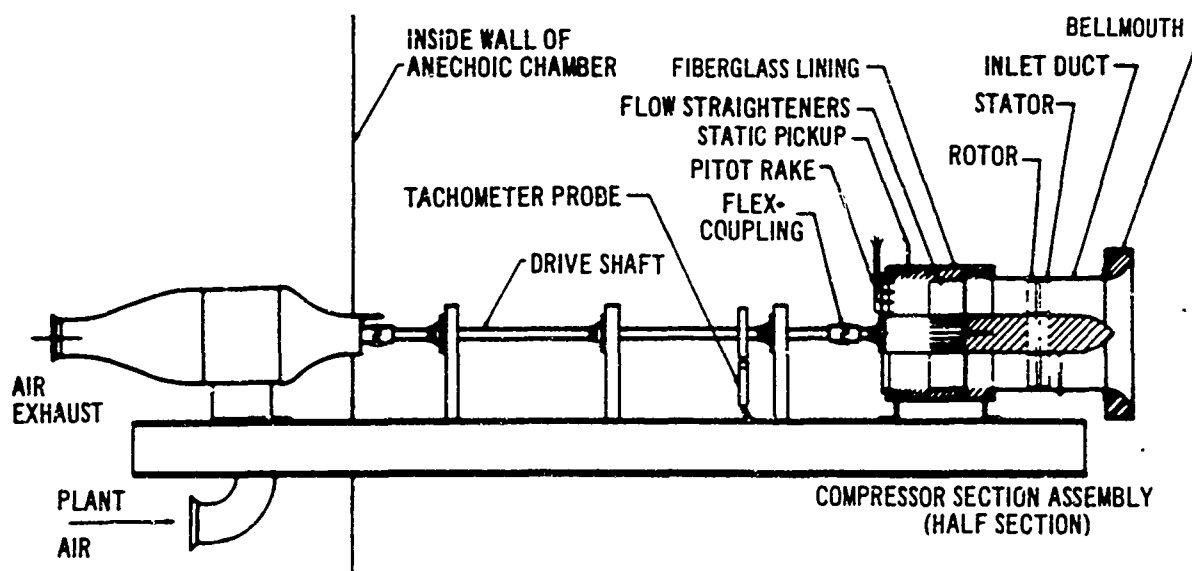


Fig. C1. Compressor Assembly Schematic

The compressor test cell is shown in Fig. C2. The walls and ceiling are made sound absorbent by installing 2 inches of fiberglass blanket material covered by a thin layer of polyurethane to retain the glass fibers. A microphone is mounted on a 6-foot boom and traverses a 90-degree arc either side of the rotational axis in front of the inlet. Its movement is remotely controlled, electrically, and it can be stopped at 15-degree intervals.

Figures C3 and C4 show the sound level data reduction system. Data are reduced "on line" to circumvent the inconvenience and added expense of using a tape recorder and the associated data reduction equipment.

Flow measurements are obtained with the pitot rake shown in Fig. C5.



Fig. C2. Compressor Test Cell

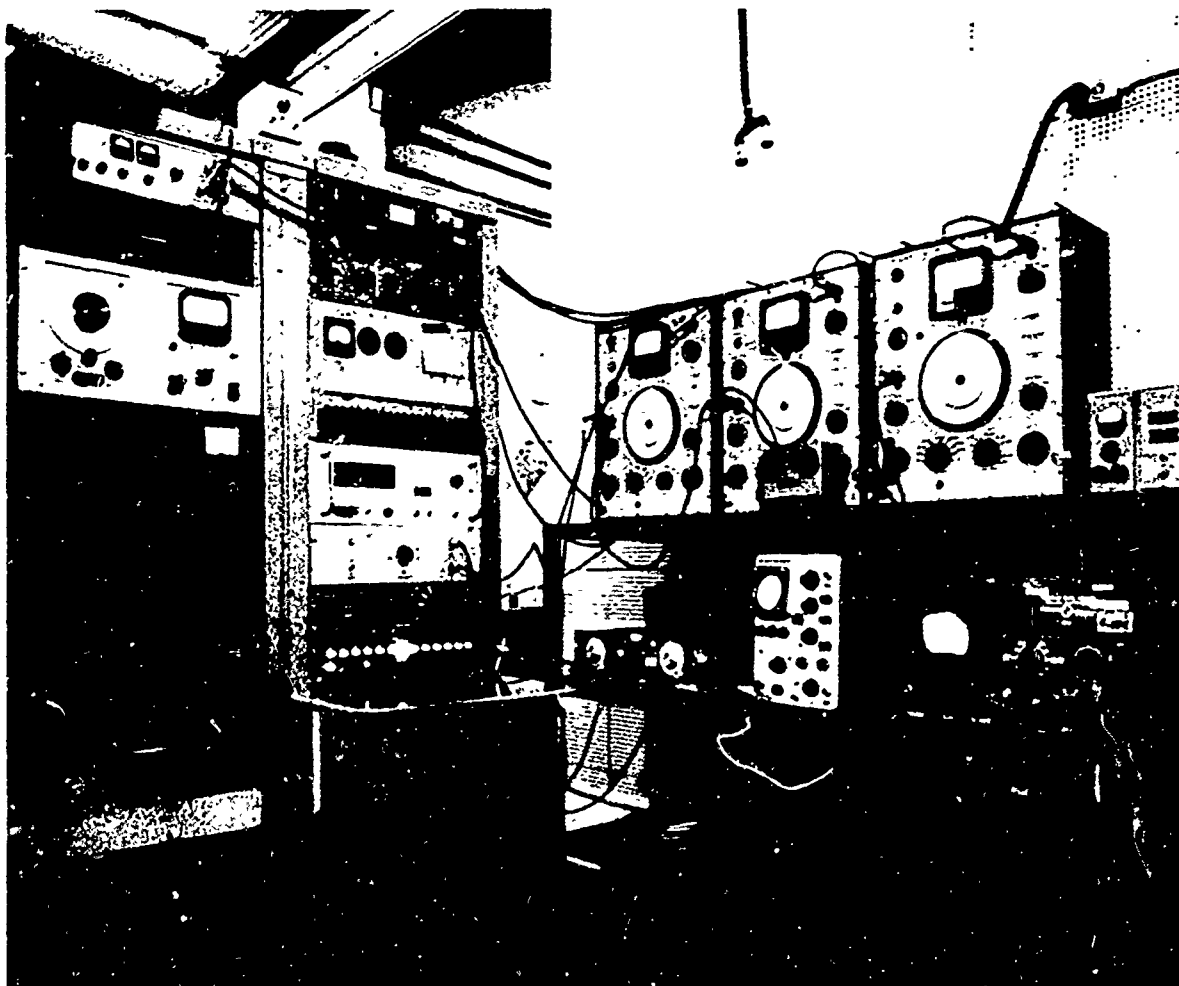


Fig. C3. Sound Level Data Reduction System

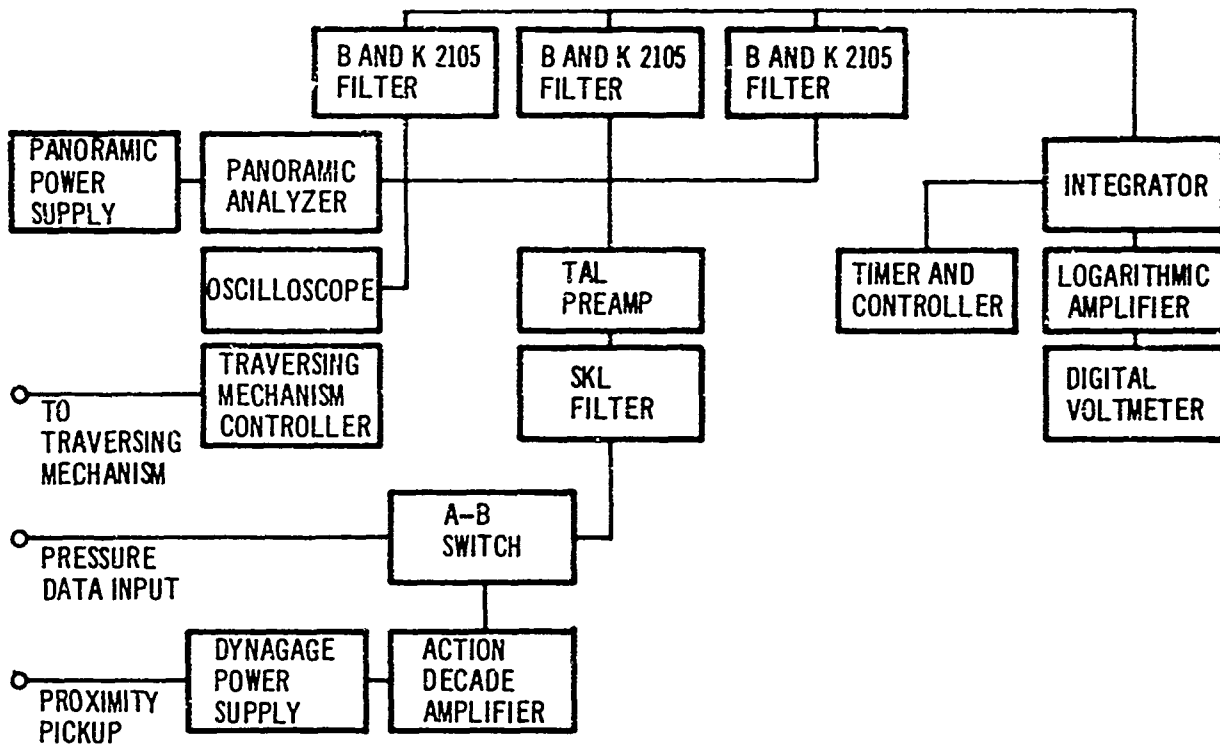


Fig. C4. Sound Level Data Reduction System Schematic

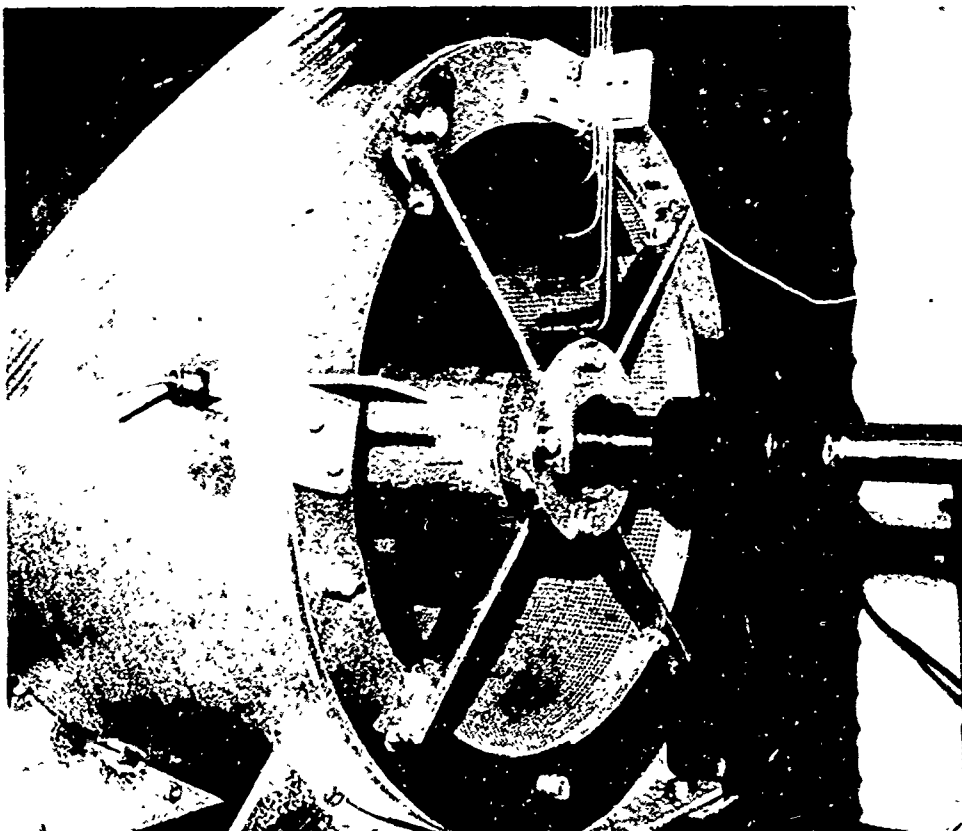


Fig. C5, Pitot Rake